ISSN 2461-4254

EUREKA: PHYSICS AND ENGINEERING

- Chemical Engineering
- Chemistry
- Computer Science
- Earth and Planetary Sciences
- Energy
- Engineering
- Materials Science
- Mathematics
- Physics and Astronomy

Volume 2(15)
2018

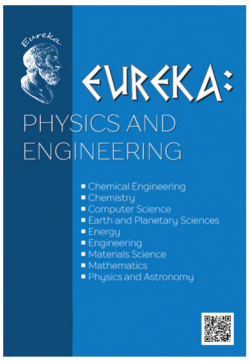

SCIENTIFIC JOURNAL

EUREKA: Physics and Engineering – scientific journal whose main aim is to publish materials allowed to see ***new discoveries at the intersection of sciences.***

- Chemical Engineering
- Chemistry
- Computer Science
- Earth and Planetary Sciences
- Energy
- Engineering
- Material Science
- Mathematics
- Physics and Astronomy
- Technology Transfer

EUREKA: Physics and Engineering
publishes
4 types of materials:
– review article,
– progress reports,
– original Research Article
– reports on research projects

PUBLISHER OÜ «Scientific Route»
European Union
Editorial office
«EUREKA: Physical Sciences and Engineering»
Narva mnt 7-634, Tallinn, Eesti
Harju maakond, 10117
Tel. + 372 602-7570
e-mail: info@eu-jr.eu
Website: http://eu-jr.eu

EDITORIAL BOARD

CONTENT

RESEARCH OF MICROBIOLOGICAL INDICATORS OF QUALITY OF SURFACE WATERS OF NATURAL ENVIRONMENTAL TERRITORIES OF THE DANUBE BASIN

Andrew Masikevych
Department of Hygiene and Ecology
Bucovinian State Medical University
2 Teatralna sq., Chernivtsi, Ukraine, 58000
masikevich.a@gmail.com

Mikhail Kolotylo
Department of Ecology and Law of Chernivtsi Faculty
National Technical University "Kharkiv Polytechnic Institute"
2 Kyrpychova str., Kharkiv, Ukraine, 61002
vyzhpark@ukrpost.ua

Valery Yaremchuk
Department of Ecology and Law of Chernivtsi Faculty
National Technical University "Kharkiv Polytechnic Institute"
2 Kyrpychova str., Kharkiv, Ukraine, 61002
vyzhpark@ukrpost.ua

Yurij Masikevych
Department of Hygiene and Ecology
Bucovinian State Medical University
2 Teatralna sq., Chernivtsi, Ukraine, 58000
yumasik@meta.ua

Valentyn Myslytsky
Department of Pathological Physiology
Bucovinian State Medical University
2 Teatralna sq., Chernivtsi, Ukraine, 58000
myslytsky@gmail.com

Ivan Burdeniuk
PhD, Assistant
Department of microbiology and virucology
Bucovinian State Medical University
2 Teatralna sq., Chernivtsi, Ukraine, 58000
microbiology@bsmu.edu.ua

Konstantin Dombrovskyi
Department of General and Applied Ecology and Zoology
Zaporizhzhya National University
66 Zhukovsky str., Zaporizhzhya, Ukraine, 69600
dombrov1717@ukr.net

Abstract

A comparative analysis of the sanitary and ecological state of surface watercourses in the upper part of the Danube basin (on the territory of Ukraine) was carried out according to microbiological indicators. Similar hygienic studies were previously conducted in the middle and lower Danube in Austria, Slovakia, Hungary and Romania. In Ukraine, the river network of the Danube River basin was not studied by microbiological indicators.

The object of research is the watercourses on the territory of various zones of the nature protection object, which are different in function. This approach makes it possible to use hygienic indicators of water in protected areas of nature conservation areas as a reference for conducting background monitoring.

The original design of the treatment plant based on the use of "Viya" fibrous carrier and "paste" technical structure is proposed. It was established that as the transition from the reserve to the economic zone occurs, the nitrate content in the water increases, the BOD increases in water, and the dissolved oxygen in the water decreases for all the watercourses studied. Significant differences in microbiological indices of watercourses of various functional zones of the protected object have been revealed.

The possibility of using the sanitary-microbiological indicators of the river network as a reliable rapid test for assessing the state of environmental safety of nature conservation areas is shown.

Keywords: nature protection areas, functional zones, surface waters, Danube basin, sanitary-microbiological indicators.

DOI: 10.21303/2461-4262.2018.00590

© *Andrew Masikevych, Mikhail Kolotylo, Valery Yaremchuk, Yurij Masikevych, Valentyn Myslytsky, Ivan Burdeniuk, Konstantin Dombrovskyi*

1. Introduction

Sanitary-microbiological indicators are successfully used as indicators of environmental pollution: water, air, soil [1–3], as well as to monitor the status of ecosystems, forecasting and modeling of development. In connection with the rapid reaction to environmental changes, bacteria proved to be ideal markers of microbial contamination of surface waters [4]. This approach is especially valuable for protected areas. Protected areas serve as background sites for assessing the ecological status and changes in the environment. Studying their condition makes it possible to predict changes in the environment to a distant future.

The object of research is the sanitary and epidemiological indicators of the water network of the Siret River. This river enters the upper part of the Danube basin and forms the basis of the hydrological network of the protected nature reserve "Vyzhnytsia National Nature Park". The Danube is one of the most important rivers of Europe and the world and, simultaneously, according to a number of authors [4], is one of the most vulnerable aquatic ecosystems. For monitoring the water quality of the Danube River, the coastal countries currently use different approaches and methods of sanitary and ecological analysis, which does not allow the formation of a holistic picture of the state of the ecosystem of an important waterway in Europe. That is why the use of microbiological analysis as a universal approach for water quality monitoring by the coastal countries of the international river Danube is relevant at this time.

2. Literature review and problem statement

To date, there is a strong demand for monitoring water quality. Researches of scientists of the Institute of Hydrometeorology from Bratislava [5] suggest the use of autoregressive models for studying the impact of natural and technogenic changes on the quality of the Danube.

In terms of monitoring the water network, the assessment of the presence of pathogenic bacteria in water is of particular interest, according to the American School of Researchers at the University of California, Davis and Iowa State University. In particular, this concerns the problems associated with the use of indicator organisms for this purpose. This approach is the main problem of protecting human and animal health [6, 7].

The results obtained by Hungarian researchers [8] indicate that the bacteriological properties of water can be a specific indicator of fecal pollution and organic contamination. That is why, according to the authors, microbiological contamination by fecal (pathogenic) bacteria is considered to be the most important issues of surface water quality, and especially in the Danube basin. The accumulation index of E. coli is one of the specific indicators of fecal contamination of the aquatic environment, and can be used for express diagnostics of the aquatic environment.

An interesting experience is the assessment of the quality of the surrounding aquatic environment of the Kingdom of the Netherlands [11]. The national program for monitoring surface water in this country, in addition to hydrochemical indicators, including also hydrobiological monitoring (including epidemiological). In a number of EU countries (most of which have their own

biological assessment of surface waters), bacteria, algae, invertebrate hydrobionts, phytoplankton are used as bioindicators [12, 13].

Researchers [9] have summarized existing methods of microbiological bioindication of the aquatic environment. It should be noted that the standards of the USSR in the field of protection of the hydrosphere operating in Ukraine do not take into account bacteriological indicators of water quality. This was, in all probability, the reason that data on the microbiological state of the upper part of the Danube basin (in the Ukrainian part: Tisza, Prut, Siret rivers) are practically absent.

Since water quality assessment is expensive [14], the development of rapid assessment methods remains an urgent problem. The introduction of this approach in many developed countries can reduce the cost of monitoring.

It should also be noted that the use of sanitary and microbiological indicators of the river network for assessing the status of protected sites, to date, is episodic [4, 10]. The question of assessing the sanitary and hygienic quality of surface waters of different purpose and status of functional zones of nature protection territories remains to be fully investigated.

The analysis of literature data confirms the need to use methods of sanitary-microbiological analysis of surface waters for assessing the ecological status of nature reserves and monitoring of aquatic ecosystems as a whole.

3. The aim and objectives of research

The aim of research is studying the epidemiological state of the surface waters of the river network of the Siret River (the upper part of the Danube basin, the Ukrainian territory) of various functional zones of the nature reserve object.

To achieve the aim, the following tasks are set:

– to determine the main sanitary and microbiological indicators (nitrite content, biological oxygen consumption, dissolved oxygen, coli-index, total microbial number), determine the quality of surface waters;

– to conduct a comparative analysis of sanitary and microbiological indicators, various in terms of the functional purpose of the zones, a nature reserve site;

– to study the possibility of using the proposed "biofilter", created on the basis of "Viya" artificial fibrous carrier and "paste" technical design, for assessing the quality of surface waters of various functional zones of a nature reserve site.

4. Materials and methods for research of surface water quality indicators

The watercourses have been studied: rivers Stebnyk, Sukhyi Strumok, Solonets entering the Ukrainian part of the Danube Basin. To assess the quality of the surface waters of the waterways of the Vyzhnytsia national nature park (NNP), Viya fibrous carrier (TU (995990)) was used. It made from a textured filament yarn (TU 6-06-C116-87, text 350) is described in [15].

Earlier [15, 16] it was established that a fibrous carrier of this type can be successfully used to construct "biofilters" for cleaning surface water. In particular, it was shown that the effectiveness of the "bioreactor" depends on the temperature, the concentration of microorganisms and that the accumulation of phytoplankton and heterotrophic microorganisms on carriers is most effective in the summer period (July-August). Using the approach described by the authors, a "biofilter" was mounted on the basis of special wooden structures – "paste", have long been used by local residents to saturate the streams with oxygen (**Fig. 1**). "Biofilter" is intended for adsorption on its surface of bacteria on hydrobionts.

The studies were carried out during the summer season 2016 and 2017. Sampling of water (23–25 °C) was carried out immediately before and after the "biofilters" from different functional zones of the waterways of the NNPs indicated in the scheme (**Fig. 2**), in accordance with the existing standard techniques. The choice of water sampling points was determined by their belonging to the functional zones of the protected object. The linking of the research region to the map of Europe is shown in **Fig. 3**.

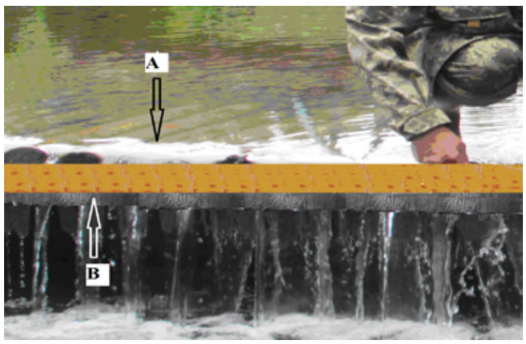

Fig. 1. When installing a cleaning structure using "Viya" fibrous carrier: A – a «paste» wooden structure; B – "Viya" fibrous carrier

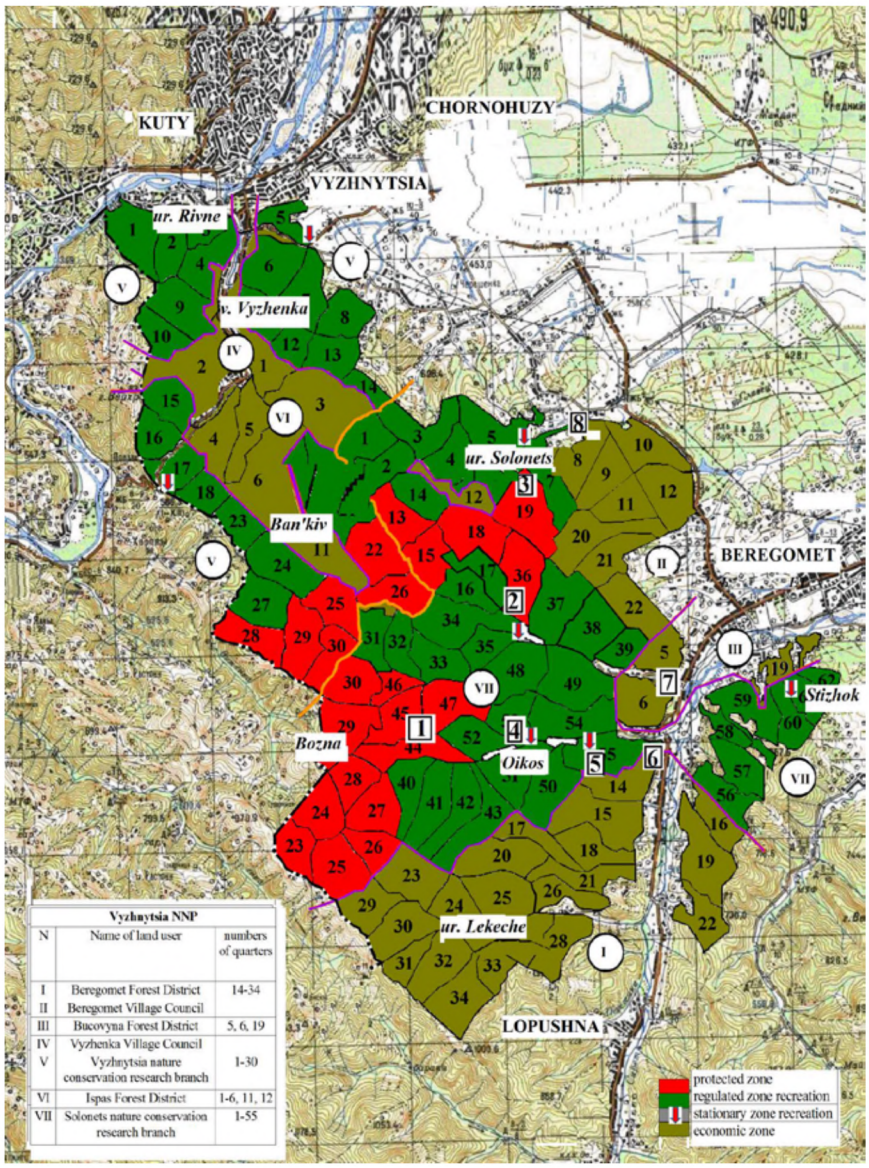

Fig. 2. Map-scheme of functional zoning of Vyzhnytsia national nature park: sampling points: 1 – the upper part of the Stebnik riverbed, 2 – the upper part of the Sukhyi Strumok canal, 3 – the upper part of the Slavets riverbed, 4 – "OIKOS" recreational zone, 5 – "Myslyvskyi budynok" recreational zone, 6 – the lower part of the Stebnik riverbed, 7 – the lower part of the Sukhyi Strumok canal, 8 – the middle part of the Solonets riverbed

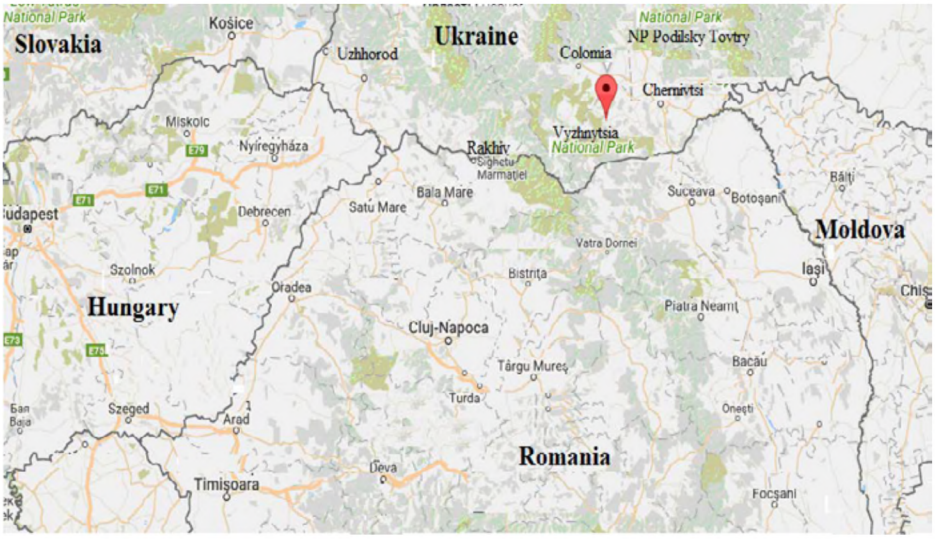

Fig. 3. Geographical location of the research area on the map of Europe

The investigated watercourses are a rather convenient model for studying the quality of surface waters of various functional zones of the nature reserve object, because they include three zones: a reserved zone in the upper part of the riverbed, a recreational zone in the middle of the riverbed and a recreational zone in the lower part.

The content of nitrates was determined in accordance with DSTU 40780-2001, biological oxygen consumption, dissolved oxygen, coli-index, total microbial number was determined by conventional methods in accordance with methodological guidelines [17].

The hydrobiological material (biocenosis of the periphyton overgrowth of the Viya" fibrous carrier) was selected in the second decade of August. The material was delivered to the laboratory in an open vessel. The infusoria, rotifers and turbolarium of the fouling biocenosis were studied in a living state under the Biola R-14 microscope, with an increase of 150–600 times. Other organisms (larvae of amphibiotic insects and nematodes) were fixed with 70° ethanol and determined their species affiliation. The species were determined according to determinants and scientific works [18, 19]. The statistical processing of the results was carried out using the computer program Excel.

5. Research results of surface water quality of various functional areas of the Vyzhnytsia NNP

The carried out researches have shown that there is an increase in the value of sanitary and microbiological indicators downstream along all these watercourses. Especially it concerned the increase in the amount of lactose-positive E. coli (E. coli) per 1 liter of water (coli-index). It should be noted that the E. coli is a sanitary indicator and indicates fecal contamination in this case of water bodies of the environment. Comparing the indices of coli-index in samples of river water of the protected zone and selected water samples in the economic zone, an increase in the coliform index was found to be 2 times on average (**Table 1**). At the same time, the total microbial number (CFU/ml) exceeded by 2–4 times the normative indicators adopted in the EU countries (Surface Water Directive: 75/440 EU) and amounted to 1500–1700 (for the protected zone), 2300–3500 (for the stationary zone recreation) and more than 5000 (for the economic zone).

Downstream of the watercourses, and the transition from the reserve to the economic zone, there is a growth in the water content of nitrates, an increase in the BOD index and a decrease in dissolved oxygen in the water. The obtained results indicate an increase in pollution of the river network by organic residues, in particular, they can be fecal connections of the economic zone where there are no existing treatment facilities.

The study of the qualitative species composition of organisms (periphyton) that inhabited the fibrous substrate showed bacteria, protozoa, fungi, algae, worms, crustaceans, bivalves and others to form fouling.

The data are presented in **Fig. 4** indicate that the "Viya" fibrous material is able to accumulate in considerable quantities the bacteria of the E. coli group (**Fig. 4**).

Table 1

The values of the main sanitary-microbiological indices of various functional zones of the Vyzhnytsia NNP*

Sampling points	BOD_{tot} (mg O_2/dm^3)	Dissolved oxygen (mg O_2/dm^3)	Coli-index (dm^3)	Microbial number (CFU/ml)	Nitrogen (mg N/dm^3)
		protected area			
1	1,8±0,10	7,5±0, 55	85±10,5	1500±85,4	0,01±0,001
2	2,3±0,12	7,1±0,50	80±8,0	1700±90,2	0,02±0,001
3	2,0±0,08	8,0±0, 70	82±12,2	1600±65,5	0,02±0,002
		zone of stationary recreation			
4	5,1±0,30	5,2±0, 60	90±11,5	2300±92,5	0,02±0,03
5	4,5±0,25	6,0±0,55	100±9,4	3500±150,4	0,05±0,004
		economic zone			
6	8,8±0,50	4,2±0, 20	120±15,3	5800±250,5	0,15±0,02
7	9,2±0,45	4,0±0,25	105±12,5	5200±280,3	0,10±0,01
8	9,5±0,40	3,8±0,20	110±14,6	5500±255,2	0,14±0,02

*Note: * – the data are reliable for p<0.05; the name of the sampling points corresponds to the notation of **Fig. 2***

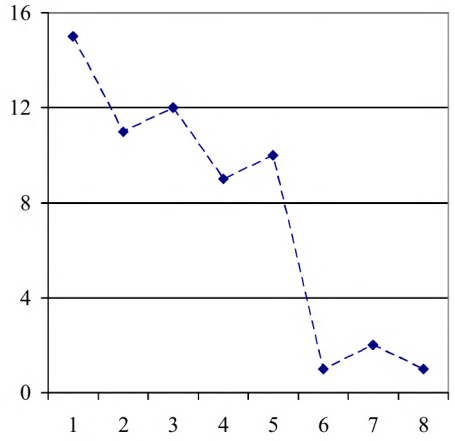

Fig. 4. The coefficient of accumulation of bacteria on fibrous carriers "Viya":
the name of the sampling points corresponds to the notation in **Fig. 2**;
coefficient of accumulation – the multiplicity of excess of content in comparison with
the surrounding water environment.

As the data in **Fig. 4** for sampling points 1, 2, 3, included in the NNP protected area is characterized by a high coefficient (from 11 to 14 times) of the accumulation of bacteria on fibrous carriers. In water samples taken in the zone of stationary recreation (points 4–5), this coefficient also has a sufficiently high index in the range of 9–10 units, that is, the carrier accumulates on its surface an order of more bacteria than the river water of the sampling points.

In the periphyton of the "Viya" fibrous carrier, 12 species and subspecies of hydrobionts were found. Most of these hydrobionts belong to amphibiotic insects (8 taxa). Rotifers and infusoria are represented by 2 taxa, respectively. Other systematic groups (ciliated worms, nematodes) were represented by one species, respectively. The species composition of the hydrobionts was supplemented with new species as the transition from the protected zone – 5 species (points 1, 2, 3) to the zone of stationary recreation – 7 species (points 4, 5) and the economic zone – 12 species (points 6, 7, 8).

6. Discussion of the research results of surface water quality of various functional zones of the Vyzhnytsia NNP

Comparison of the obtained results (**Table 1**) with the normative indicators adopted in the EU countries (Surface Water Directive: 75/440 EU) give grounds to assert that the surface waters of the river network of the NNP reserve and recreational zone refer to the permissible level of pollution. At the same time, the river water of the economic zone does not meet the sanitary and hygienic requirements and refers to a moderate and high pollution degree. The use of water of this pollution degree, without proper cleaning, can lead to the appearance of a number of diseases in the population.

The conducted studies showed (**Fig. 4**) that in the protected zone and the zone of NNP stationary recreation, the maximum values of the accumulation coefficient of bacteria on fibrous carriers take place. This coefficient characterizes the multiplicity of exceeding the amount of E. coli group on a synthetic carrier in comparison with the surrounding aqueous medium. It is known that the presence of E. coli group in water indicates fecal contamination and, accordingly, the possible contamination of water by pathogenic microorganisms of the intestinal group (typhoid, paratyphoid, dysentery, etc.) [8]. However, the detection and isolation of pathogens is complicated by the low concentration of bacteria in surface waters, the high financial costs and the length of detection technology [23]. The use of natural adsorbents is well-established in this regard [24]. In order to overcome this methodological obstacle, "biofilter" based on a synthetic material such as "Viya" was used. It was mounted on special «paste» wooden structures. The data in Fig. 3 indicate that the use of the "biofilter" makes it possible to concentrate the E. coli group for their identification and possible destruction.

It is also shown that as the transition to the economic zone and the increase in the amount of organic pollution of waterways, there is a sharp increase in the magnitude of the coli-index and the microbial number (**Table 1**). At the same time, the accumulation coefficient of E. coli group on the "biofilter" is characterized by minimal indicators. This can be explained by the saturation of the absorption surface by microorganisms, and also by their partial incorporation into nutrient chains.

One of the proofs of this statement is an increase in the species composition of hydrobionts on the "biofilters" of the watercourses of the economic zone. Thus, representatives of rotifers, copepods (and other lithophilic species) prevailed in water samples collected in the protected zone (upper part of the current). At the same time, in the water of the economic zone, with the growth of organic detritus, the species composition of the fouling is replenished at the expense of detritophages, incl. nematodes, oligochaetes, dreissena and others.

Thus, a specific "biofilter" in the form of an artificially created microecosystem is formed downstream on fibrous carriers. In this microecosystem fibrous carrier serves as a kind of "home" for microorganisms, plant and invertebrate animal organisms, they are able to accumulate, which is the basis for cleaning reservoirs. In addition, some bacteria, in all probability, become an element of the feeding chain and serves as food for invertebrate hydrobionts. Thus, water reservoirs are cleaned in two stages: due to adsorption on synthetic carriers in the first stage and trophic chains on the second stage.

In general, in the estuary part of the tributaries of the Siret basin there is a significant contamination of surface waters (III-IV quality class), which is consistent with the results of studies [25], which showed that it is the Siret and Prut rivers that are significant factors in the pollution of the lower part of the Danube riverbed.

7. Conclusions

1. It is shown that as the transition from the protected to the economic zone occurs, the nitrate content in the water increases, the BOD index increases and the dissolved oxygen in the water decreases for all the investigated watercourses.

2. "Viya" fibrous carrier is capable of effective accumulation on the adsorbing surface of microorganisms of bacteria of the group of Escherichia coli and invertebrate hydrobionts for watercourses with insignificant content of organic pollutants.

3. Significant differences in microbiological indices of watercourses of various functional zones of the protected object have been established. The total microbial number (CFU/ml) was 1500–1700 (for the protected zone), 2300–3500 (for the zone of stationary recreation) and more than 5000 (for the economic zone).

3. It is shown that during the growth of organic pollution of water bodies, especially in the economic zone of nature protection territories, a kind of "biofilters" – artificial microecosystems – are formed on fibrous carriers.

4. The obtained results supplement the idea of the sanitary and ecological state of the Danube basin in its upper part on the territory of Ukraine. Pollution of the upper part of the Siret river basin ultimately determines the level of pollution of the lower part of the Danube riverbed, and actually affects the state of the ecosystem of this international waterway of Europe.

References

[1] Sumampouw, O. J., Risjani, Y. (2014). Bacteria as Indicators of Environmental Pollution: Review. International Journal of Ecosystem, 4 (6), 251–258.

[2] Ashbolt, N. J. (2015). Microbial Contamination of Drinking Water and Human Health from Community Water Systems. Current Environmental Health Reports, 2 (1), 95–106. doi: 10.1007/s40572-014-0037-5

[3] Hermans, S. M., Buckley, H. L., Case, B. S., Curran-Cournane, F., Taylor, M., Lear, G. (2016). Bacteria as emerging indicators of soil condition. Applied and Environmental Microbiology, 83 (1). doi: 10.1128/aem.02826-16

[4] Pall, E., Niculae, M., Kiss, T., Sandru, C. D., Spinu, M. (2013). Human impact on the microbiological water quality of the rivers. Journal of Medical Microbiology, 62, 1635–1640. doi: 10.1099/jmm.0.055749-0

[5] Pekarova, P., Onderka, M., Pekar, J., Roncak, P., Miklanek, P. (2009). Prediction of Water Quality in the Danube River Under extreme Hydrological and Temperature Conditions. Journal of Hydrology and Hydromechanics, 57 (1), 3–15. doi: 10.2478/v10098-009-0001-5

[6] Pandey, P. K., Kass, P. H., Soupir, M. L., Biswas, S., Singh, V. P. (2014). Contamination of water resources by pathogenic bacteria. AMB Express, 4 (1), 51. doi: 10.1186/s13568-014-0051-x

[7] Pandey, P. K., Soupir, M. L. (2013). Assessing the Impacts ofE. coliLaden Streambed Sediment onE. coliLoads over a Range of Flows and Sediment Characteristics. JAWRA Journal of the American Water Resources Association, 49 (6), 1261–1269. doi: 10.1111/jawr.12079

[8] Bayoumi Hamuda, H. E. A. F., Patko, I. (2012). Ecological monitoring of Danube water quality in Budapest region. American Journal of Environmental Sciences, 8 (3), 202–211. doi: 10.3844/ajessp.2012.202.211

[9] Ryl's'kyi, O. F., Masikevych, Yu. G. (2012). Mikrobiolohichna bioindykatsiyi dovkillya zabrudnenoho vazhkymy metalamy ta inshymy ksenobiotykamy. Visnyk Zaporiz'koho natsional'noho universytetu, 3, 139–147.

[10] Mudrak, O. V. (2012). Zbalansovanyy rozvytok ekomerezhi Podillya: stan, problemy, perspektyvy. Vinnytsya, 914.

[11] Schets, F. M., van Wijnen, J. H., Schijven, J. F., Schoon, H., de Roda Husman, A. M. (2008). Monitoring of Waterborne Pathogens in Surface Waters in Amsterdam, The Netherlands, and the Potential Health Risk Associated with Exposure to Cryptosporidium and Giardia in These Waters. Applied and Environmental Microbiology, 74 (7), 2069–2078. doi: 10.1128/aem.01609-07

[12] Farcas, A. N., Curtean-Banaduc, A., Kifor, C. V. (2013). Ecological assessment as a first step in the evaluation of ecosystem services provided by lotic ecosystems. Management of Sustainable Development, 5 (2), 9–12. doi: 10.2478/msd-2013-0009

[13] Azzoni, R. (2015). Il controllo della qualita delle acque del fiume Adda mediante un metodo di analisi biocenotica. Boll. chim. Unione ital. lab. Prov., 31 (6), 293–305.

[14] Klochenko, P., Shevchenko, T., Barinova, S., Tarashchuk, O. (2014). Assessment of the ecological state of the Kiev Reservoir by the bioindication method. Oceanological and Hydrobiological Studies, 43 (3), 228–236. doi: 10.2478/s13545-014-0137-8

[15] Gvozdyak, P. I. (2003). Za pryncypom biokonveyera. Biotexnologiya oxorony dovkillya. Visnyk NAN Ukrayiny, 3, 29–36.

[16] Masikevych, A., Masikevych, Yu., Myslytsky, V., Burdeniuk, I. (2016). Valuation hydroecological and sanitary-hygienic condition of the river network of Pokutsko-Bukovinisn Carpathians policy. Water Security. Mykolaiv: PMBSNU, Bristol: UWE, 308.

[17] Sanitarno-virusolohichnyy kontrol' vodnykh ob»yektiv: metod. vkazivky MV 10.2.1-145-2007. Pro zatverdzhennya metodychnykh vkazivok «Sanitarno-virusolohichnyy kontrol' vodnykh ob»yektiv» (2007). Ministerstvo okhorony zdorovia Ukrayiny, No. 284. Dodatok 1. Available at: http://www.moz.gov.ua/docfiles/8203_dodatok.rar Last accessed: 18. 01.2018

[18] Berger, H. (2008). Monograph of the Amphisiellidae and Trachelostylidae (Ciliophora, Hypotricha). Salzburg, 736. doi: 10.1007/978-1-4020-8917-6

[19] Kutikova, L. A., Starobogatov, Ya. I. (1977). Opredelitel presnovodnykh bespozvonochnykh Evropeyskoy chasti SSSR (plankton i bentos). Leningrad, 511.

[20] Barinova, S. (2017). On the Classification of Water Quality from an Ecological Point of View. International Journal of Environmental Sciences & Natural Resources, 2 (2). doi: 10.19080/ijesnr.2017.02.555581

[21] Odume, O. N.; Tutu, H. (Ed.) (2017). Ecosystem Approach to Managing Water Quality. Water Quality. doi: 10.5772/65707

[22] Directive 2000/60/EC of the European Parliament and of the Council of 23 October 2000 establishing a framework for Community action in the field of water policy (2000). Official Journal of the European Communities, 43, 72.

[23] Thompson, D. E., Rajal, V. B., De Batz, S., Wuertz, S. (2006). Detection of Salmonella spp. in water using magnetic capture hybridization combined with PCR or real-time PCR. Journal of Water and Health, 4, 67–75.

[24] Malyovanyi, M., Sakalova, G., Chornomaz, N., Nahurskyi, O. (2013). Some kinetic regularities of intracellular substance extracting. Chemistry and chemical technology, 7 (3), 198–208.

[25] Kirschner, A. K. T., Kavka, G. G., Velimirov, B., Mach, R. L., Sommer, R., Farnleitner, A. H. (2009). Microbiological water quality along the Danube River: Integrating data from two whole-river surveys and a transnational monitoring network. Water Research, 43 (15), 3673–3684. doi: 10.1016/j.watres.2009.05.034

Original Research Article: full paper

(2018), «EUREKA: Physics and Engineering»
Number 2

DEVELOPMENT OF THE MANAGEMENT SYSTEM OF ORDERS OF THE COMPANIES AND ORGANIZATION OF THE STAFF WORK

Svitlana Popereshnyak
Department of Software Systems and Technologies
Taras Shevchenko National University of Kyiv
64/13 Volodymyrska str., Kyiv, Ukraine, 01601
spopereshnyak@gmail.com

Anastasia Vecherkovskaya
Department of Software Systems and Technologies
Taras Shevchenko National University of Kyiv
64/13 Volodymyrska str., Kyiv, Ukraine, 01601
vecherkovskaia90@gmail.com

Abstract

In the course of the study, the activity of Ukrainian enterprises was analyzed. It was revealed that the main aspects that require increased attention, regardless of the industry, are staff management and order management.

The activity of any enterprise consists of fulfilling orders and, as a consequence, satisfying customers.

It is proposed to develop an automated system that will enable to keep records of orders, namely: the time of order receipt, the number of products, the urgency, the necessary material and time resources, the priority of the order, the executor, the predicted and actual time of the order. This system will help to organize the work of staff, namely: to optimize the working hours of employees due to the dynamic scheduling of the task list; to introduce responsibility for an order that is tied to a specific employee, to keep records of shifts and working hours, automatically form a payroll with due account of worked shifts/hours. The work designed an automated system for managing orders and staff at middle-class enterprises. The requirements for this system are defined and two types of architecture are proposed. For a better understanding of the design phase of the automated system, a class diagram, activity diagram and interaction diagrams are presented.

In the process of research, the end product was created with a user-friendly and intuitive user interface that maximally satisfies all the requirements that have been defined for this system. For today the system works in a test mode at the enterprise of Ukraine. The introduction of the system to the filter element manufacturing company allowed to improve the interaction with customers by 40 % due to faster fulfillment of orders; 80 % facilitate the work of managers to track and control the execution of orders; and also, by 20 % increase the efficiency of the staff department. What on the whole positively affected the work of the enterprise as a whole.

Keywords: automated system, order management, staff work organization, system architecture, UML diagrams.

DOI: 10.21303/2461-4262.2018.00588

1. Introduction

The success of the production and economic activities of any enterprise or organization is necessarily connected and directly depends on the leader's leadership qualities and its ability to organize the production process and all staff. It should be managed in such way that everything that needs to be done to achieve corporate goals has been carried out in a timely, qualitative and rational manner in terms of resources spent on it.

In modern conditions, the need to use the latest technologies in staff management and organization of work at the enterprise is becoming increasingly urgent. They are designed to optimize order management, improve the quality of the final product, improve methods and production technology and optimize the use of temporary resources. The use of the latest information technologies in this field makes it possible:

– significantly improve the distribution of time in the company;
– increase the number of tasks on which the team works simultaneously;
– clearly define the main and secondary tasks;
– accelerate the exchange of information and data in the company;

– quickly obtain statistical data;

– significantly reduce the time and financial costs associated with the organization of staff time.

The success of any business depends, first of all, on the qualification of the staff of the enterprise, its ability and desire to work productively. An important role in optimizing the management of enterprise employees belongs to automated human resources management systems (the so-called Human Resource Systems) [1]. Staff is the long-term factor of competitiveness and survival of the enterprise.

It is also difficult to ignore one of the most important components of a successful operation of an enterprise ensuring effective order management and as a result a satisfied customer.

Order management is an area of activity during which clear goals are defined and achieved when balancing the amount of work, resources, time, quality, aimed at achieving a certain result under the specified constraints. Order management application of knowledge, skills, tools and methods for planning and implementing actions aimed at achieving the goal in the framework of specified requirements. When managing orders, the following steps can be distinguished:

– work planning;

– risk assessment;

– assessment of the necessary resources;

– work organization;

– attracting human and material resources;

– assigning tasks;

– leadership;

– control over the progress of implementation (to control the effectiveness of the execution of orders, the method of utilized volume is used);

– progress report;

– analysis of the results based on the findings.

In this paper, the aim was set, in detail, to investigate the process of developing such an automated system that would help the enterprise's employees organize their work and the work of subordinates in such way that the short-term and long-term aims set for the company were achieved in the shortest possible time and with the minimum spent on it resources. In other words, to help the company's staff in practice follow the principles of time management of technology for rational planning and distribution of working time, taking into account the fulfillment of orders in a given timeframe and priorities, with the aim of releasing opportunities [2, 3].

2. Literature review

The issue of automation of staff management is widely studied both in Ukraine and around the world [4–17]. So, in works [4–6] the main attention is paid to the necessity of automation of the enterprise by introducing the accounting of employees' working hours. Issues of visualization of risks, taking into account the multilevel management at the enterprise, are devoted to works [7, 8]. The main systems that require automation are customer service systems for working with customers in various industries, some aspects of which are discussed in [9]. In works [10, 11] attention is paid to the issues of architecture and the design of automated enterprise management systems.

Most of the work on staff management is devoted to the differences between executives and executors and the use of this understanding for effective work [12], as well as a lot of literature on staff motivation [13, 14]. Today's management of an enterprise requires a number of capabilities, which include finding quick solutions for the shortage of employees with a field of certain qualities. In work [15] it is proposed to apply the selected schedules to facilitate mobile staff management.

An important matter is the relationship between the involvement of staff and the joint creation of the product. In [16], various types of products and categories of staff, as well as the relationships between them, are considered. And in [17] a hierarchical control system with several agents is proposed.

However, the task of managing orders, with reference to a particular employee, and organizing their work is not adequately described in the literature and requires additional research.

Automation of order management processes and staff should help to organize the enterprise correctly with a minimum amount of initial investment and maximum benefit from the implementation of this system.

The expected benefits from the introduction of an automated order management system and staff can be the following:

– increase of the enterprise efficiency;
– timeliness of making managerial decisions;
– rational allocation of time between orders and tasks;
– effective staff management;
– increase the efficiency of staff work;
– effective control over the performance of tasks;
– effective management of enterprise funds;
– control over the performance of the enterprise and the like.

For many enterprises, it is essential to gradually introduce an information system with the possibility of first-priority automation of the most problematic areas. It is possible to implement modules that will allow for the phased introduction of the information system. For example, it is possible first automate the activities of individual units, then connect to the accounting system, which will create conditions for monitoring the movement of resources. After that, it is possible to put in operation the budgeting system, automate the formation and control of the order list, as well as other elements of the information system.

Usually, order management automation systems contain the following structural elements:

– funds for calendar-and-network planning (CNP-systems);
– means for solving individual problems (the formation of the list of orders, the prioritization of orders, the appointment of the responsible executor, the deadline for the completion of the order, risk analysis, contract management, time, budget);
– means for organizing communications between contractors;
– means for automatic payroll, depending on the number of shifts hours worked and/or the amount of work.

As a result of work to achieve the aforementioned goal, the software product “OrderBook” was created, which provides ample opportunities for users to effectively manage orders, staff and their time. This system is focused mainly on small and medium-sized businesses (the number of workers is up to 200 people), which can be used by staff of enterprises of any industry, whole companies or individual departments.

Let’s consider the requirements that were put before the system:

1. Allow the user to log in to the system under his account.
2. Ability to work with the system on PCs, tablets and telephones.
3. Create and manage orders, determine the order manager/executor, the start date for the work on it, and the end date.
4. Create tasks related to orders.
5. Create and manage tasks, define their performers, status and priority, start and end dates for the task.
6. Manage your own calendar, create entries for important meetings and events.
7. View the list of staff contacts of the company.
8. Place ads on the corporate virtual bulletin board.
9. View and publish important documents, templates and other company files to your computer.

3. Materials and Methods

To implement the functionality stated in the previous section, the automated system was divided into several divisions, each of which would perform a specific set of tasks for the user’s needs.

The system has the following sections:

1) Personal calendar;
2) Order book;

3) Task log;
4) Ad Log;
5) Contact log;
6) Company files.

When implementing the order management system and staff work, it is important to ensure the financial feasibility of its use. It is important that the cost of development does not exceed the amount of possible damage that will be incurred in the case of the development and operation of this system without an information security system.

3. 1. Physical structure of the system

Let's consider two possible options for deploying the OrderBook system in the company:

1) Closed system for internal use in the local network (**Fig. 1**).

Each company will have its own local server All data on this company is stored on it. Users of the system will connect to the server through the local network. Connection is possible both with the help of cable connection, and Wi-Fi. The system will work stably locally, without requiring connections over the Internet.

In this structure it is very easy to update the system. Since all data is on the server, the user automatically receives all the innovations with minimal interruptions in the work.

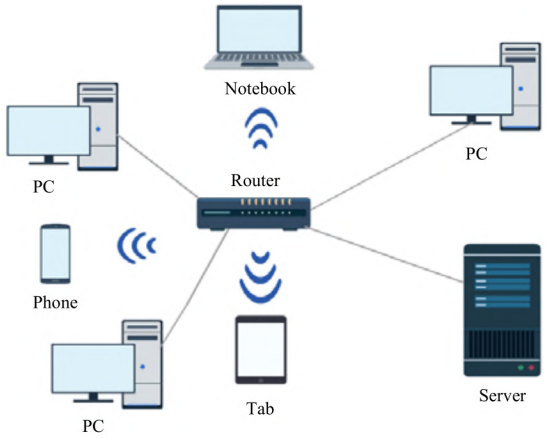

Fig. 1. The structure of a closed system for internal use in the local network

This approach is very convenient for software engineers who support the system and saves their time.

2) Open system with the ability to access it from the Internet (**Fig. 2**).

In this structure, the server is hosted on a virtual hosting. Users of the system will connect to the server over a wide area network. Connection is possible, both with the help of cable connection, and Wi-Fi.

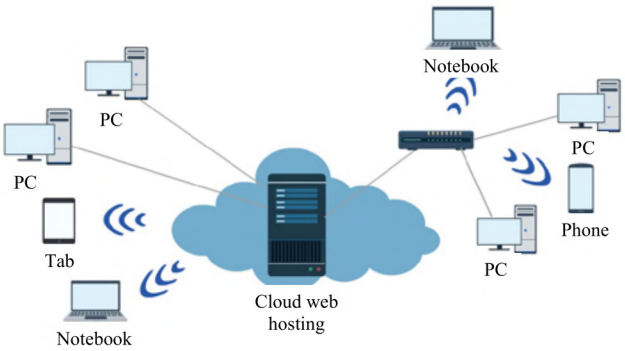

Fig. 2. The structure of an open system with the possibility of access to it from the Internet

The advantage of this structure is that it can be used in case the organization of the local network is problematic or in some way restricts the use of the system. The update is also very convenient for both users and technical staff, supports the company's software.

3. 2. System architecture

The system architecture is a structural diagram of the components of the system interacting with each other through interfaces. Components can consist of a sequence of smaller components and interfaces. The system architecture is constructed by defining the system's objectives, its input and output data, decomposing the system into subsystems, components or modules and developing its general structure.

When building the architecture of the order management system and staff work, the Model-View-Controller (MVC) architectural template was used (**Fig. 3**).

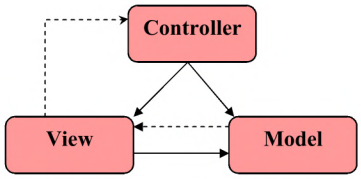

Fig. 3. Diagram of interaction between the components of the MVC template

4. Experimental procedures

4. 1. Development of the activity diagram

So, the activity diagram (in UML) is a visual representation of the graph of activities. The graph of activities is a kind of graph of states of a finite automaton which vertices are certain actions, and transitions occur after completion of actions.

Action is the fundamental unit of behavior definition in the specification. The activity specification (at higher compatibility levels) can allow the execution of several (logical) flows, and the existence of synchronization mechanisms to ensure that the actions are performed in the correct order.

For the OrderBook system, an activity diagram is created that depicts the process of working with orders in the system (**Fig. 4**).

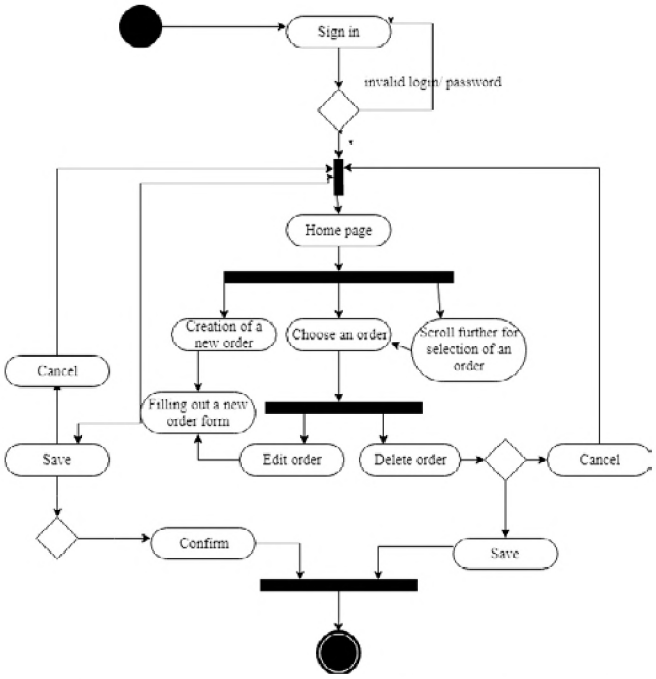

Fig. 4. Diagram of activity according to the precedent "Process of work with orders in the system"

The user must log in by entering a username and password. Further from the main page, which has a bookmark "orders" it has the ability to view existing ones, create new ones, edit and delete orders.

4. 2. Development of the interaction diagram

Most often at the specification stage of requirements it is necessary to show not only the algorithm of actions or change of the state of the object, but also the exchange of messages between individual objects of the system. This problem is solved by the interaction diagram.

The interaction diagram is one of the models describing the behavior of interacting groups of objects in the UML, describing the behavior only within one use case.

The interaction diagram is intended for modeling relationships between objects (roles, classes, components) of the system within a single use case.

This type of diagram reflects the following aspects of the projected system:

– exchange of messages between objects (including in the framework of messaging with third-party systems);

– constraints imposed on the interaction of objects;

– events that initiate the interaction of objects.

Unlike the activity diagram, it shows only the sequence (algorithm) of the system operation, the interaction diagrams emphasize the developers' attention to messages initiating the call of certain operations of the object (class) or is the result of the operation.

Two main types of interaction diagrams are divided:

– sequence diagram;

– collaboration diagram.

Extending the notation of interaction diagrams in UML allows analysts at a more detailed level to work out the requirements as much as possible to replace activity diagrams with interaction diagrams.

Thus, the main target audience for the interaction diagram will be the development team. For the customer, this kind of diagrams will be of interest only in the framework of modeling the interaction between the projected IS and extraneous Systems operating on the Customer's side.

4. 2. 1. Development of a sequence diagram

The sequence diagram illustrates the order in which objects interact with time operations and reflects the objects and classes involved in the scenario, next to the message chains exchanged between objects in the execution of the functions specified in the scenario.

According to the OrderBook project, a sequence diagram was created with the precedent "Creation of a new order" (**Fig. 5**).

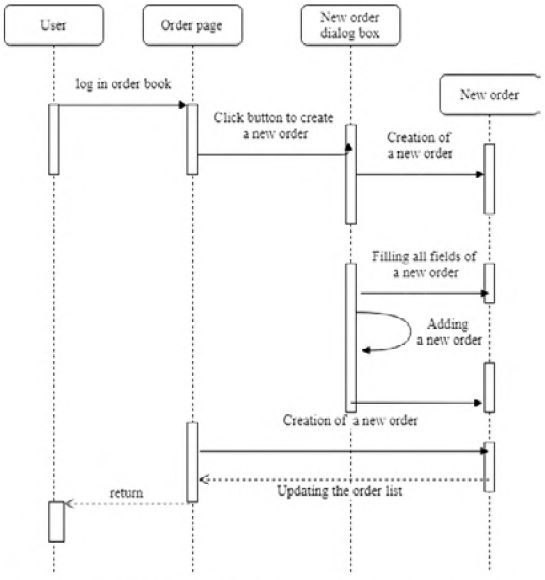

Fig. 5. Sequence diagram behind the use case "Creation of a new order"

Each object in the sequence diagram is associated with a timestamp, denoted by a dashed line segment, and the messages exchanged between the two objects are represented by an arrow connecting the source object to the receiver object.

4. 2. 2. Development of a collaboration diagram

The collaboration diagram represents an alternative way of describing the scenario. The collaboration concept is used to denote the set of objects interacting with a specific purpose in the general context of the modeled system. The goal of the collaboration itself is specification of the specific features of the implementation of the individual most significant operations in the system. Collaboration determines the structure of the system's behavior in terms of the interaction of participants in this collaboration.

According to the OrderBook project, a cooperative diagram was created according to the precedent "Creation of a new job" (**Fig. 6**).

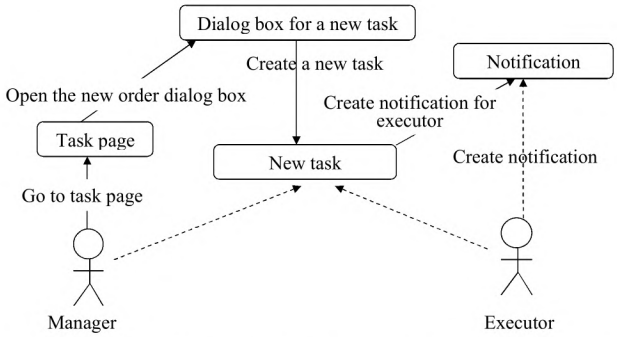

Fig. 6. The collaboration diagram after the precedent "Creation of a new job"

When constructing a sequence diagram, the emphasis is on the temporal aspect, while in constructing the collaboration diagram, the static interaction of the objects of the system is considered.

5. Results

As a result of the work, a system for managing orders and organizing the staff work is created.

Working with the OrderBook system starts with the main page, which welcomes the user and plays the role of the business card of the system, providing an accurate description of the main functionality of the system.

The OrderBook system allows to manage users of the system, for which the Colleagues page was created. For the administrator, it allows to add a new user, edit it and delete it from the system, for a regular user, it allows to view the list of your colleagues in a convenient format.

In order for a new user to start working with the system, it is necessary that his account be created by the administrator. To do this, the administrator must go to the main page and log in by entering a username and password.

It is important to note that the new user's page addition page has validation of the data entered by the administrator, which was implemented using the jQuery Validation plug-in. For example, if not all required fields are entered, or data that has been entered does not meet certain requirements, the system does not accept such information and issues an error message. If all fields are entered correctly, a new user is created on the system and displayed in the general list, which all other users see.

6. Discussion

For today the system works in a test mode at the enterprise of Ukraine. The introduction of the system into the enterprise for the manufacture of filter elements allowed:

– improve interaction with customers by 40 % due to faster execution of orders;

– 80 % facilitate the work of managers to track and control the execution of orders;

– increase the efficiency of the HR department by 20 %.

The implementation of the OrderBook system at Unifilter, which specializes in the development and production of filter elements, has had a positive impact on the work of the enterprise as a whole. The peculiarity of the work of this enterprise is in servicing a large number of customers. Orders consist of the main parameters, including: the scope of the filter element, the filter diameter (internal and external), the length, the number of filter layers, the filter requirements for the due date. These are the main parameters that are necessary for determining the manufacturing process of filter elements [18–20]. In the process of work, each order is assigned the code, priority, time for execution, estimated time of order execution and the responsible executor. These data make it possible to trace the status of the order, the number of produced filter elements, to form a provisional value and, in the case of rejection, to analyze on which shift and by whom of the employees the order was executed.

For the correct operation of this automated system requires the correct introduction of information by managers and timely filling out a report on the manufactured filter elements by employees. Employees must include the order code and the number of manufactured items. To do this, it is necessary to provide workers with access to a portable device, such as a tablet, in which they will see the task that must be performed and note what is done for the shift and/or hour.

The introduction of this system requires additional technical resources, as a rule, these are computers for managers and a tablet in the working area for production workers. One of the constraints faced by this company is the human factor: reluctance to perform additional actions by shop workers who produce filter elements and time for their training on the use of this system.

In general, the system is quite universal and does not depend on the field of application. It can be widely used in enterprises that work with customers, fulfill orders and have the need to bind the order to the date of implementation and to the responsible executor.

7. Conclusions

In recent decades, changes in the external environment of the functioning of enterprises, institutions and organizations have been taking place at an extremely high pace. Today, effective management of orders and staff is impossible without the use of modern software, as the size of companies, employees, orders, volumes of information grow.

In the course of the work the following is accomplished.

First, the automation of order management and staff work at enterprises in Ukraine and in the world is analyzed, and the benefits and advantages of information systems for order management and staff work are found.

Secondly, an automated system for order management and staff work at middle-class enterprises is designed. The requirements for this system are determined and the architecture is built.

Thirdly, the system for managing orders and organization of staff work is designed in detail: class diagram, activity diagram and interaction diagrams are developed.

Fourthly, a user's instruction is developed and some screen displays for demonstrating work with the system are provided.

In the process of work, the end product is created with a user-friendly and intuitive user interface that maximally satisfies all the requirements that have been defined for this system.

References

[1] Beardwell, I., Holden, L., Claydon, T. (Eds.) (2004). Human Resource Management. Harlow: Prentice Hall.

[2] Popereshnyak, S. (2016). Combination of methods of time management in dynamic task scheduler. Science and practice: Collection of scientific articles. Melbourne: Thorpe-Bowker, 85–90.

[3] Popereshnyak, S. (2010). Informatsiini systemy kholdynhovykh orhanizatsii ta systema upravlinnia vzaiemovidnosynamy z kliientamyurl. Naukovi pratsi Don NTU. Seriia: Ekonomichna, 38-3, 115–125. Available at: http://ea.dgtu.donetsk.ua:8080/jspui/bitstream/123456789/18533/1/115.pdf

[4] Popereshnyak, S. (2016). Project control system and organization of work staff. Economics, management, law: socio-economic aspects of development, 217–224.

[5] Wang, C., Zhang, T., Ma F. (2015). A multi-agent based hierarchical control system for DERs management in islanded micro-grid. 2015 Chinese Automation Congress (CAC). doi: 10.1109/cac.2015.7382713

[6] Louis, J.-N., Calo, A., Leiviska, K., Pongracz, E. (2015). Environmental Impacts and Benefits of Smart Home Automation: Life Cycle Assessment of Home Energy Management System. IFAC-PapersOnLine, 48 (1), 880–885. doi: 10.1016/j.ifacol.2015.05.158

[7] Sarshar, S., Haugen, S. (2018). Visualizing risk related information for work orders through the planning process of maintenance activities. Safety Science, 101, 144–154. doi: 10.1016/j.ssci.2017.09.001

[8] Paraforos, D. S., Vassiliadis, V., Kortenbruck, D., Stamkopoulos, K., Ziogas, V., Sapounas, A. A., Griepentrog, H. W. (2017). Multi-level automation of farm management information systems. Computers and Electronics in Agriculture, 142, 504–514. doi: 10.1016/j.compag.2017.11.022

[9] Johansson, C., Larsson, T., Tatipala, S. (2017). Product-Service Systems for Functional Offering of Automotive Fixtures: Using Design Automation as Enabler. Procedia CIRP, 64, 411–416. doi: 10.1016/j.procir.2017.03.006

[10] Zhang, J., Li, X., Xing, T., Tang, X. (2017). Study on Architecture and Application Technology of Ubi-bus Network of Building Automation System. Procedia Engineering, 205, 1286–1293. doi: 10.1016/j.proeng.2017.10.382

[11] Nayak, R., Padhye, R. (2018). Introduction to automation in garment manufacturing. Automation in Garment Manufacturing, 1–27. doi: 10.1016/b978-0-08-101211-6.00001-x

[12] Dutton, B. G. (1973). Staff management and staff participation. Aslib Proceedings, 25 (3), 111–125. doi: 10.1108/eb050398

[13] Forsyth, P. (2006). Motivating your staff [positive staff motivation]. Engineering Management, 16 (1), 22–23. doi: 10.1049/em:20060104

[14] Pearce, C. (2007). Ten steps to staff motivation. Nursing Management, 13 (9), 21–21. doi: 10.7748/nm2007.02.13.9.21.c4334

[15] Encheva, S. (2017). Towards mobile staff members management. AIP Conference Proceedings. doi: 10.1063/1.4992765

[16] Merrilees, B., Miller, D., Yakimova, R. (2017). The role of staff engagement in facilitating staff-led value co-creation. Journal of Service Management, 28 (2), 250–264. doi: 10.1108/josm-10-2015-0326

[17] Diakaki, C., Papageorgiou, M., Papamichail, I., Nikolos, I. (2015). Overview and analysis of Vehicle Automation and Communication Systems from a motorway traffic management perspective. Transportation Research Part A: Policy and Practice, 75, 147–165. doi: 10.1016/j.tra.2015.03.015

[18] Vecherkovska, A., Popereshniak, S. (2018). Avtomatyzatsiia vyrobnytstva elementiv z porystoho polipropilenu metodom pnevmoekstruzii. Visnyk natsionalnoho tekhnichnoho universytetu «KhPI». Seriia: Mekhaniko-tekhnolohichni systemy ta kompleksy, 44 (1266), 116–121. Available at: http://mtsc.khpi.edu.ua/article/view/124899

[19] Vecherkovska, A., Popereshniak, S. (2017). Osoblyvosti pobudovy avtomatyzovanoi systemy vyhotovlennia filtruiuchykh elementiv. Vcheni zapysky Tavriiskoho natsionalnoho universytetu imeni V. I. Vernadskoho. Seriia: Tekhnichni nauky, 12.

[20] Vecherkovskaya, A., Popereshnyak, S. (2018). Software for calculation of productivity of polypropylene filtering element in dependence from its application. Technology audit and production reserves, (1 (3 (39)), 14–23. doi: 10.15587/2312-8372.2018.124288

Original Research Article: full paper

(2018), «EUREKA: Physics and Engineering»
Number 2

APPLICATION OF ROTATED FILM APPARATUS AT PRODUCTION OF MULTI-COMPONENT FRUIT PASTS

Oleksandr Cherevko
Department of Processes, Devices and Automation of Food Production
Kharkiv State University of Food Technology and Trade
333 Klochkivska str., Kharkiv, Ukraine, 61051

Valeriy Mykhaylov
Department of Processes, Devices and Automation of Food Production
Kharkiv State University of Food Technology and Trade
333 Klochkivska str., Kharkiv, Ukraine, 61051
v.mykhailov@hduht.edu.ua

Aleksey Zagorulko
Department of Processes, Devices and Automation of Food Production
Kharkiv State University of Food Technology and Trade
333 Klochkivska str., Kharkiv, Ukraine, 61051
zagorulko@hduht.edu.ua

Andrii Zahorulko
Department of Processes, Devices and Automation of Food Production
Kharkiv State University of Food Technology and Trade
333 Klochkivska str., Kharkiv, Ukraine, 61051
zagorulkoAN@hduht.edu.ua

Abstract

The aim of the study is to probate the improved rotated film apparatus (RFA) at producing high-quality multi-component fruit pasts. The construction of the improved RFA with an innovative solution as to the system of heating its working chamber at the expanse of using a radiating heater – FFREhRT is developed. The designed construction is resource-effective and allows to concentrate fruit puree by using saving non-inertial thermal regimes (50...60 °C) with processing duration 0,65...0,8 min to content 25...30 % of RM. At the researches there was realized the probation of the improved RFA at concentrating offered multi-component fruit purees, based on apple, cranberry and haw.

The high quality of obtained multi-component fruit pasts was confirmed as a result of studying their structural-mechanical and color characteristics. Structural-mechanical parameters of studied fruit purees allowed to determine the influence of each component of the composition on the dispersed stability of an obtained structure of puree. It was established that the best disperse stable structure is inherent to the composition with percent content of apples, cranberries and haws as 60÷30÷10 with the mean radius of microcapillaries $\bar{r} = 1{,}51$ nm.

As a result of concentrating fruit purees, there were determined their color characteristics by CIELab system. And the comparisons of the studied sample before and after concentration indicate their unessential change. Thus, for the recipe composition with best organoleptic indices: apple, cranberry, haw in ratio 60÷30÷10, the brightness index for puree is: T=37,8 %, and for the concentrated past – T=36,4 % respectively. All obtained compositions are characterized by the red-orange color that totally confirms preservation of their physical-chemical characteristics at thermal processing.

The improved RFA construction may be implemented at enterprises of tinned production for processing and getting high-quality fruit pasts for providing needs of food industry of the country.

Keywords: rotated film apparatus, fruit puree and pasts, structural-mechanical properties, color.

DOI: 10.21303/2461-4262.2018.00599

1. Introduction

Everyday growth of the demand for natural food products conditions the necessity in implementing innovative solutions for their production [1]. It especially concerns the equipment and

processing methods of natural fruit raw materials, because the existent technical equipment in most cases is characterized by certain defects, among which: metal-consumption, difficulties for maintenance, automation and other designing shortcomings [2]. And for providing artificial enrichment of multi-component mass with fruit raw materials with the essential content of biologically active substances (BAS) and acquiring treating-prophylactic properties by them, it is necessary to improve methods of its processing [3]. Just that is why, there is offered one of innovative solutions of existent constructive-technological tasks of tinned food industry of Ukraine.

The aim of the work is to conduct the probation study of the improved rotated film apparatus (RFA) at producing high-quality multi-component fruit pasts with offering the recipe ratio at mixing fruit raw materials that provides the artificial increase of BAS content and treating-prophylactic properties. And also the methods of determining the change of structural-mechanical features of obtained products depending on a mass share of each component and confirming conservation of quality characteristics of obtained products at the expanse of using methods of analyzing their color.

The offered innovative solutions allow to raise technical parameters of the equipment for concentrating natural raw materials using a suitable temperature regime and widening the assortment of high-quality multi-component fruit semi-products.

2. Materials and Methods

Experimental studies were conducted in the laboratories of Kharkiv state university of food and trade (Ukraine).

2. 1. Experimental device of the rotated film apparatus

The studies of concentrating multi-component fruit puree were realized on the improved RFA that differs from a prototype by using a flexible film resisting electric heater of the radiating type (FFREhRT) [4]. The general look of the experimental device is presented on **Fig. 1**.

Fig. 1. Look of the improved experimental device RFA

The construction of the improved scheme of the experimental device RFA (**Fig. 2**) consists of the following elements: turning of the rotor drive is realized by electric motor 1 using wedge-pass transmission 2. The number of rotor turns is determined by tachometer 3. The product from chamber 4 is transmitted in the working chamber of RFA by pinion pump 5.

The external surface of chamber with product 4 is enveloped by FFREhRT 7 of heating the output product. Chamber 4 contains blade mixer 8 for mixing puree-like mass. Regulation of the heating temperature and turning the speed of the mixer is realized by measuring block 9 with the insert electric motor and potentiometer CSP -2. Regulation of product consumption is provided by bypass line with valves 10.

Consumption of the final product and condensate is measured by flow meter 11. Secondary steam is condensed in tube condenser 12. Vacuum in the apparatus is created by the vacuum-pump and controlled by vacuum-meter 13.

The temperature of the apparatus wall, product in chamber 4, and temperature of the product on input and output of the working chamber are measured using chromel-copel thermocouples 14, combined with the potentiometer CSP-2, fixed in measuring block 9.

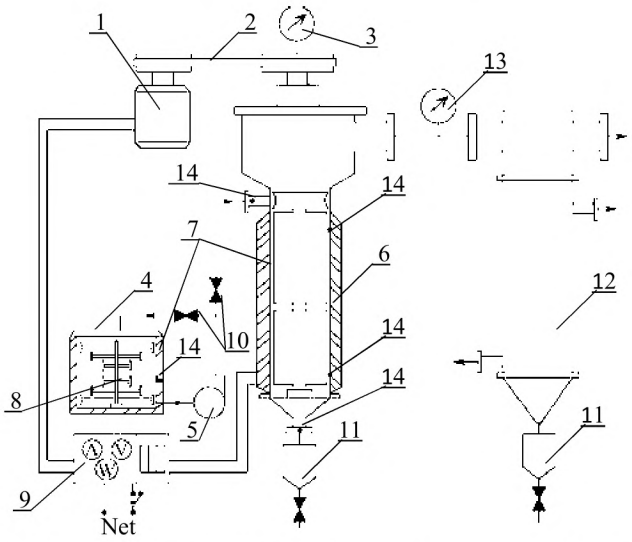

Fig. 2. The scheme of the experimental device for studying concentration processes that take place in RFA: 1 – electric motor; 2 – wedge-pass transmission; 3 – tachometer; 4 – chamber for the output; 5 – pinion pump; 6 – working chamber of RFA; 7 – flexible film resistant electric heater of radiating type (FFREhRT); 8 – blade mixer; 9 – measuring block C-50 with the fixed electric motor and potentiometer CSP -2; 10 – bypass line with valves; 11 – capacious consumer-meter; 12 – condenser; 13 – vacuum-meter; 14 – termocouples

The working surface of RFA is heated by FFREhRT, which external surface is enveloped by isolating material. The upper part of the apparatus body is spread and the separation space for the secondary thermocouple is created. The rotor with film-creating elements (blades) turns along the apparatus. The distribution ring that distributes the product that comes to the apparatus is fixed on the rotor shaft. The upper part of the cylinder contains a connecting pipe for conducting a product to the apparatus. The branch pipe for unloading a ready product is placed below the model [4].

For producing high-quality fruit semi-products taking into account their thermo-labile properties, there is offered to use the suitable temperature regime (50...60 °C) with the processing duration as 0,65...0,8 min for the content 25...30 % of RM. The offered perpetual apparatus is characterized by the low metal-consumption, transient thermal processing of a product and easy regulation. Just this fact provides maximal storage of food value of natural fruit raw materials.

2. 2. Materials, methods of studying compositions of multi-component fruit semi-products

At studying multi-component fruit semi-products, the main raw materials were chosen as apples (Antonyvka variety), cranberry (Hoves) and haw (Krymsky variety) (**Fig. 3**) with treating-prophylactic properties and also puree pasts on their base. Apples with the high content of a pectin substance that provides interaction with other components were used as the main share of multi-component semi-products. Wild cranberries have treating properties. Cranberries contain such important microelements as phosphorus, potassium, calcium, magnesium, iron, cobalt and iodine [5]. Berries contain vitamins C and P, and also B_1 and B_2 [5]. They also contain much ursolic acid, which structure and genetics are familiar to many physiologically important hormones. They are used at catarrhal and infectious diseases, hypertonic ones and so on [5].

For preparing multi-component fruit semi-products, there is offered the recipe ratio of components (apple, cranberry, haw) in compositions:

a) 60÷30÷10;

b) 65÷25÷10;

c) 55÷40÷5.

Haw fruits contain antioxidants, so they favor the blood circulation improvement, regulate heart muscle rates and help to clean vessels. Ursolic acid reveals cardio-stimulating action spread vessels. That is why berries are used at angina, hypertension, arrhythmia, neurosis and insomnia [5].

a *b* *c*

Fig. 3. Look of studied samples: *a* – apple; *b* – cranberry; *c* – haw

The total acidity was determined by the standard titrometric method by SS 26188-84, mass share of dry substances – by SS 28561-90 [6, 7].

According to the offered recipe ratio of fruit components in multi-component composition, there were determined their influences on the formation of structural-mechanical properties (strength) in obtained food masses.

As a result of the experimental studies, it was established, that multi-component fruit mass changes previous structural-mechanical properties at the expanse of redistributing moisture by bound forms. For determining the influence of each multicomponent mass on forming the structural-mechanical properties in obtained food masses at changes of components ratio, there was used the dispersity of the product, namely the differential function of pores distribution by radiuses f(r), characterized by the mean radius of the porous structure of the product $\overline{r}$ [8].

$$\overline{r} = \int_{r\,min}^{r\,max} rf(r)dr, \tag{1}$$

where r_{min} – minimal radius of microcapillaries; r_{max} – maximal radius of microcapillaries.

Tensometric method of Van-Bammelen was used for building sorption isotherms. Equation (2) was used for describing sorption-desorption isotherms [8]:

$$u = u_0 \exp\left(-\frac{a_{293} \ln(r) + b_{293}}{r}\right), \tag{2}$$

where u – relative humidity of the sample, rel.; u_0 – hygroscopic humidity at sorption, rel., un.; r – current radius of capillaries, nm; α_{293}; b_{293} – stable, found regarding the look of experimental sorption-absorption isotherms at T=293 K.

The distinctive feature of this methodology is the fact that constants a and b, included in equation (2), at the same time are included in analytic expression (3) that describes DFS.

$$f(r) = \frac{b_{293} - a_{293} + a_{293} \ln(r)}{r^2} \exp\left(-\frac{a_{293} \ln(r) + b_{293}}{r}\right). \tag{3}$$

It essentially facilitates DFS determination for combined masses and food products in whole. The use of equation (3) at the correspondent choice of values of the parameters a, b, W_0 allows to find values of balanced humidities of sorption-desorption curves in the whole diapason

of the relative humidity of air up to its hygroscopic value. For raising the exactness of the obtained values a, b, W_0 it is necessary to sort out values (φ) and to average determined values of parameters of curve (1) [8].

The passage from the relative humidity of air (φ) to radiuses of microcapillaries (r) is realized by formula (4):

$$r_1 = \frac{2\sigma V}{RT\ln\phi}, \quad (4)$$

where σ – surface tension of water; V – molar volume of water steam; R – gas constant.

Such approach allows to determine the parameters a and b (and W_0 if necessary) easily by experimental points of sorption-absorption isotherms and to assess the dispersity of experimental samples by formulas (3), (5):

$$Q_\phi = \frac{(T_2 r_2 - T_1 r_1)RT_1\ln\phi}{(T_2 - T_1)r_1}, \quad (5)$$

where r_1 – maximal radius of microcapillaries, filled at the expanse of sorption of water steam at the relative humidity of air φ and temperature T_1=293 K, found by Tompson formula [8].

The obtained experimental data of balanced humidity for recipe compositions, presented in **Table 1**, allow to construct DFS isotherms.

Table 1

Experimental values of initial humidity of fruit compositions and calculating values of isotherm and DFS parameters

Constant isotherms	Composition samples			Control (apple puree)
	a	b	c	
W_0	0,35	0,34	**10,2**	**0,65**
$W_{0,2}$	0,08	0,06	0,08	0,12
$W_{0,4}$	0,12	0,10	**0,15**	**0,14**
$W_{0,6}$	**0,18**	0,12	0,11	**0,15**
$W_{0,9}$	0,30	0,28	0,18	0,35
a_{313}	0,40	0,46	0,06	1,4
$в_{313}$	1,17	1,48	0,5	1,8
$\Theta_{0,5}$	**2,82**	**2,8**	**6,3**	**1,05**
$\Theta_{0,7}$	**1,78**	**1,83**	**4,5**	–
$\Theta_{0,9}$	**1,52**	0,7	**1,7**	**0,10**
$\sum\Theta$	**6,2**	**5,6**	**12,6**	**1,16**

As a result of the analysis of obtained experimental data of multicomponent fruit masses and their mathematical processing according to the methodology, presented in work [8], there were calculated the results of average radiuses of microcapillaries of muticomponent natural compositions.

Color-creating parameters were determined by MCO method (International system of coordinates CIELab by the parameters L, a, b) [9]. The studies of diffuse reflection of samples were realized on the spectrophotometer SF-2000 (producer «SDB Spectrum», Russia) in the diapason 380…700 nm with the step in 10 nm and number of accumulation cycles – 20. After that, color characteristics of the studied samples in CIELab system were determined using inset SFScan software [10].

3. Results

At determining changes structural-mechanical properties of multicomponent fruit masses, apple puree was used as a control. As a result of the studies as to pores distribution by radius (DFS) for offered recipe compositions, it was established, that the higher dispersity of samples, the more number of microcapillaries with less radius of pores. Just this fact results in forming the large contact surface between components of compositions and provides creation of combined products.

As a result of analyzing DFS, there was compared the influence of the mass share of cranberries on the dispersity of the obtained compositions of multicomponent fruit purees taking into account preliminary calculated values of mean radiuses of capillaries: a – $\overline{r} = 1,51$ mn, b – $\overline{r} = 1,69$ nm, c – $\overline{r} = 1,7$ nm. It may be stated, that at increasing the cranberry content from 25 to 30 % (compositions b and a) there is observed the increase of the dispersity of the studied puree.

At the experiment there were obtained and compared color-creating parameters in the international system of coordinates by CIELab system, brightness and color in the experimental multicomponent fruit compositions (puree, pasts). The obtained results were compared in **Table 2.**

Table 2

Comparison of color-creating parameters of experimental multicomponent fruit compositions by CIELab system

Samples of compositions ratio	Puree				Past				Visual color of fruit composition
	L	a	b	Brightness, T, %	L	a	b	Brightness, T, %	
a (60÷30÷10)	18	26	24	37,8	15	23	21	36,4	Red-orange
b (65÷25÷10)	17	27	19	36,2	15	22	18	35,7	Red-orange
c (55÷40÷5)	16	25	22	35,2	14	21	19	34,5	Red-orange

The analysis of the data of experimental samples of multicomponent fruit compositions (purees, pasts), presented in **Table 2**, confirms the minimal change of their physical-chemical properties, because at using the appropriate temperature regime the brightness of samples is saved by the inherent red-orange color. Taking it into account, it is possible to state the maximal conservation of BAS and treating-prophylactic properties in the final product – multicomponent pasts. It became possible at the expanse of using the improved RFA.

4. Conclusions

There was developed the construction of the rotor film apparatus with the innovative solution as to the system of heating its working chamber at the expanse of using the radiating heater – FFREhRT. It provides getting multicomponent fruit pasts of the high quality. Such construction is resource-effective and allows to concentrate fruit purees using saving non-inertial heat regimes (50...60 °C) with processing duration 0,65...0,8 min for content 25...30 % RM. The studies probated the improved RFA at concentrating the offered multicomponent compositions of fruit purees, based on apples (Antonyvka variety), cranberries (Hoves variety) and haws (Krymsky variety).

The high quality of obtained multi-component fruit pasts was confirmed as a result of studying their structural-mechanical and color characteristics. Structural-mechanical parameters of studied fruit purees allowed to determine the influence of each component of the composition on the dispersed stability of the obtained structure of puree. It was established, that the best disperse stable structure is inherent to the composition with percent content of apples, cranberries and haws as 60÷30÷10 with the mean radius of microcapillaries $\overline{r} = 1,51$ nm.

As a result of concentrating fruit purees, there were determined their color characteristics by CIELab system. The comparison of the studied samples before and after concentrating indicates their unessential change. Thus, for the recipe composition with best organoleptic parameters: apple, cranberry, haw in ratio 60÷30÷10, the brightness parameter for puree is: T=37,8 %,and for concen-

trated past – T=36,4 % respectively. All obtained compositions are characterized by the red-orange color that totally confirms saving their physical-chemical properties at thermal processing.

The further development of the studies is planned to be directed on elaborating waste-free production of fruit pats and dried powders on its base. The improvement of the correspondent equipment for preliminary thermal processing of vegetable raw materials is aimed at decreasing resource consumption.

The improved construction of RFA may be implemented at enterprises of tinned food production for processing and obtaining high-quality fruit pasts. Fruit pasts may be recommended in food rations as an independent product and also for producing non-alcoholic and vodka drinks, confectionary and bakery products and other needs of food industry of the country.

References

[1] Shazzo, R. I., Ovcharova, G. P. (2005). Produkty detskogo pitaniya iz rastitel'nogo i myasnogo syr'ya infrakrasnoy sushki. Khranenie i pererabotka sel'khozsyr'ya, 1, 50–52.

[2] Magomedov, G. O., Magomedov, M. G., Zhuravlev, A. A., Lobosova, L. A. (2015). The development of plants for the production of concentrated pastes of fruit and vegetable raw materials. Proceedings of the Voronezh State University of Engineering Technologies, 3, 13–16.

[3] Magomedov, G. O., Magomedov, M. G., Astredinova, V. V., Litvinova A. A. (2012). Technology concentration of fruit and vegetables. Proceedings of the Voronezh State University of Engineering Technologies, 4, 86–89.

[4] Cherevko, A. I., Kiptelaia, L. V., Mihailov, V. M., Zagorulko, A. E. (2009). Progressivnye protsessy kontsentrirovaniia netraditsionnogo plooovoshchnogo syr'ia. Kharkiv: KhSUFTT, 241.

[5] Eitenmiller, R. R. (2002). Vitamin analysis for the health and food sciences.2 Ed. CRC Press, 675.

[6] GOST 26188-84. Produkty pererabotki plodov i ovoshhey, konservy myasnye i myasorastitel'nye. Metod opredeleniya rN (s Izmeneniem N 1) (1985). Moscow: Izdatel'stvo standartov, 3.

[7] GOST 28561-90. Produkty pishhevye konservirovannye. Metody opredeleniya sukhikh veshhestv ili vlagi (Vzamen GOST 13340.3-77) (2011). Moscow: Izdatel'stvo Standartinform, 9.

[8] Cherevko, A. I., Kiptela, L. V., Zaharenko, V. A., Zagorulko, A. N. (2013). Pat. No. 83943 UA. Method of determining the strength of the multicomponent structure of plant pastes. MPK G01N 30/00, A23L 1/06/. No. u201302710; declareted: 04.03.2013; published: 10.10.2013, Bul. No. 19, 4.

[9] Mizhnarodna komisiia z osvitlenosti. Available at: https://uk.wikipedia.org/wiki/Міжнародна_комісія_з_освітленості

[10] Kiptela, L. V., Zagorulko, A. M., Zagorulko, O. Ye. et. al. (2017). Analiz isnuiuchykh sposobiv vyznachennia yakosti produktiv kharchuvannia za kolorom. Prohresyvni tekhnika ta tekhnolohii kharchovykh vyrobnytstv restorannoho hospodarstva i torhivli, 2 (26), 354–363.

Original Research Article: full paper

(2018), «EUREKA: Physics and Engineering»
Number 2

ANALITIC INVESTIGATION OF THE REGULARITIES OF CHANGING DUST CONCENTRATION DURING THE ABRASIVE DECREASE OF STONE STRUCTURES

Ala Bezpalova
Department of Building Management and Labor Protection
Odessa State Academy of Civil Engineering and Architecture
4 Didriksona str., Odessa, Ukraine, 65029
bespalova-a-v@mail.ru

Vladimir Lebedev
Department of Structural Materials Technology and Materials
Odessa National Polytechnic University
1 Shevchenko ave., Odessa, Ukraine, 65044
wlebedev29@rambler.ru

Yuri Morozov
Department of higher mathematics and systems simulation
Odessa National Polytechnic University
1 Shevchenko ave., Odessa, Ukraine, 65044
morozovyu@gmail.com

Abstract

In the process of repair or restoration of building structures, it is often necessary to strengthen building structures from limestone-shell rock, concrete, reinforced concrete, hard materials-granite, basalt, etc. by cutting or making cuts of the required size with detachable circles of synthetic diamond and cubic boron nitride (CA and CBN).

The cutting process is accompanied by considerable dust formation, which can be both harmful and dangerous factor in the work.

The aim of the work is studying the process of dust sedimentation and the regularity of the change in dust concentration during the abrasive cutting of concrete and stone materials.

Mathematical models have been developed – dust emission from under the wheel, speed of sedimentation of dust particles depending on their material, size and shape, and also depending on temperature, pressure and humidity, the concentration of dust in the working space and the concentration change during the cutting cycle are calculated.

It is shown that the velocity of the sedimentation of particles depends significantly on the shape. The higher the sphericity, the higher the sedimentation rate. The ambient temperature has little effect on the sedimentation rate, in the temperature range (–20→+40 °C) at which the operation takes place.

The sedimentation rate of dust particles generated by cutting the most common building stone materials also differs slightly. Almost the same sedimentation rate has dust particles obtained by cutting basalt and concrete. A bit higher is the sedimentation rate of particles from granite.

The sedimentation rate of particles of generated dust is about 600–700 cm/h or 10–11 cm/min for particles measuring 6 μm. This means that at a production height of about 2 m (200 cm) during the operating cycle (about 3 min), the dust will remain at an altitude of about 1.5 m, i. e. practically remains in the working area. This gives grounds to assert about a high concentration of dust during the cutting cycle (about 4.8 108/m^3).

Keywords: cutting of stone structures, dust formation, dust sedimentation, dust concentration, sedimentation rate, sedimentation time.

DOI: 10.21303/2461-4262.2018.00584

1. Introduction

In work [1] the mechanism of dust generation during abrasive cutting of stone structures was shown. A minute concentration of dust in the working space was shown. However, the concentration of dust is not exhausted by this, so let's consider this issue in more detail. In the process

of repair and restoration of buildings, it is often necessary to strengthen structures that have great destruction. In this case, auxiliary structures are introduced into the walls, foundations and floors, for which they have to cut openings and nests, where reinforcing elements are built.

Such works are often performed in limestone-shell, concrete, granite, basalt by cutting or making cuts to the required size with detachable circles of synthetic diamond and cubic boron nitride (CA and CBN). Cutting of solid building materials is carried out by disk diamond circles and circles from CBN rotation speed, which, and, consequently, the cutting speed is 35–50 m/s. In view of the high intensity of the cutting process and intensive micro-striking, the cutting process is accompanied by considerable dust formation, as indicated in [1]. The dust concentration in the working space can't be characterized by only a minute concentration. The cutting process is long, at least a few minutes. If divide the dust into minute portions, it is obvious that after the first portion has arrived, it is partially in the air for some time. When it is in the air, a second portion of dust enters the working space, followed by a third, and so on. Thus, the longer the dust sedimentation time, the higher its concentration in the working space.

The time of dust sedimentation depends on many factors – the height at which the cutting takes place (when cutting through the window openings this height can be about three meters), the size of the dust particles, the shape of the dust particles, the state of the environment, the dust particles.

It should be noted that when cutting metal objects, the separation of chips and dust occurs as a result of plastic shear deformation. In this case, the shape of the shavings – a speck of dust – is close to the shape of a "comma", which can be taken into account in practical calculations. However, when cutting a brittle material from which stone building structures are made, the formation of a dusty mote occurs as a result of brittle fracture, in which the shape of the dust particles is arbitrary, which naturally affects the sedimentation rate (sedimentation) of the dust particle.

Building structures can consist of dissimilar materials – different density and hardness. Dusts of different chemical composition, even with the same size and shape, will have different rates of sedimentation, and, consequently, will be deposited at different times.

It is not difficult to see that when cutting, dust from under the circle literally flies out along the tangent to the circle. The direction can be arbitrary depending on the position in which work is performed, including upwards, that will add the height of the dust ejection.

In addition, it is necessary to take into account the state of the environment – temperature and humidity, which will affect the density of this environment and the Archimedean forces that act on the dust particle.

All these factors should be taken into account, both in theoretical calculations and in experiments, if the latter are to be performed.

It is more reasonable to have mathematical models of dust ejection, sedimentation rate and sedimentation time to determine all these dependencies, depending on the above factors.

The existence of such models can make it possible to conduct a computational experiment, establish the necessary dependencies, determine the concentration of dust during working hours, which in turn will provide material for improving and, if necessary, developing new means of individual and collective protection of workers.

2. Analysis of literary data and the formulation of the problem

At present, there are theoretical models of dust sedimentation.

So work [5] has mathematical models of dust sedimentation, which take into account the various forces that act on the dust particle during its waking in the air. However, the calculations refer to dust emitted from chimneys of considerable height 40 to 50 m. Thus, it is rather a matter of soot particles. The shape of the particles is not taken into account, it is known that the basic shape of the particles is flaky. The mineral composition of dust and the dependence of the speed of sedimentation on this composition are not considered.

In work [6] there are mathematical models of dust sedimentation in production shops of construction enterprises, however without sources of dust generation. The height with which the dust precipitates is not specifically indicated, however, the authors consider the shape of the dust

grains, although the main calculations are made for spherical dust particles. One type of material is considered – mineral wool. Pathogenic properties of this type of dust are very high, however, dust of other mineral composition is not considered.

In work [2] there are models of dust sedimentation in ventilation ducts. The authors tried to take into account all types of forces that act on the speck of dust while it is in the air. Mathematical models basically take into account the spherical shape of the particles. The mineral composition of the dust is also not considered.

In work [3], the sedimentation velocities of particles from various materials – minerals, biomaterials, biomineral in water – are considered. The mathematical apparatus takes into account all the forces acting on the particle, but the environment in which the sedimentation occurs differs from the air environment, although the main regularities remain.

The paper [9] deals with the sedimentation of mineral dust from the atmosphere in Japan. Satellite observations with remote sensing are used. The work has an ecological aspect. Dependences of dust sedimentation on time and space factors are investigated. The work uses satellite observations, and it can be considered as experimental. There are also training aids, for example, [8] which outlines the main provisions of theoretical calculations of the movement of dust or aerosols.

Indeed, all mathematical models combine the fact that in all we take into account gravity, the Archimedes' force and the viscous drag force of the medium, written as a rule in a differential form. However, the considered models do not consider the dust generated during abrasive cutting of stone structures consisting of a large number of minerals. In addition, the effects of the shape of particles and the state of the environment are almost not considered. Naturally, the issues of dust emission from under the cut circle, the concentration of dust in the working area and the issues of the cutting cycle duration are not considered.

Bearing in mind the considered materials in the introduction and in the review of the literature, the aim and objectives of this paper can be formulated as follows.

3. The aim and objectives of research

The aim of research is performing an analytical study of the change in the concentration of dust formed during the abrasive cutting of stone structures, depending on the rate of its sedimentation, which is a function of the size and shape of the dust, the material being cut, the temperature and the humidity of the environment.

To do this, it is necessary to solve the following tasks:

1. Develop a mathematical model of dust release from under the circle, and determine the distance to which it is ejected, depending on the rotation speed of the cutting circle.

2. Develop a mathematical model that adequately reflects the speed of sedimentation of dust particles depending on their material, the size and shape of these particles, and also depending on the state of the environment – temperature, pressure and humidity.

3. Using the obtained materials, as well as data from previous works published by the authors, which consider the intensity and productivity of dust generation during abrasive cutting of stone structures, calculate the dust concentration in the working space during the cutting cycle.

4. Mathematical model of the dust release from under the circle. The general equation of motion

In practical problems, as a rule, not individual particles are considered, but a cloud of particles of a dispersed phase, which includes hundreds and millions of individual particles. However, in the case of their low concentration, the motion of each particle does not depend on neighboring particles. And then, knowing the trajectory and velocities of individual particles, it is possible to calculate the behavior of the entire disperse system. The condition for the applicability of this approach is the low value of the volume concentration of particles.

The general vector equation of motion of a particle has the form [2, 3, 9, 10]

$$m_p \frac{d\mathbf{v}}{dt} = \mathbf{F},$$

$$\frac{d\mathbf{R}_p}{dt} = \mathbf{v}, \quad (1)$$

where m_p is the mass of a particle; $\mathbf{R}_p$ is the radius vector of the particle coordinate; F is the vector of forces acting on the particle.

Forces acting on a particle (a speck of dust):

In the gravitational field, the gravitational force $\mathbf{F}_g=\rho_p V_p \mathbf{g}$ and the Archimedes force $\mathbf{F}_A= =-\rho V_p \mathbf{g}$ act on the particle (both resting and moving), which are written as the sum of the forces

$$\mathbf{F}_B = (\rho_p - \rho)V_p \mathbf{g},$$

where V_p is the volume of a particle; $\mathbf{g}$ is the acceleration vector of gravity; ρ_p, ρ – the density of the particle material and the density of the dispersion medium, respectively.

Force of viscous resistance of medium

$$\mathbf{F}_S = -C_D \frac{\rho S_m}{2} |\mathbf{u}_R| \mathbf{u}_R,$$

where S_m is the area of the median section of the body (the maximum cross-sectional area of the body in the plane perpendicular to the direction of its motion); $\mathbf{u}_R=\mathbf{v}-\mathbf{u}$ is the velocity vector of the relative motion of the body and the carrier medium; the vectors v, u are the velocities of the particle and the carrier medium, respectively; C_D – empirical coefficient of resistance depending on the Reynolds number

$$\mathrm{Re} = \frac{\rho |\mathbf{u}_R| d_p}{\mu},$$

μ – coefficient of the dynamic viscosity of the dispersion medium, if expressed through the coefficient of kinematic viscosity $\nu=\mu/\rho$, then the Reynolds number will take the form

$$\mathrm{Re} = \frac{|\mathbf{u}_R| d_p}{\nu};$$

d_p is the particle diameter. Dependences of the C_D values on the Reynolds number are presented in **Table 1** [9, 10]

Table 1

Dependences of C_D values on the Reynolds number

Reynolds number, Re	C_D
$\mathrm{Re} < 0.1$	$24/\mathrm{Re}$
$0.1 < \mathrm{Re} < 2$	$C_D = \frac{24}{\mathrm{Re}}[1 + \frac{3}{16}\mathrm{Re} + \frac{9}{160}\mathrm{Re}^2 \ln(2\,\mathrm{Re})]$

When the particle is unsteady ($d\mathbf{u}_p/dt \neq 0$), an additional resistance force acts on it, due to the need to report acceleration to the motion of the mass of the carrier medium displaced by the particle

$$\mathbf{F}_R = -\frac{1}{2}\rho V_p \frac{d\mathbf{v}}{dt}. \quad (2)$$

This force, called the force of the attached masses, is directed opposite to the particle acceleration vector.

When the particle moves in a shear flow (with a non-uniform velocity profile of the carrier medium), the Saffman force (lift) acts on it, directed perpendicular to the particle motion vector. At low Reynolds numbers and in the absence of rotational motion of the particle, the Saffman force is given by Eq.

$$\mathbf{F}_S = C_S d_p \mathbf{u}_R \sqrt{\rho\mu\left|\frac{d\mathbf{u}}{dy}\right|}\,\mathrm{sgn}\left(\frac{d\mathbf{u}}{dy}\right), \tag{3}$$

where $C_S = 1.615$, $d\mathbf{u}/dy$ is the transverse velocity gradient.

Substituting all the forces that are significant for the problem under consideration in equation (1), it is possible to obtain the differential equation of motion of the particle for each particular problem.

In the case of particles with a low inertia, the velocity of the dispersed phase is determined from the dynamic balance of forces acting on the particles. Thus, it is not necessary to solve the complete differential equations of motion, but it is sufficient to consider the equation of the dynamic balance of forces.

Let's start from the following assumptions:

– the motion of the particle is determined by the force of Archimedes $\mathbf{F}_A$ and the force of resistance $\mathbf{F}_S$;

– the particle velocity vector $\mathbf{v}$ at the initial instant of time is parallel to the acceleration vector caused by the Archimedes force $\mathbf{F}_A$;

– there is no interaction between the particles;

Taking into account the above assumptions, the equation of motion of a single particle can be represented in the following form:

$$m\frac{d\mathbf{v}}{dt} = -C_D\frac{\rho S_m}{2}|\mathbf{v}|\,\mathbf{v} + (\rho_p - \rho)V_p\mathbf{g}. \tag{4}$$

Let's build the trajectories of dust particles on the basis of the Runge-Kutta integration of the equations of motion (1), which for the two-dimensional case, taking into account that the velocity of the medium is zero, will be written as follows

$$\frac{dv_i}{dt} = -C_D\frac{\rho S_m}{2m_p}|v|\,v_i - \frac{(\rho_p - \rho)}{m_p}V_p g_i\delta_{i2},\quad |v_i| = \sqrt{v_1^2 + v_2^2},$$

$$\frac{dx_i(t)}{dt} = v_i(t), \tag{5}$$

where $x_i(t)$ are the coordinates of the particle position; $v_i(t)$ is the velocity of the particle; δ – the symbol of Kronecker.

With the initial conditions $x_i(0) = 0,\ i = 1,2,\ \{v_1(t), v_2(t)\}\big|_{t=0} = \{v_1^0, v_2^0\}$.

In the case of a spherical particle, the system (1.3) will be written as

$$\frac{dv_i}{dt} = -C_D\frac{3}{4d_p}|v|\,v_i - \frac{(\rho_p - \rho)}{\rho_p}g_i\delta_{i2},\quad |v| = \sqrt{v_1^2 + v_2^2},$$

$$\frac{dx_i(t)}{dt} = v_i(t). \tag{6}$$

Numerical studies of the dependence of the velocity of particles and the height on which they rise as a function of the geometrical parameters of the particle are shown in **Fig. 1.**

The present and subsequent calculations are carried out for conditions: atmospheric pressure 100 kPa, air humidity 60–80 %. Under these conditions, work is usually done and fluctuations in air density are insignificant.

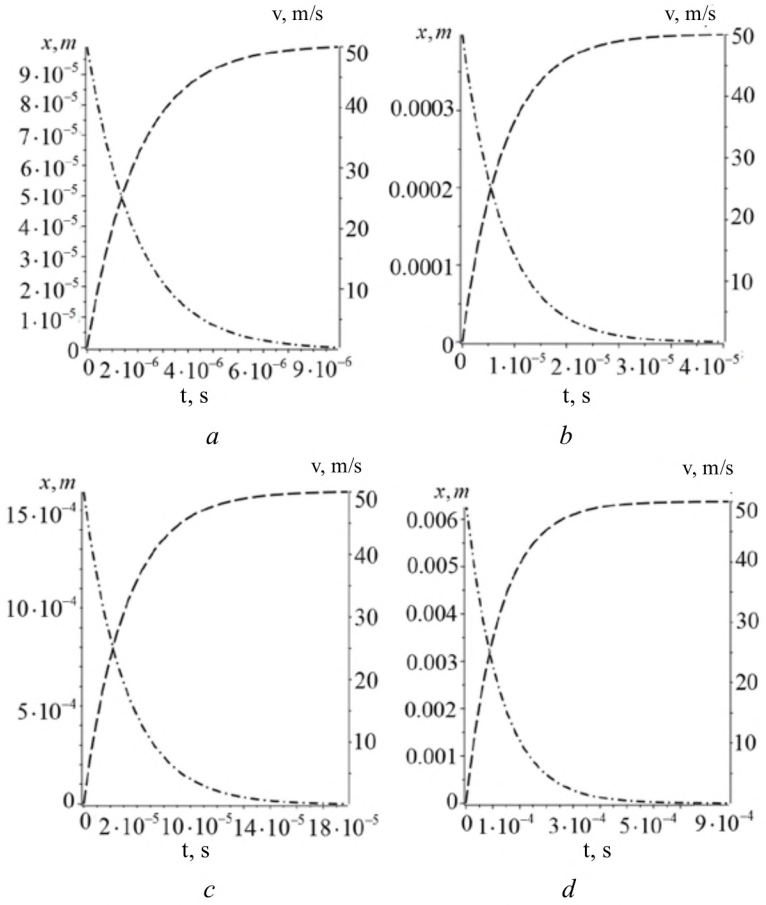

Fig. 1. Dependence of particle velocity and lift height as a function of time and particle diameter d_p. The particle velocity is a dash-dot line; the height of the emission of particles is a dashed line. The material is basalt, *a* – d_p=0.5 μm, *b* –d_p=1 μm, *c* – d_p=2 μm, *d* – d_p=4 μm

From **Fig. 1** it can be seen that at a certain moment of time the velocity of the particle will drop to zero and the particle becomes to a so-called suspended state.

Velocity and sedimentation time of particles.

The basic condition necessary for finding a particle in the suspended state, and, consequently, determining the sedimentation of particles is the condition for the dynamic balance of forces (2), which in the case of gravitational sedimentation of particles, ie, in the stationary mode (dv/dt=0), can be represented as follows

$$-C_D \frac{\rho S_m}{2m} |v_s| v_s + \frac{\rho_p - \rho}{m} V_p g = 0, \quad (7)$$

where v_s – the rate of steady-state sedimentation of the particle (sedimentation rate).

Using the solution of equation (5), it is possible to determine such characteristics as the sedimentation time t_s and the sedimentation length l_s as follows:

$$t_s = \frac{\rho}{\rho - \rho_p} \frac{v_s}{g},$$
$$l_s = v_s t_s. \quad (8)$$

The sedimentation rate can be considered as a scale characteristic characterizing the velocity of the particle in a resisting medium.

Influence of the particle shape on the sedimentation rate.

The shape of the particles of the dispersed phase can differ from the spherical phase (snowflakes, polyhedra, ellipsoids, plates, fibers, etc.), **Fig. 2**.

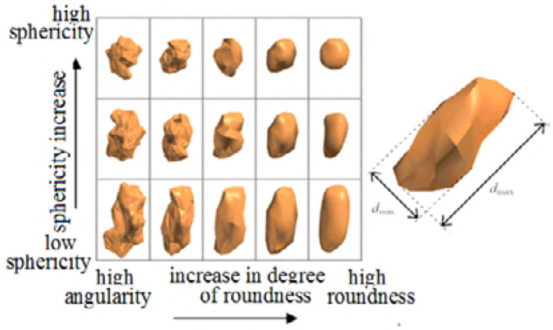

Fig. 2. Forms of dispersed phase particles

Since the methods of dispersion analysis do not, in their majority, allow fully characterize each particle of a disperse system in three dimensions, let's use an approximation, in other words, the replacement of particles of real material by equivalent particles of regular geometric shape. When analyzing a particle under a microscope, its planar projection is visualized, in which case the particle can be characterized by a number of different dimensional parameters. It is important to understand that each method of determining the size is based on measuring the various physical characteristics of particles (maximum length, minimum length, volume, surface area etc.), and as a result, the sizes obtained by different methods will differ. **Fig. 3** shows the various options for answering the question what is the particle size. At the same time there are no erroneous results – each answer is subjectively correct – it reflects a physically measured characteristic.

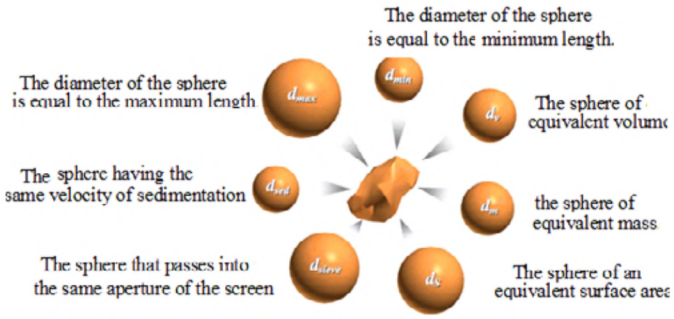

Fig. 3. Equivalent diameters of dispersed phase particles

When calculating the motion of non-spherical particles in the corresponding equations instead of d_p d_{pe} is substituted. It should be noted that in the case of flow past particles whose shape differs from spherical, this approach gives only an estimated result. For clarification, it is necessary to carry out experiments with a spherical and predetermined particle (for example, gravitational sedimentation in a viscous liquid) and introduce a correction factor (geometric coefficient).

For non-spherical particles, a formula for C_D was proposed in [10] for, taking into account the sphericity factor Φ_p

$$C_D = \frac{24}{Re}\left[1+\frac{3}{16}Re+\frac{9}{160}Re^2\ln(2Re)+\frac{10(1-\Phi_p)}{\Phi_p}Re^{0.35}\right],\quad Re<2, \tag{9}$$

where $\Phi_p = \pi(6V_p/\pi)^{2/3}S_p^{-1}$; V_p – the equivalent volume of a particle.

For particles of complex shape, the difficulties that arise when the dynamic and geometric parameters of the particles are compared can be overcome by replacing real particles with ellipsoids close in shape.

Let's consider a particle in the form of an elongated ellipsoid:

$$\Omega : x^2/a^2 + y^2/b^2 + z^2/b^2 = 1, \quad a > b,$$

$$V_p = 4\pi ab^2/3,$$

$$S_p = 2\pi b^2 (1 + \lambda e^{-1} \arcsin(e)),$$

$$\lambda = a/b > 1,$$

$$e = a^{-1}\sqrt{a^2 - b^2}, \tag{10}$$

where V_p is the volume of the particle, and S_p is the surface area of the particle.

Then, the sphericity factor Φ_p is written as follows:

$$\Phi_p = \Phi_p(\lambda) = 2\lambda^{2/3}(1 + \lambda^2(\lambda^2 - 1)^{-1/2} \arcsin\sqrt{1 - \lambda^{-2}})^{-1}. \tag{11}$$

The projected area A_p will depend on the orientation of the main axis of the ellipsoid relative to the vertical. The orientation will depend on the initial conditions, particle inertia and environmental conditions. If consider a rotation θ in the (x, y) plane, it is an ellipse in the projection. For randomly oriented particles, the projected area A_p is replaced by a spherically averaged value

$$\hat{A}_p = \left[4\int_0^{\pi/2} \pi b a_{proj}(\theta) d\theta\right]\left[4\int_0^{\pi/2} d\theta\right]^{-1} = 2baE(e), \tag{12}$$

where E(e) is a complete elliptic integral of the second kind.

Finally, let's obtain an expression for the equivalent diameter d_{pe} as a function of λ

$$d_{pe} = d_{pe}(\lambda) = 2(S_p/\pi)^{1/2} = 2b(1 + \frac{\lambda^2}{(\lambda^2 - 1)^{1/2}} \arcsin\sqrt{1 - \lambda^{-2}})^{1/2} = b\Psi_d(\lambda). \tag{13}$$

Substituting the obtained expressions into the equation of the balance of forces (7), let's obtain

$$v_s = \frac{(\rho_p - \rho)}{12}\frac{d_p V_p g}{\mu S_m} = \frac{(\rho_p - \rho)}{18\mu}\frac{\pi d_p^2}{\Psi_d(\lambda)E(e)}, \quad Re < 1, \tag{14}$$

$$\left[1 + \frac{3}{16}\left(\frac{\rho v_s d_p(\lambda)}{\mu}\right) + \frac{9}{160}\left(\left(\frac{\rho v_s d_p(\lambda)}{\mu}\right)\right)^2 \ln\left(\frac{2\rho v_s d_p(\lambda)}{\mu}\right) + \right.$$
$$\left. + \frac{10(1 - \Phi_p(\lambda))}{\Phi_p(\lambda)}\left(\frac{\rho v_s d_p(\lambda)}{\mu}\right)^{0.35}\right] v_s = \frac{(\rho_p - \rho)}{18\mu}\frac{d_p^2(\lambda)\pi g}{E(e)\Psi_d(\lambda)}, \quad 1 < Re < 2. \tag{15}$$

Equation (15) is nonlinear with respect to v_s and must be solved numerically.

In **Fig. 4** is shown the dependence of the particle sedimentation rate (cm/h) on its geometric parameters and temperature at atmospheric pressure for the case $Re < 1$.

In **Fig. 5** is shown the dependence of the sedimentation rate as a function of the material and the geometric parameters of the particle at atmospheric pressure for the $Re < 1$ case.

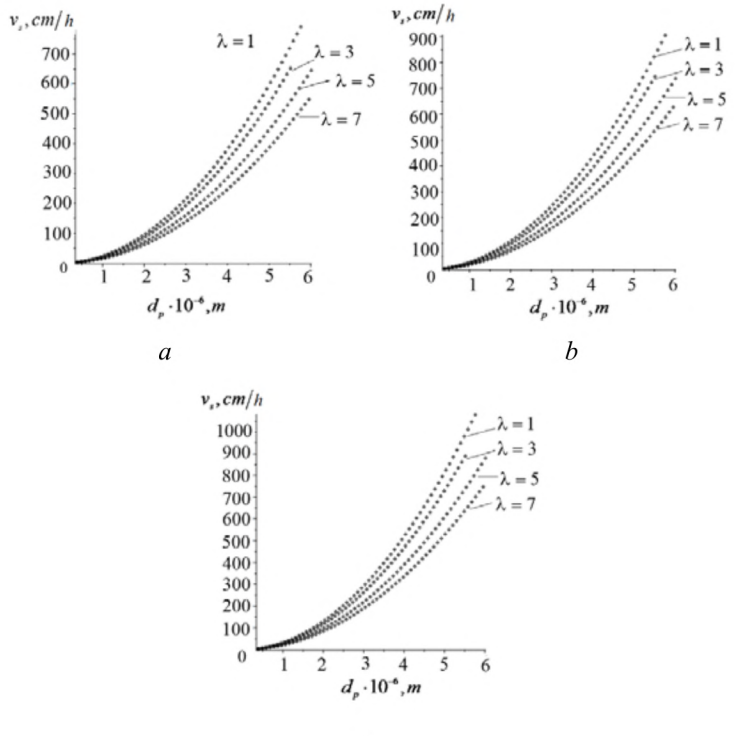

Fig. 4. Dependence of the sedimentation rate (cm/h) on the geometric parameters of the particle and the ambient temperature. At λ=1 (spherical particle), diameters d_p=0.4...6 μm, when taken, λ=3.5.7, the value of b was chosen so that d_{pe}=d_{pe}(λ)=0.4..6 μm. Cut material – basalt, *a* – T=20 °C, *b* − T=40 °C, *c* – T=–20 °C

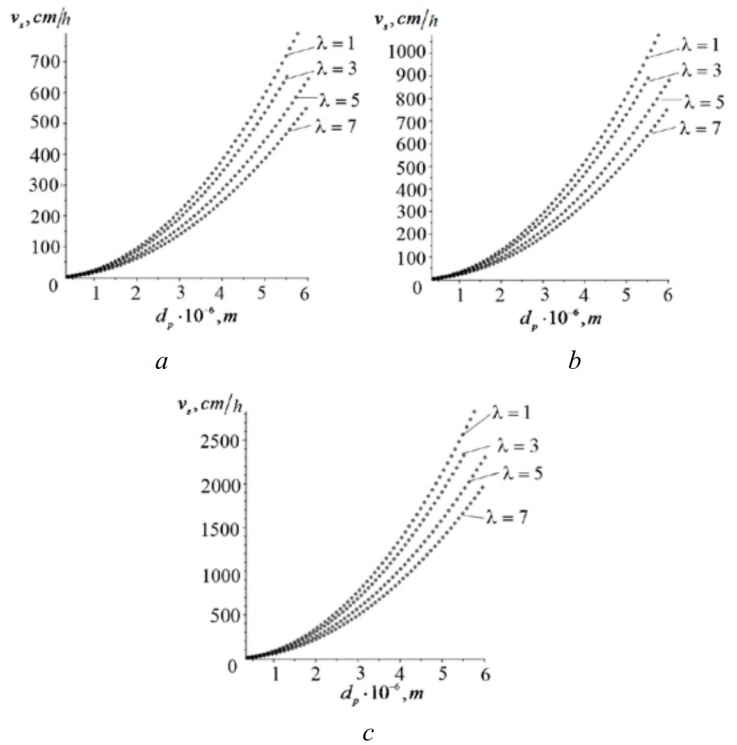

Fig. 5. Dependence of sedimentation rate (cm/h) on the type of material being cut and the geometrical parameters of the particle: *a* – concrete (ρ_p=2200 kg/m^3), *b* – granite (ρ_p=3000 kg/m^3), *c* – steel 40X (carbon 0.4 %, chromium 1 %, ρ_p=7850 kg/m^3)

Model for determining the concentration of particles

The concentration of dispersed particles is also one of the most important characteristics on which the behavior of the disperse system depends on various physicochemical processes. There are countable C_n, volumetric C_V and mass C_m concentration of particles:

C_n is the number of particles per unit volume of a two-phase medium;

C_m is the total mass of particles per unit volume of a two-phase medium;

C_V is the total volume of particles per unit volume of a two-phase medium.

The relationships between C_n, C_m, C_V for polydisperse systems (consisting of particles of different sizes) are presented in (**Table 2**) [8]. For such systems, the dispersed composition is characterized by a differential function of the countable particle size distribution $f(D) = (a/D)\cdot\exp(-b\ln(\beta D)^2)$.

Table 2

Relationships between concentrations for polydisperse media [8]

	C_n	C_m	C_V
C_n	C_n	$C_m\left[\frac{\pi\rho_p}{6}\int_0^\infty D^3 f(D)dD\right]^{-1}$	$C_V\left[\frac{\pi}{6}\int_0^\infty D^3 f(D)dD\right]^{-1}$
C_m	$C_n\frac{\pi\rho_p}{6}\int_0^\infty D^3 f(D)dD$	C_m	$C_V\rho_p$
C_V	$C_n\frac{\pi}{6}\int_0^\infty D^3 f(D)dD$	$C_m\frac{1}{\rho_p}$	C_V

Let's consider the countable concentration of dust $C_n \equiv C(y,t)$, for the calculation of which, using gravitational sedimentation, we use the following differential equation, which is a two-dimensional transport equation

$$\frac{\partial C_i(y,t)}{\partial t} - u_{s,i}\frac{\partial C_i(y,t)}{\partial y} = Q_i(t)\delta(y-y_i),$$

$$C_i(y,t)\big|_{t=0} = 0,\ \ C_i(y,t)\big|_{y=y_i} = 0, \qquad (16)$$

where $C_i(y, t)u_{s,i}$, respectively, the concentration and velocity of the i-th fraction of the dust; $Q_i(t) = Q\sum_{j=1}^{60}\eta(t-j)$ − intensity of dusting; $\eta(t-\tau)$ is the Heaviside function; $\delta(y-y_i)$ is the Dirac delta function by which the height of the i-th fraction of dust is taken into account.

In order to avoid the application of the Laplace transform and difficulties with its treatment, we proceed as follows. Let's divide the time interval T into M-intervals of length $h=TM^{-1}$ and in formula (16) replace the derivative with respect to time by the difference relation:

$$\frac{\partial\zeta}{\partial t} = \frac{\zeta_j - \zeta_{j-1}}{h},\ \ \zeta_j(y) = \zeta(y, jh),\ \ j = 1,2,...$$

As a result,

$$\frac{\partial C_{i,j}(y)}{\partial y} - \frac{1}{u_{s,i}h}C_{i,j}(y) = \frac{1}{u_{s,i}}Q_{i,j}\delta(y-y_i) - \frac{1}{u_{s,i}h}C_{j-1}(y),\ \ j = 1..N,$$

$$C_{i,0}(y) = 0, \quad C_{i,j}(y)\Big|_{y=y_i} = 0. \tag{17}$$

Suppose $j = 1$, the equation takes the form

$$\frac{\partial C_{i,1}(y)}{\partial y} - \frac{1}{u_{s,i}h} C_{i,1}(y) = \frac{1}{u_{s,i}} Q_{i,1}\delta(y - y_i), \quad j = 1..N. \tag{18}$$

With allowance for the initial conditions, the solution of equation (18) has the form

$$C_1(y) = Q_{i,1}[\eta(y - y_i) - 1/2]e^{\frac{y-y_i}{h \cdot u_{s,i}}},$$

substituting it in (17) and continuing the iterative process, let's obtain the values of the concentration of the i-th dust fraction over time.

At each model time Δt=1 s. $4.6 \cdot 10^5$–$2.8 \cdot 10^6$ particles of different diameters arrive in the work zone [1]. Using (15), it is found that the minute concentration of dust during the cutting of a stone (in the dimensions of the working zone 0.5·0.5·0.5 m=0.125 m^3) is in the range $0.28 \cdot 10^8$–$1.68 \cdot 10^8$ pcs/m^3, for the cutting time of 3 m let's obtain a concentration of $0.84 \cdot 10^8$–$4.8 \cdot 10^8$ pcs/m^3. The range of sizes of dust particles is 0.35–6 μm.

6. Discussion of the results of the analytical study

The results of the calculations show that the sedimentation velocity of particles depends significantly on the shape. The higher the sphericity, the higher the rate of sedimentation. Obviously, irregularly shaped particles experience greater medium resistance and greater Archimedean forces, which somewhat compensates for the gravity force under which the dust particle "falls". The temperature state of the environment has little effect on the sedimentation rate, in any case in the accepted temperature range at which work can occur. This can be explained by a slight change in the density of air, as a result of which the force of the medium's resistance and the Archimedean force vary insignificantly.

The sedimentation rate of dust particles generated by cutting the most common building stone materials also differs slightly. So practically the same sedimentation rate has dust particles obtained by cutting basalt and concrete. A bit higher is the rate of sedimentation of particles from granite. This can be explained by the fact that the structure of these materials is fragile, as a result of which the dust particles have a similar shape and the sedimentation rate is affected only by the density, which differs insignificantly. As for particles of chips – dust when cutting steel reinforcement, the influence of a higher density of steel is clearly visible here. In addition, the chips formed as a result of plastic deformation are likely to have a more "streamlined" shape and experience less air resistance. This circumstance, however, requires additional study.

The sedimentation rate of particles of generated dust, taking into account the actual shape for shearing strain (λ=5–7), is approximately 600–700 cm/h or 10–11 cm/min for particles measuring 6 μm. This means that at a production height of about 2 m (200 cm) during the operating cycle (about 3 min), the dust will remain at an altitude of about 1.5 m, i. e. practically remains in the working area. This gives grounds to assert about a high concentration of dust (as indicated by the order of $4.8.10^8$ pcs/m^3). It should be noted that particles of 4–6 μm in size were taken into account. Taking into account smaller particles, this concentration will be somewhat higher.

The advantage of the analytical study can be considered that mathematical models make it possible to evaluate the generation of dust when cutting various materials, for example, ceramic tiles from aluminum oxides and zirconium.

It should be noted that the study does not exhaust the topic of dust generation in the abrasive cutting of stone materials. Further research should be directed to the investigation of air currents arising during the rotation of the circle, the interaction of these flows with dust and with cooling liquids.

7. Conclusions

1. A mathematical model of dust extraction from under the circle is developed, the distance to which it is ejected is determined, depending on the rotation speed of the cutting circle, and is on the order of 7–10 mm with a particle size of 4–6 μm, with a circle rotation speed of about 35–50 m /s.

2. A mathematical model has been developed that adequately reflects the sedimentation velocity of dust particles depending on their material, size and shape, and also depending on the state of the environment. It is shown that the sedimentation velocity of dust particles with dimensions of 4–6 μm is 10–11 cm/min. The more a dust particle differs from a spherical shape, the lower its sedimentation rate. The state of the environment under the conditions under which the work is performed has little effect on the rate of dust sedimentation. The type of cutting stone material – basalt, granite, concrete – has little effect on the sedimentation velocity, since the densities of these materials are quite close. Dimensions of dust particles significantly affect the sedimentation rate. So when the size of dust particles decreases from 6 to 2 μm, i.e. 3 times, the sedimentation rate decreases by 7 times.

3. The conducted research allows to determine the dust concentration in the working space in the amount of $4.8 \cdot 10^8$ pcs/m^3 during the working cycle of cutting, that allows in each case to formulate the requirements shown to means of individual and collective protection of workers.

References

[1] Bezpalova, A., Lebedev, V. (2017). Investigation of the formation process of hazardous and harmful production factors when cutting a stone for construction works. EUREKA: Physics and Engineering, 5, 30–38. doi: 10.21303/2461-4262.2017.00416

[2] Gao, R., Li, A. (2011). Modeling deposition of particles in vertical square ventilation duct flows. Building and Environment, 46 (1), 245–252. doi: 10.1016/j.buildenv.2010.07.020

[3] Maggi, F. (2013). The settling velocity of mineral, biomineral, and biological particles and aggregates in water. Journal of Geophysical Research: Oceans, 118 (4), 2118–2132. doi: 10.1002/jgrc.20086

[4] Dust and respiratory tract. All about spontaneous pneumothorax. Available at: http://www.spontan.ru/pnevmokoniozy/186-pyl-i-dyxatelnye-p.uti.html

[5] Mushchenko, B. L. (2009). Calculation of the rate of incidence of dust particles and the evaluation of the degree of influence of various forces acting on the particle. Scientific Bulletin of the Voronezh State University of Architecture and Civil Engineering, 2, 58–63.

[6] Azarov, V. N., Bessarab, O. I., Kabaev, O. V. (2010). Theoretical studies of sedimentation rate of fine dust in the air of working rooms of engineering and construction industry enterprises. Bulletin of Volg-GASU. Series: Str-in and the architect, 17 (36), 102–105.

[7] Osada, K., Ura, S., Kagawa, M., Mikami, M., Tanaka, T. Y., Matoba, S. et. al. (2014). Wet and dry deposition of mineral dust particles in Japan: factors related to temporal variation and spatial distribution. Atmospheric Chemistry and Physics, 14 (2), 1107–1121. doi: 10.5194/acp-14-1107-2014

[8] Arkhipov, V. A., Usanina, A. S. (2013). A877 Movement of aerosol particles in a stream. Tomsk: Publishing House of Tomsk State University, 92.

[9] Clift, R., Grace, J. R., Weber, M. E. (1978). Bubbles, Drops, and Particles. Academic Press, 380.

[10] Gu, Z., Zhao, Y., Li, Y., Yu, Y., Feng, X. (2006). Numerical Simulation of Dust Lifting within Dust Devils–Simulation of an Intense Vortex. Journal of the Atmospheric Sciences, 63 (10), 2630–2641. doi: 10.1175/jas3748.1

Original Research Article: full paper

(2018), «EUREKA: Physics and Engineering»
Number 2

SYNTHESIS OF THE LAWS GOVERNING THE NON-HOLONOMIC MODEL OF A TWO-LINK ROAD TRAIN WITH REVERSE MOTION (OFF-AXLE HITCHING MODEL)

Dmitry Tatievskyi
Department of Software of Automated Systems
Zaporizhzhia State Engineering Academy
226 Soborny ave., Zaporizhzhia, Ukraine, 69006
dtdissert@gmail.com

Abstract

The complexity of the control of the road train is due to the pronounced nonlinearities, as well as the instability of the control object during the movement in the backward motion (jackknifing). For the road trains, the location of the towing device behind the tractor's rear axle is quite typical. In this study, a synthesis of control laws for road trains with offset of coupling devices relative to the rear axle of the tractor (off-axle hitching) is proposed. The controllers have been implemented both to ensure a stable circular motion and for rectilinear motion with a given orientation angle, and the behavioral features of this model have been studied on the basis of them.

Based on the analysis of the approaches to the synthesis of the laws governing the road train with the coupling out, it was decided to synthesize the required control laws using the Lyapunov function method.

Synthesized controllers can be directly used to program the robotic systems of the respective models. It is also possible to use them for the development of the Dubins machine for the investigated model. They can be used to build automatic control systems that would help the driver to drive a car with a trailer while driving backward.

In this research, a study was made of the state of the solution of the problem associated with the reverse movement of a road train consisting of a tractor and a semitrailer with a coupling, synthesized laws made it possible to study the features of such model, determined by its linear dimensions.

For comparison of the synthesized laws, the analysis of phase portraits of trajectories, angles of folding and control, orientation angles was carried out, and also the analysis of the quality of transient processes with the change in the speed of the road train was performed.

Keywords: road train, kinematic model, on-axle hitching, off-axis hitching, route curve, controller, non-holonomic system, control law.

DOI: 10.21303/2461-4262.2018.00592

1. Introduction

Road trains consisting of a tractor and passive semitrailers belong to the class of nonlinear, non-holonomic, structurally unstable (with reverse motion) dynamic systems. Because of this, the task of controlling their movement is relevant both from the point of view of theory and from the point of view of the practical implementation of programmed motion with given constraints.

But, there is a problem of controlling such system when driving reverse (parking, entry into a limited space ("dock"), maneuvering when going back out of the dock, etc.). Without proper control action, the links of the road train will "squeeze out" each other, which is accompanied by an unlimited increase in the angle of folding. This phenomenon, known as jackknifing, while moving forward the semitrailer will track the tractor's heading angle. Therefore, autonomous cargo transportation systems are, at present, the object of numerous research projects, among which it is possible to single out works on the synthesis of control laws for the reverse movement of such systems.

The problem of controlling the movement of a road train with a semitrailer under the assumption of non-holonomic constraints (the absence of lateral slippage of the support wheels) is of great theoretical and practical importance. Research in this field is stimulated by numerous applied problems.

It should be noted that work in this direction is actively conducted abroad, especially in recent years. In this case, as a rule, separately considered models are "on-axle hitching" and "off-axle hitching", the control laws for which are synthesized by various methods.

For the investigated model, management and planning methods are proposed using a diverse mathematical apparatus. Among the most frequently used methods, let's single out the method of feedback linearization [1, 2] and chain systems [3]. Due to the fact that such systems are differentially flat, the technique proposed by the authors of [4, 5] is well applicable to them.

Methods are also used, which are exclusively due to the geometric features of the kinematics of the "off-axle hitching" model, formulated in cascade form [6]. The apparatus of Lie algebras [7] and fuzzy logic [8] is also applied. A cascading control strategy (VFO) is used [6]. Linear quadrature controllers [9], nilpotent approximation [10], and so on are used.

A qualitative analysis of such systems is carried out in [11].

The main aim of research is synthesis of the laws governing the wheel module of the road train with the displacement of the coupling device relative to the tractor's rear axle, when driving with the reverse. This ensures the movement of the road train in the specified corridor, and is achieved by imposing restrictions on the values of the angles of folding between the links of the road train.

In applied works, based on the mathematical theory of control, the model of a controlled object, called the Dubins machine [12], is very popular. Such model is given by a nonlinear system of third-order differential equations. Two phase variables characterize the geometric position of the controlled object on the plane, the third variable angle of the direction of the velocity vector. The speed is considered constant. The scalar control action, constrained by the geometric constraint, determines the instantaneous turning radius. Obviously, in this capacity, it is possible to consider the proposed model, and solve for it the task of achieving a given aim.

In this paper, the synthesis of the control law is based on the Lyapunov function method [13]. It is possible to note that the direct Lyapunov method has already been successfully applied for the synthesis of a tractor control law with one semitrailer with a hitch in the "on-axle hitching" model [14].

Maple system is used for symbolic calculation of control laws, numerical integration and modeling. At the same time, the structure of the script in the internal language of the Maple system has a modular structure: the synthesis of the control law in symbolic form, the recording of the CDS, the input of data, numerical integration, the mapping of phase portraits.

2. Materials and methods

At the heart of the mathematical model of the controlled motion of the road train, the classical positions of the mechanics of the system of solids lie in the reverse (taking into account the presence of non-holonomic constraints). The task of synthesizing programmed controlled motion was solved on the basis of rigorous approaches to the theory of automatic control and control of dynamical systems. The correctness of the obtained results is verified on the basis of independent numerical simulation of the system, namely:

1. The kinematic model of a three-link road train with non-holonomic constraints (no lateral slippage of the wheel system) with an off-axle hitching coupling model is considered.

2. To stabilize the movement of the reverse of such system, the Lyapunov function method is used (Lyapunov second method). The property of stability is considered from the point of view of the definition of Lyapunov stability.

3. When implementing the method, the necessary symbolic calculations are performed in the Maple environment.

4. Numerical simulation (integration) of the equations of controlled motion of the road train model is also carried out in the Maple environment.

The empirical study consists in realizing the controlled motion of a large-scale physical model, registering the angles of folding and controlling the impact, which allowed the optimal adjustment of the regulators for both synthesized control laws.

3. Synthesis of control laws. Kinematic model of the system

The movement of a system consisting of a tractor with a passive semi-trailer, connected by the "off-axle hitching" model, describes the single-track kinematic model quite accurately at low

speeds. This model does not take into account the slip between the wheels and the roadway. Angular displacements in vertical planes are also not taken into account (**Fig. 1**).

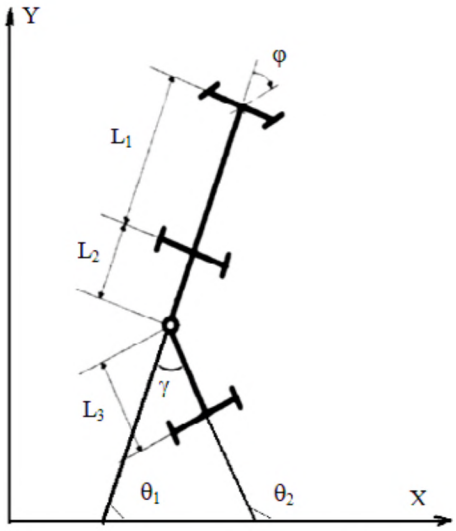

Fig. 1. The kinematic scheme of the system

Here θ_1, θ_2 – the orientation angles of the system objects, L_1, L_2, L_3 – their linear dimensions, φ – the steering wheel angle of the tractor unit, $\gamma=\theta_2-\theta_1$ – the angle of folding between the tractor and the semitrailer. At this angle, a restriction is $|\gamma|<\pi/2$, the restrictions on the angle φ are determined by the technical control capabilities.

Such scheme is described by the following system of differential equations (1), obtained on the basis of the studies [15]:

$$\dot{x}_1 = v\cdot\cos(\theta_1),$$

$$\dot{y}_1 = v\cdot\sin(\theta_1),$$

$$\dot{\theta}_1 = v\cdot\tan(\phi)/L_1,$$

$$\dot{\theta}_2 = -(L_2\cdot\dot{\theta}_1\cdot\cos(\gamma)+v\cdot\sin(\gamma))/L_3, \quad (1)$$

where $v<0$ – the linear speed of the tractor.

Compared with the system used to describe the on-axle hitching model, the latter equation contains the angular velocity of the tractor as a factor, complicating the synthesis of the control law. The same factor is also contained in the equation of trailer speed v_1 (2) [16]:

$$v_1 = -L_2\cdot\dot{\theta}_1\cdot\sin(\gamma)+v\cdot\cos(\gamma), \quad (2)$$

which makes it difficult to control and stabilize the system.

Obviously, the first term on the right-hand side of (2) is determined by the rotational motion of the tractor (at $v=0$), and the second by the forward motion of the tractor (if its angular velocity is zero).

For numerical integration and modeling, the following design parameters are used: $L_1=5$ m, $L_2=2$ m, $L_3=4$ m, Cauchy conditions of a rather general form $\theta_1(0)=-\pi/10$, $\theta_2(0)=\pi/15$ – zigzag, desired folding angle and orientation $\gamma_{ref}=\theta_{2ref}=\pi/5$, $v=-1$m/s, the time intervals varied for clarity of phase portraits. Specifically, the change in these parameters is discussed when studying the behavioral features of this model.

4. Synthesis of a circular controller

Let's define the tracking error $e=\gamma_{ref}-\gamma$, where y_{ref}=const – the desired folding angle and choose the Lyapunov function (3) that satisfies the necessary conditions (4):

$$V_1 = e_1^2 / 2. \tag{2}$$

$$V(0) = 0,$$

$$V(x(t)) > 0, \quad x \neq x_0,$$

$$\dot{V}(x(t)) \Leftrightarrow e \cdot \dot{e} \leq 0, \forall t > 0. \tag{3}$$

Its derivative $\dot{V} = e \cdot \dot{e} = e \cdot \dot{\gamma}$, since γ_{ref} has a constant value.

In the Maple system, calculate the derivative for the folding angle γ, substituting the necessary expressions from the system (1), taking into account the relationship $\gamma = \theta_2 - \theta_1$, **Fig. 2**.

```
=
> diffG := simplify(diffTheta2 - diffTheta1);
=          diffG := -(L1sin(g(t))cos(φ) + sin(φ)(cos(g)(t))L2 + L3)V / cos(φ)L1L3
```

Fig. 2. The derivative of the folding angle

The control law is obtained from the condition of its negative semidefinite, assuming its value is equal to ke, where k>0 and, solving this equation with respect to control φ, let's obtain **Fig. 3**.

```
=
> Ex := diffG – k · e;
Ex := –(gRef – g(t))k – (L1sin(g(t))cos(φ) + sin(φ)(cos(g)(t))L2 + L3)V / cos(φ)L1L3
=
> Phi := simplify(solve(Ex = 0, phi));
Φ := –arctan((L1(Vsin(g(t))) + kL3(gRef - g(t))) / V(cos(g(t))L2 + L3))
```

Fig. 3. Synthesis of the control law

Consequently, the circulation controller has the form (4):

$$\phi = -\text{arctg}((L_1 \cdot v \cdot \sin()\gamma + k \cdot L_3 \cdot e) / (L_2 \cdot v \cdot (\cos(\gamma) + L_3))). \tag{4}$$

The derivative of the Lyapunov function, however, is negative semidefinite, which ensures the asymptotic stability of the circular motion of the system, and the synthesized controller can be directly used for program control of the investigated system.

Based on the results of numerical simulation, the obtained phase portraits present in the figures below (**Fig. 4**–**6**).

In this case, before the beginning of the program motion with a given folding angle, it is possible to calculate the curvature radius of the circular trajectory by solving equation (5) [15] with respect to R, taking its norm (6):

$$\gamma_{ref} = \pi - \arctan(R / L_2) - \arccos(L_3^2 / (R^2 + L_2^2)^{1/2}), \tag{5}$$

$$R = \left|(L_2 \cdot \cos(\gamma_{ref}) + L_3) / \sin(\gamma_{ref})\right|. \tag{6}$$

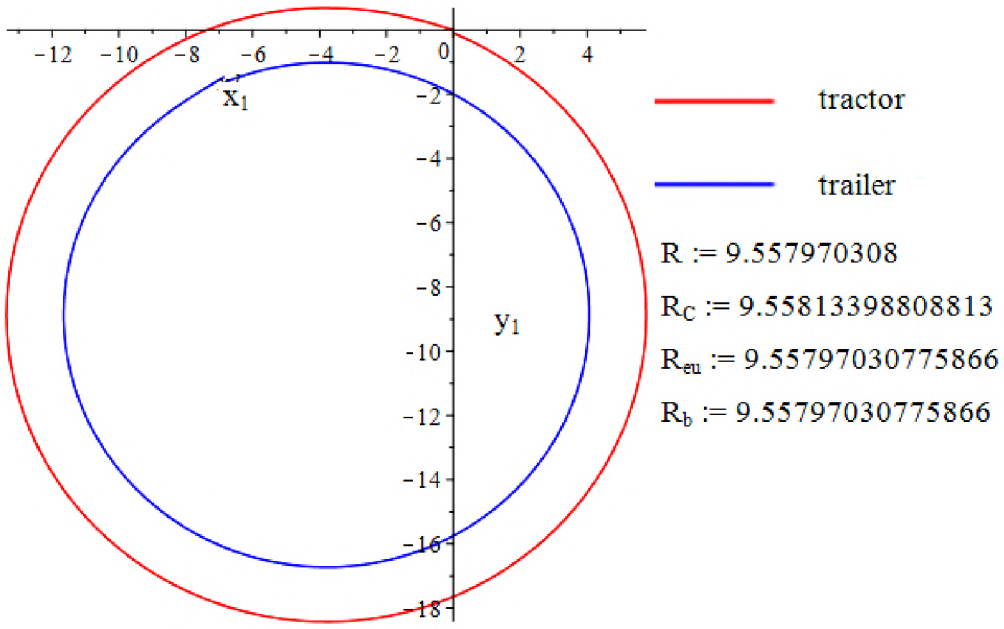

Fig. 4. Trajectories of circular movement

The value of R calculated in this way practically coincides with the values of the radii calculated from the results of numerical integration. The values of the radii in **Fig. 4** calculated from the coordinates of the trajectory (R_c), according to the Euler formula (R_{eu}), using the control value (R_u). For the last three formulas, the last values in the arrays generated by the Maple tools for phase portraits are used (**Fig. 5**).

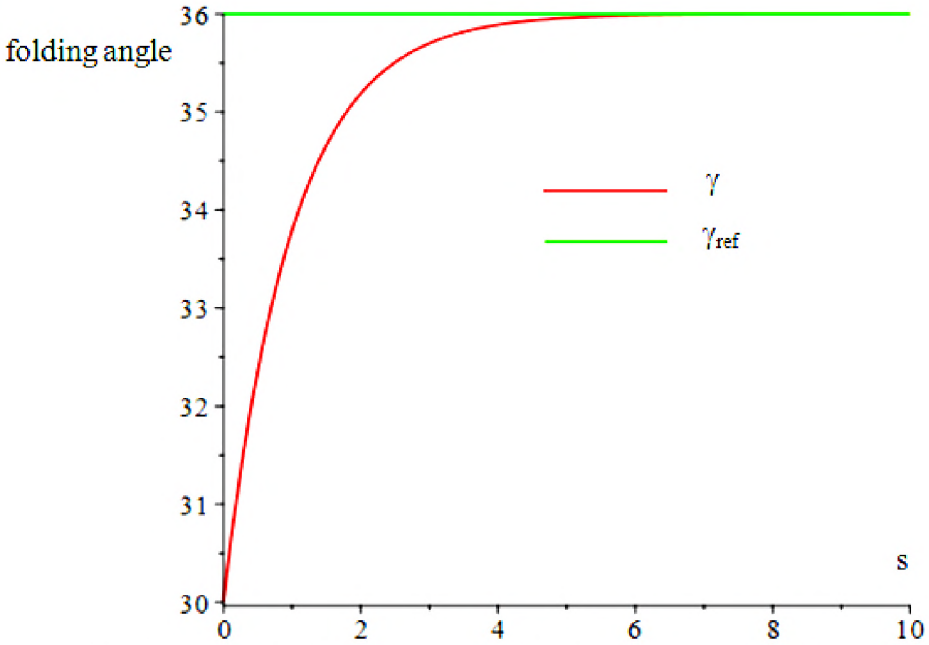

Fig. 5. Dynamics of the folding angle with reverse curvilinear motion

Also, it is possible to calculate the asymptotic value of the control using the radius of the circle R calculated above (trajectory of the track) $\phi_{ref} = \arctan(L_1/R)$, and display it on the phase portrait (**Fig. 6**).

In this case, the control coefficient k in the control law was chosen to be 1.4, which made it possible to optimally adjust the control value and the transient time.

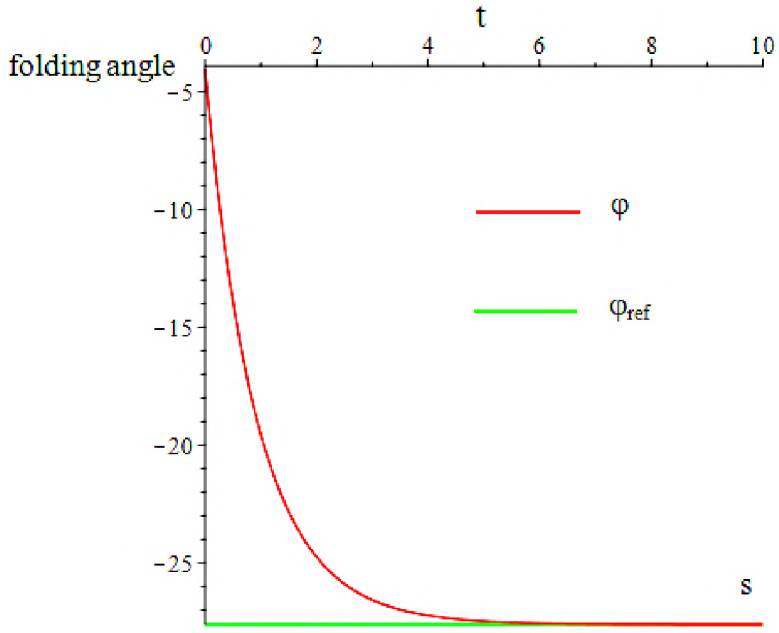

Fig. 6. Dynamics o of the road train control

5. Synthesis of the orientation controller

The control law for this controller (motion with a given orientation angle) is synthesized on the basis of the previous law, selecting the tracking error $e=\gamma_{ref}(t)-\gamma(t)$ and demanding the condition $\gamma_{ref}(t)=\theta_{2ref}-\theta_2$, where θ_{2ref}=const – desired orientation angle of the semitrailer.

The derivative of the Lyapunov function (2) (**Fig. 7**):

$$> \text{diffG} := \text{simplify}(\text{diffTheta2} - \text{diffTheta1})$$

$$\text{diffG} := -\frac{V(L_1 \sin(g(t))\cos(\phi) + \sin(\phi)(\cos(g)(t))L_2 + L_3))}{\cos(\phi)L_1 L_3}$$

Fig. 7. The derivative of the folding angle

From the condition of negative semidefinite (assuming its value is equal to ke, where k> 0), the control law follows (**Fig. 8**) (7):

$$> E_x := diffG - k \cdot e;$$

$$> \text{Phi} := \text{simplify}(\text{solve}(E_x = 0, \text{phi}));$$

$$\Phi := -arctan\left(\frac{L_1(V\sin(g(t))) - kL_3(g(t) - \text{theta2Ref} + \theta 2(t))}{V(\cos(g(t))L_2 + L_3}\right)$$

Fig. 8. Synthesis of the control law

$$\text{phi} = -\arctan((L_1 \cdot (v \cdot \sin(\gamma(t)) - \\ -k \cdot L_3 \cdot (\gamma(t) - \theta_{2ref} + \theta_2(t)))) / (v \cdot (\cos(\gamma(t) \cdot L_2 + L_3)))). \quad (7)$$

For the synthesized orientation controller, the phase portraits presented in the figures below are obtained (**Fig. 9**–**12**).

In this case, the value of the orientation angle computed along the path of the phase portrait

$$\theta = \arctan(\delta Y / \delta X) = 35.9999948305423,$$

at a specified desired angle of 36°.

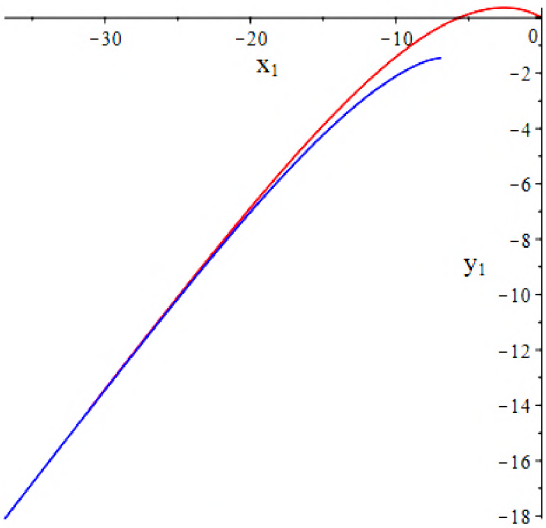

Fig. 9. Trajectory of tractor and trailer movement

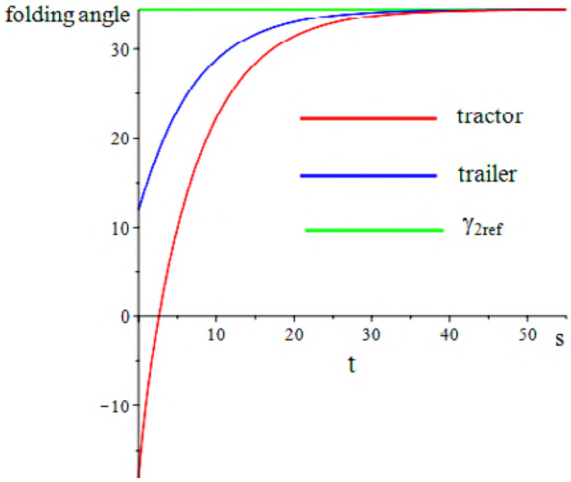

Fig. 10. Orientation angles of tractor and trailer

Control dynamics.

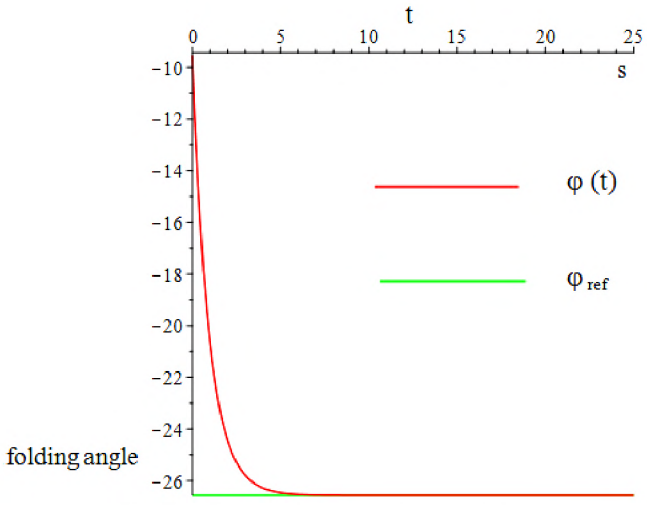

Fig. 11. Steering wheel deflection angle (control)

The folding angle (blue) and the control (red) in this case tend to zero (**Fig. 12**).

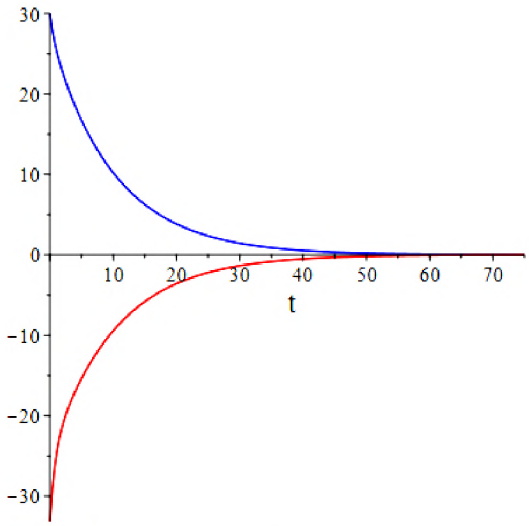

Fig. 12. Dynamics of the folding and control angles

6. Synthesis of the law for realizing the movement of a road train on a given route curve

As is known, two types of tracking automatic control systems are used for driving vehicles: a "trajectory tracking" system and a control system for "path following".

In the first case, the trajectory specifies the desired change in state variables as a function of time. In the second case, the desired route curve (a combination of lines and arcs of a circle of radius R) in the workspace is set, which is not a function of time.

The laws synthesized above successfully solve the first problem. To solve the second, let's use the dependence (5), calculating the desired folding angle over a given radius of curvature.

When a radius value is received at the input of the Maple script, the desired folding angle is computed and the motion along the circumference (**Fig. 13**) occurs according to the law synthesized for the circular controller.

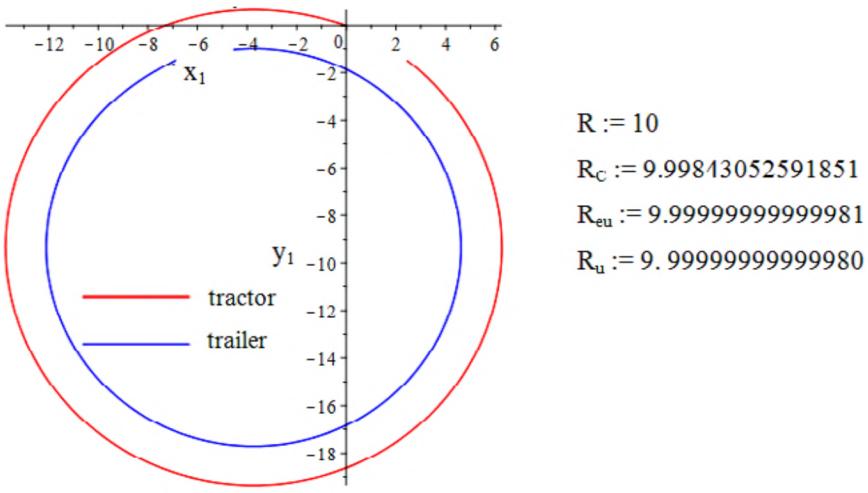

Fig. 13. Movement along a curve of a given radius

The curves in **Fig. 13** are the values of the radii, calculated in various ways: on the coordinates of the trajectory (R_c), according to the Euler formula (R_{eu}) and taking into account the control (R_u). For the last three formulas, the last values of the arrays generated by the Maple tools for phase portraits were used. In this case, the value of the angle calculated from (5) is equal to γ_{ref} 34.4°.

Dynamics of control when using this law is shown in **Fig. 14**, the asymptotic value of the control is calculated by the formula $\phi_{ref} = a\tan(L_1 / R)$.

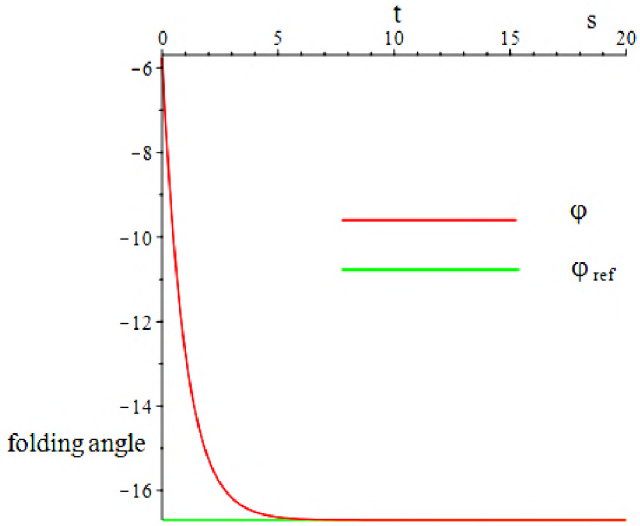

Fig. 14. Dynamics of control when driving on a given route curve

In this case, it should be borne in mind that in the case of $R->\infty$ or $\gamma_{2ref}->0$ the movement of the road train will tend to rectilinear.

7. Investigation of the off-axle hitching model features

Let's use synthesized controllers to study the features of this model. Changing its geometry – linear dimensions, it is possible to draw the following conclusions.

A decrease in the parameter L_2 (L_3=const) leads to an increase in control (**Fig. 15**), which reaches its maximum in the limiting case L_2=0 (on-axle hitching model).

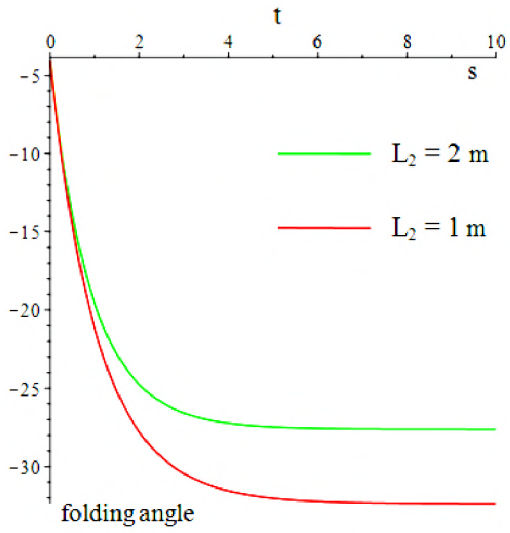

Fig. 15. Increase in the amount of control when the coupling decreaes

With an increase in the length of the semitrailer with a constant length of the coupling, the amount of control decreases (**Fig. 16**) and vice versa.

In this case, the best stability of the movement, in the sense of the speed of the trailer, is ensured when L2=L3, the semitrailer and tractor track a single trajectory (**Fig. 17**).

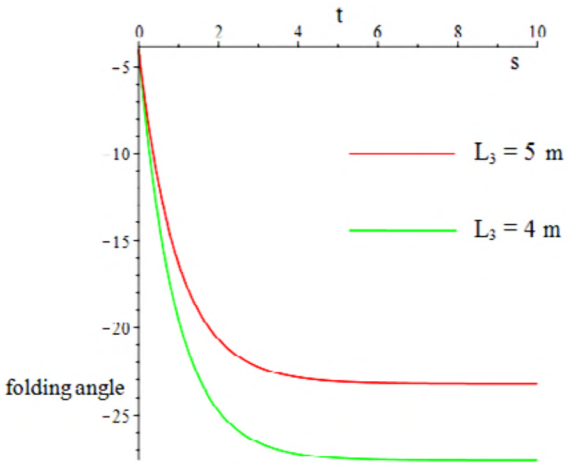

Fig. 16. Decrease in the amount of control as the length of the semitrailer increases

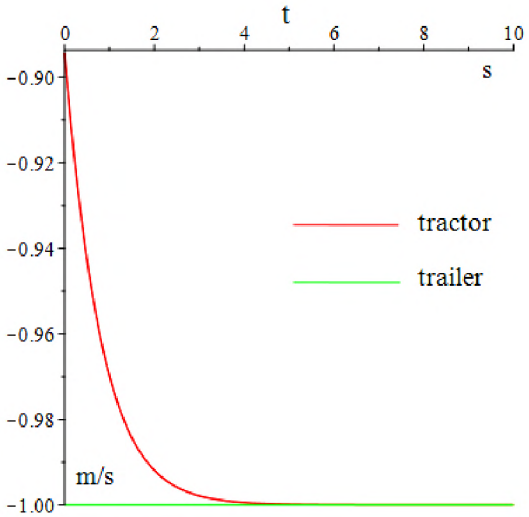

Fig. 17. Optimum stability of motion

Trailer speeds for other values of the length of the couplings (large and smaller than 4 m) are shown in **Fig. 18**.

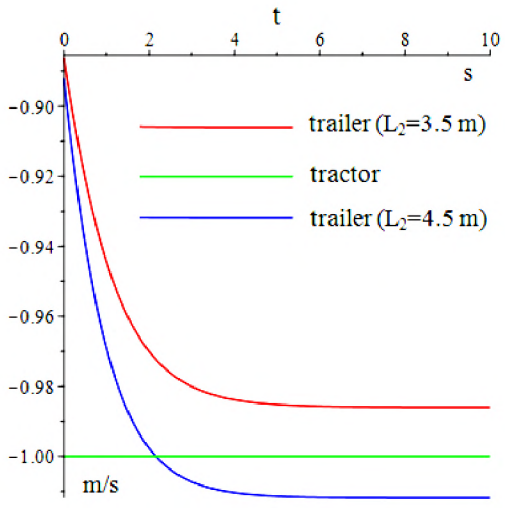

Fig. 18. Dynamics of trailer speeds for different coupling lengths (curvilinear motion)

For rectilinear motion (using the orientation controller and circular) with the condition or, changing the linear dimensions of the system has practically no effect on the amount of control. At the same time, the speed of the semitrailer maximally tends to the tractor speed (**Fig. 19**).

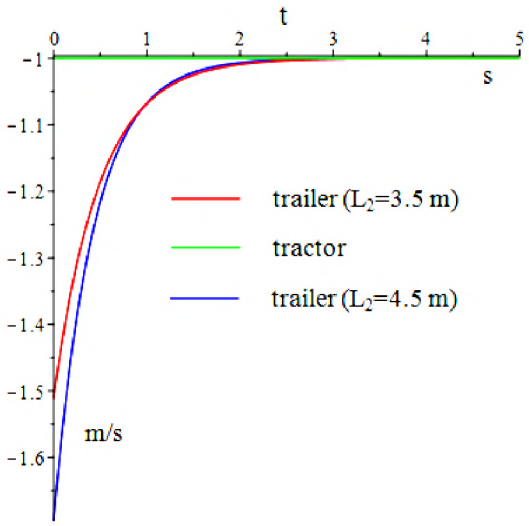

Fig. 19. Dynamics of orientation controller speeds

Thus, synthesized controllers can be useful in the development of robotic systems for their compliance with the necessary technological requirements.

8. Conclusions

1. A review of the existing complexes of theoretical and empirical methods is performed, the combination of which makes it possible to study the object with the greatest certainty in order to select the optimal mathematical apparatus for achieving the goal of synthesizing control laws for the reverse motion of a road train with coupling out.

2. The synthesis of such laws using the Lyapunov function method and using the Maple system for performing this synthesis, intermediate calculations and numerical integration of a system of differential equations is realized.

3. A control system has been synthesized for following a road train along a route curve defined by its curvature radius.

4. The features of the off-axle hitching model, determined by the ratio of its linear dimensions and the conditions for its maximum stability, are investigated.

5. A special feature of the study is that, unlike the approaches to synthesizing control laws for the studied model, the Lyapunov function method is used, we are not aware of the work on the synthesis of the orientation controller. The synthesized orientation controller now allows solving the problem of achieving the target by a road trains along the optimal trajectory within a certain reachable range without the use of switching. The efficiency of the method of Lyapunov functions will allow it to be used in the future in the backstepping method to solve the problem of reverse motion of road trains with an increasing number of links.

The practical value of this research is that synthesized control laws can now be applied for the programmatic management of the robot train. Such robotic system is under implementation. To control it, it is planned to integrate the synthesized controllers into a controller developed according to fuzzy logic.

In addition, the subject of further research will be the development of the Dubins machine based on synthesized control laws to ensure a stable rectilinear motion, with a given orientation angle and curvilinear, with a given radius to solve the problem of achieving the aim.

References

[1] Bolzern, P., DeSantis, R. M., Locatelli, A., Masciocchi, D. (1998). Path-tracking for articulated vehicles with off-axle hitching. IEEE Transactions on Control Systems Technology, 6 (4), 515–523. doi: 10.1109/87.701346

[2] Altafini, C. (2003). Path following with reduced off-tracking for multibody wheeled vehicles. IEEE Transactions on Control Systems Technology, 11 (4), 598–605. doi: 10.1109/tcst.2003.813374

[3] Murray, R. M., Sastry, S. S. (1993). Nonholonomic motion planning: steering using sinusoids. IEEE Transactions on Automatic Control, 38 (5), 700–716. doi: 10.1109/9.277235

[4] Fliess, M., Levine, J., Martin, P., Rouchon, P. (1995). Design of trajectory stabilizing feedback for driftless flat systems. Proc. 3rd European Control Conf. Rome, 1882–1887.

[5] Rouchon, P., Fliess, M., Levine, J., Martin, P. (1993). Flatness and motion planning: the car with n trailers. Proceedings of the 32nd IEEE Conference on Decision and Control. Available at: http://cas.ensmp.fr/~rouchon/publications/PR1993/ECC93.pdf

[6] Michalek, M. (2012). Application of the VFO method to set-point control for theN-trailer vehicle with off-axle hitching. International Journal of Control, 85 (5), 502–521. doi: 10.1080/00207179.2012.658524

[7] Sklyarenko, E. G., Shumakher, V. (2010). Stabilizatsiya zadnego khoda avtopoezda s dvukhosnym pritsepom metodom linearizatsii obratnoy svyaz'yu po sostoyaniyu. Visn. Nats. tekhn. un-tu «KHPI», 28, 275–278.

[8] Cheng, J., Wang, B., Zhang, Y., Xu, Y. (2016). Backward Path Tracking Control for Mobile Robot with Three Trailers. China, 32–41. doi: 10.1007/978-3-319-70136-3_4

[9] Evestedt, N., Ljungqvist, O., Axehill, D. (2016). Motion planning for a reversing general 2-trailer configuration using Closed-Loop RRT. 2016 IEEE/RSJ International Conference on Intelligent Robots and Systems (IROS), 3690–3697. doi: 10.1109/iros.2016.7759544

[10] Ardentov, A. A. (2016). Controlling of a mobile robot with a trailer and its nilpotent approximation. Regular and Chaotic Dynamics, 21 (7-8), 775–791. doi: 10.1134/s1560354716070017

[11] Martynyuk, A. A., Nikitina, N. V. (2018). O kachestvennom analize odnoy modeli transportnykh mashin. Prikladnaya mekhanika, 2, 110–115.

[12] Dubins, L. E. (1957). On Curves of Minimal Length with a Constraint on Average Curvature, and with Prescribed Initial and Terminal Positions and Tangents. American Journal of Mathematics, 79 (3), 497–516. doi: 10.2307/2372560

[13] Lyapunov, A. M. (1956). Collected Papers. Vol. 2. Moskow: Izd. Akd. Nauk SSSR, 472.

[14] Tatievskyi, D. (2017). The synthesis of steering rules for stabilizing road train reverse motion to solve the task of reaching a set goal. Technology Transfer: Fundamental Principles and Innovative Technical Solutions, 37–39. doi: 10.21303/2585-6847.2017.00482

[15] Cariou, C., Lenain, R., Thuilot, B., Berducat, M. (2010). Autonomous maneuver of a farm vehicle with a trailed implement: motion planner and lateral-longitudinal controllers. 2010 IEEE International Conference on Robotics and Automation. Anchorage. doi: 10.1109/robot.2010.5509447

[16] Lee, J.-H., Chung, W., Kim, M., Song, J.-B. (2004). A Passive Multiple Trailer System with Off-axle Hitching. International Journal of Control, Automation, and Systems, 2 (3), 289–297.

Original Research Article: full paper

(2018), «EUREKA: Physics and Engineering»
Number 2

THE PROPAGATION OF THE TEMPERATURE WAVE IN MYOCARDIUM

Vladyslav Shlykov
Department of Biomedical Engineering
National Technical University of Ukraine "Igor Sikorsky Kyiv Polytechnic Institute"
37 Peremogy ave., Kyiv, Ukraine, 03056
v.shlykov@kpi.ua

Abstract

The method for estimating the rate of propagation of temperature waves in the myocardium during hypothermia and hyperthermia of the heart based on noninvasive temperature control on the heart surface in conditions of cardiopulmonary bypass is proposed. The solution of the heat conduction equation for temperature waves in the myocardium is presented, which allows determining at each point of the medium the temperature change function, as well as the amplitude and phasing velocity of the temperature wave upon cooling and warming of the heart in conditions of cardiopulmonary bypass. The velocity distribution for the temperature field on the surface of the myocardium and in the depth of tissues during the hypothermia and hyperthermia of the heart is obtained.

The thermographic images of the heart during controlled hypothermia and hyperthermia of the heart under cardiopulmonary bypass are obtained. The study of the conditions for spreading the temperature wave in the myocardium is performed, which allows to improve the means of intraoperative protection of vital organs and tools for controlling its effectiveness. The results of introduction of methods of non-invasive temperature control in cardiac surgery and the process of intraoperative cardiac protection in the temperature range from +10 °C to +38 °C are presented.

Keywords: heart temperature, temperature waves, hypothermia, hyperthermia, cardiopulmonary bypass.

DOI: 10.21303/2461-4262.2018.00580

1. Introduction

The propagation of temperature waves in the heart during the process of hypothermia and hyperthermia is a periodic change in the temperature distribution in a homogeneous medium – the myocardium, which is associated with periodic fluctuations in the density of the heat flows entering the environment from the contour of cardiopulmonary bypass.

The temperature waves contain information on the properties of the myocardium (heat, temperature, conductivity, density) and the nature of the processes and phenomena that give rise to them (blood flow in the contour of artificial blood circulation, oscillatory processes of the temperature in the operating field, the frequency of rotation of the rollers of the cardiopulmonary bypass). Thermal conductivity is the main mechanism of transferring heat to tissues that are not directly exposed to heat, and the temperature is the main physical value that characterizes all thermal interactions in the myocardium with hypothermia and hyperthermia under artificial blood circulation.

The temperature waves in the myocardium are characterized by some features that distinguish them from electromagnetic and acoustic waves in biological objects. When distributed in biological tissues, the temperature waves are strongly suppressed with penetration, they are characterized by a significant variance – the dependence of the rate of propagation on the frequency of heat sources.

The change in the depth of penetration of the temperature wave depends on the frequency of thermal defectoscopy depending on the frequency, which allows them to be used to detect microcavities in the tissues, disturbance of blood supply and zones of ischemia in the myocardium.

2. Analysis of literary data and problem statement

In the conditions of artificial blood flow effects of uneven distribution of temperature in tissues of the human body appear during controlled cooling and warming of the heart and brain.

Useful and important empirical approaches are presented in several well-developed published studies [1–3]. The patterns of heartwarming are based on the method of contrast X-ray examination of blood vessels and a detailed experimental display of isolated hearts. In the above studies, the heat transfer in the myocardium is also measured by various experimental methods.

In a series of studies to obtain images that show the anisotropy of the tissues of the heart [4–6], the technique of diffusion tensor image was used. Such method of measuring the heat transfer can provide high-quality data that can be used in computer models.

Methods of study of temperature distribution [7], which are based on the empirical approach, can significantly help to verify the parameters of the models developed by the theoretical approach. But this requires correct averaging of the data obtained by displaying isolated samples of the heart. The most important issue of obtaining qualitative information about the coronary flow was not so easy to solve, since open heart operations for controlling the temperature available the only visible side of the heart. At the same time, modern devices and information technologies provide new solutions that can be useful in studies of temperature distribution and distribution of temperature waves in the myocardium.

3. The purpose and tasks of the study

The purpose of the work is studying the conditions for the propagation of the temperature wave in the myocardium and development of a method for evaluating the rate of propagation of temperature waves in the process of controlled hypothermia and hyperthermia on the basis of non-invasive control of temperature on the surface of the heart.

To achieve this purpose, the following tasks were set:

1. To solve heat conduction equation taking into account the influence of heat sources in the myocardium, which cause the occurrence of temperature waves.

2. To determine a temperature function in the layer of the myocardium, as well as the amplitude and phase velocity of the temperature wave during cooling and warming of the heart.

3. To get a dependence of the rate of distribution of the heat flow in the myocardium from the temperature in the layer of myocardium in the process of hypothermia and hyperthermia.

4. Materials and methods of research

The method of evaluation the rate of propagation the temperature waves in the myocardium in the process of hypothermia and hyperthermia of the heart is realized on the basis of non-invasive control of temperature on the surface of the heart under artificial blood circulation. For realization the method of noncontact control of temperature and digital processing of video data thermograms in conditions of artificial blood circulation, the FLIR i7 thermocouple with a spectral range of 7,5–13 microns is used on the basis of non-cooling digital matrix elements 320×240 size, minimum focal length 0,6 m and temperature sensitivity <1 °C. The FLIR i7 thermograph allows to obtain a sequence of infrared heart images at a frequency of 9 Hz, presented in the form of a sequence of frames. The obtained temperature distribution is the input data for solving the heat equation for temperature waves. The analysis of thermograms allows to determinate the function of distribution of temperature and rate of distribution of heat flux on the surface of the myocardium and at the depth of tissues in the process of hypothermia and hyperthermia of the heart under artificial blood circulation.

5. Temperature waves in the theory of thermal conductivity

For different degrees of temperature field heterogeneity, the flow velocity vector must satisfy the law of conservation of the mass of heat transferred, or the equation of continuity, which has the form [8]:

$$\frac{\partial \rho}{\partial t} + \mathrm{div}(\rho \vec{u}) = 0, \quad (1)$$

where $\vec{u}$ – vector of the heat flux rate, m/s, ρ – the density of the myocardium, kg/m^3, t – the time of distribution of heat flow, s.

Thus, the generalized differential equation of heat conduction taking into account the convection flow in the myocardium takes the form [9]:

$$\begin{cases} \rho C_p \dfrac{\partial T}{\partial t} + \operatorname{div}\left(\rho \vec{u} \dfrac{\partial T}{\partial t}\right) = -\operatorname{div}\left(\vec{q}_c\right) - \operatorname{div}\left(\vec{q}_R\right), \\ \dfrac{\partial \rho}{\partial t} + \operatorname{div}\left(\rho \vec{u}\right) = 0, \end{cases} \tag{2}$$

where C_ρ – the specific heat of the myocardium, J/(kg×K), q_C – the heat flux density due to heat transfer, q_R – the density of the heat flow due to heat transfer, W/m^2.

In the general one-dimensional case, the properties of the myocardium and the parameters characterizing the heat flux can vary in the same direction in which the flow occurs – in parallel with the axis X (**Fig. 1**). In addition, the heat flux can change over time. Therefore, the density of the flow of heat q(x, t) should be regarded as a function of coordinate x and time t.

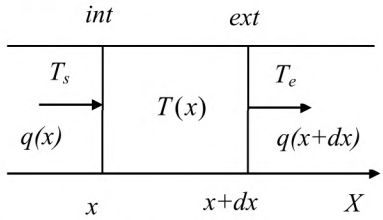

Fig. 1. The direction of the heat flow in the myocardium

To determine the thermal interaction at the boundary of two media, it is necessary to observe the condition equality of temperature and heat flows on both sides of the boundary of the section. The density of the heat flux q is a vector that coincides in the direction with the direction of heat propagation and is numerically equal to the amount of heat passing for one second through the area of the myocardium. To obtain the heat conduction equation for an infinitesimal area of the myocardium, one can consider a section of the surface in the form of a cylinder with forming, which is parallel to the axis X with a length dx. The amount of heat Q_{int} entering the cylinder due to the area of the cross section S in time dt, and the amount of heat Q_{ext} coming out at the same time through the cylinder's base, is:

$$Q_{int} - Q_{ext} = \left(q(x) - q(x + dx)\right) \cdot S \cdot dt = mC_\rho dT, \tag{3}$$

where m – mass of the cylinder (areas of the myocardium), dT – temperature change in myocardium.

If heat is not supplied through the lateral surface of the cylinder, then the total amount of heat entering the time dt through the examined part of the myocardium is determined by the formula:

$$\left(q(x) - q(x + dx)\right) \cdot S \cdot dt = -\left(\frac{\partial q(x,t)}{\partial x}\right) \cdot S \cdot dxdt. \tag{4}$$

Equating both expressions and making reductions, we obtain the equation of heat conductivity for an infinitely small part of the myocardium in the one-dimensional case:

$$\rho C_\rho \frac{\partial T}{\partial t} = -\frac{\partial q(x,t)}{\partial x}. \tag{5}$$

A heat flux occurs only when the temperature of the medium varies from one place to another. The simplest is the case of an infinite homogeneous medium – the thickness of the myocardium δ. If on one border of the myocardium (int) temperature is maintained as T_s, but on the other (ext) – temperature is T_e, and $T_s > T_e$, then the heat flux is proportional to the temperature ΔT. For infinite-

ly thin layer and the axis X is directed towards the lowering of temperature, then $\delta=dx$, $T_s=T(x)$, $T_e=T(x+dx)$, and the flow of heat in the myocardium is determined by the expression:

$$q_s = -\gamma_\rho \frac{(T_e - T_s)}{\delta} = -\gamma_\rho \frac{\partial T}{\partial x}, \quad (6)$$

where $\Delta T=T_s-T_e$ – temperature gradient in the myocardium in the direction of distribution of heat flow, °C, γ_ρ – coefficient of thermal conductivity of the myocardium, W/(m×K), which depends only on the physical properties of the myocardium.

The obtained formula is also valid in the case of an inhomogeneous medium with an arbitrary temperature distribution for all three spatial coordinates x, y, z, if consider the infinitely thin layer of the myocardium perpendicular to the direction of the heat flow. Such layer of myocardium can be considered homogeneous, and its thermal conductivity γ_ρ will be the function of all three spatial coordinates x, y, z. In one-dimensional case, the thermal conductivity will depend only on one spatial coordinate x: $\gamma_\rho=\gamma(x)$.

When the medium is homogeneous and the heat conductivity γ_ρ does not depend on temperature, let's obtain the solution of the heat conduction problem for an infinite small and homogeneous portion of the myocardium from one spatial coordinate:

$$\rho C_\rho \frac{\partial T}{\partial t} = -\frac{\partial^2 T}{\partial x^2} \text{ and } \frac{\partial T}{\partial t} = -\alpha \frac{\partial^2 T}{\partial x^2}, \quad (7)$$

where $\alpha=\gamma_\rho/\rho C_\rho$ – temperature conductivity of the medium (myocardium).

If the sources of heat present in the myocardium, which is characteristic for the process of starting the heart, then the equation of heat conductivity for a homogeneous site has the form:

$$\rho C_\rho \frac{\partial T}{\partial t} = -\frac{\partial^2 T}{\partial x^2} + q_j(x), \quad (8)$$

where q_j – the amount of heat released by sources in the volume of the myocardium.

The heat can be released, for example, as a result of perfusion or passing of an electric current through a myocardium.

6. The solution of the heat equation for temperature waves

The temperature waves in the myocardium are periodic changes in the distribution of temperature in the environment, associated with periodic fluctuations in the density of heat flowing from the cooling and warming of the heart. If in a myocardium the temperature periodically changes in time, it leads to periodic changes of temperature in all other parts of the heart. The validity of this statement is due to the fact that the variables x i t in the heat conduction equation, as well as the coefficient of thermal conductivity α are values of substance.

Let's accept the hypothesis that the temperature on the surface of the heart varies over time in a sinusoidal or cosine- law, fluctuating around some average value that is characteristic for convection of heat on the surface of the heart under artificial blood circulation. In the simplest case, when the myocardium is a homogeneous medium and fills the space limited by the plane x=0, and the direction of heat transfer is the axis X directed inside the medium and perpendicular to its boundary, the average value of the temperature fluctuation around a certain set value can be assumed to be zero if agree to deduct from it the temperature.

Then the complex function of changing the temperature in the myocardium has the form:

$$T(x,t) = T_s\left[\cos(\omega t - kx) + i\cdot\sin(\omega t - kx)\right] = T_s e^{i\cdot(\omega t - kx)}, \quad (9)$$

where k – constant value, ω – frequency change of direction of heat flow.

The differentiation of the temperature change function T(x, t) gives the following expressions:

$$\frac{\partial T}{\partial t} = i\omega T_0 e^{i(\omega t - kx)} = i\omega T, \quad \frac{\partial^2 T}{\partial x^2} = -k^2 T_s e^{i(\omega t - kx)} = -k^2 T. \tag{10}$$

Substituting these expressions into the heat conduction equation, we obtain the dependence of the temperature conductivity of the medium (myocardium) on the frequency of temperature fluctuations ω when heat convection on the heart surface:

$$i \cdot \omega = -\alpha \cdot k^2. \tag{11}$$

Execution of this condition means that the complex function of temperature change T(x, t) will be the solution of the heat equation for any value continuously T_s. If the value is ω is real and positive, then constant k will be a complex value, and may have two meanings:

$$k = \sqrt{-i\,\omega/\alpha} = \pm\sqrt{\omega/2\alpha}(1 - i). \tag{12}$$

Since the temperature fluctuations begin to be excited on the surface of the myocardium and transmitted to the environment, then these oscillations should creep as far away from the surface of the heart. Therefore, physical meaning has only an expression for the function of change in the myocardium temperature of the following type:

$$T(x) = T_s \exp\left(-\sqrt{\frac{\omega}{2\alpha}}x\right)\exp i\left(\omega t - \sqrt{\frac{\omega}{2\alpha}}x\right). \tag{13}$$

From the complex solution for the function of change in the myocardium temperature it is possible to go to the substance form using the Euler formula:

$$T(x) = \begin{cases} T_s \exp\left(-\sqrt{\frac{\omega}{2\alpha}}x\right)\cos\left(\omega t - \sqrt{\frac{\omega}{2\alpha}}x\right), \\ T_s \exp\left(-\sqrt{\frac{\omega}{2\alpha}}x\right)\sin\left(\omega t - \sqrt{\frac{\omega}{2\alpha}}x\right). \end{cases} \tag{14}$$

If fix the coordinate x, then at each point of space the function of temperature T(x, t) represents harmonic vibrations in time with the period $\tau=2\pi/\omega$ and the phase of these oscillations, which varies from one part of the medium to another. Perturbations, which describe at each point of space a function of temperature change T(x, t), represent a temperature wave propagating in a myocardium with a phase velocity υ. Length of the temperature wave λ is defined as the distance that passes through the wave for a periodτ:

$$\lambda = \upsilon\tau = 2\pi\sqrt{\pi\alpha\tau}. \tag{15}$$

The amplitude of the temperature wave decreases in the medium y e- times for each plot length $l=1/\alpha=\lambda/2\pi$ in the direction of wave propagation:

$$T(x) = T_s \exp(-\Omega \cdot x), \quad \Omega = \sqrt{\omega / 2\alpha} = 2\pi / \lambda, \tag{16}$$

where Ω – coefficient of attenuation of the temperature wave.

Limit and initial conditions that satisfy the solution for the temperature change function T(x, t), can be obtained if set the initial values x=0 and time t=0:

$$T_{t=0} = T_s \exp\left(-\sqrt{\frac{\omega}{2\alpha}}x\right)\cos\sqrt{\frac{\omega}{2\alpha}}x, \quad T_{x=0} = T_s \cos\omega t. \tag{17}$$

The heat equation retains the properties of linearity and homogeneity only in a given temperature range, in which the temperature conductivity γ_ρ myocardium is a constant value.

7. Temperature field in conditions of artificial blood circulation

The distribution of the temperature field in the myocardium describes the temperature values for all points of space at a given time. Since in the real conditions of artificial blood circulation the initial distribution of temperature can be arbitrary, the problem setting for finding the boundary conditions may be as follows:

– on the myocardium surface at a time t=0 harmonious fluctuations of temperature are excited, and then they are maintained indefinitely for a long time;

– no additional sources of heat other than blood coming from the contour of artificial blood circulation, inside the myocardium;

– at the end of a long period of time, all fluctuations of temperature in the environment are extinguished, except for forced oscillations;

– the forced oscillations will have the same periodicity in time as the temperature fluctuations on the surface of the myocardium.

The differential heat equation, which takes into account the rate of distribution of the heat flux in the medium for an infinitesimal area υ of the myocardium in the one-dimensional case, has the form:

$$\rho C_\rho\left(\frac{\partial T}{\partial t} + \upsilon\nabla T(x,t)\right) = -\nabla q(x,t), \tag{18}$$

where υ – the rate of distribution of the heat flow in the myocardium.

If the heat flow occurs at one boundary of the medium (int) with surface temperature T_s, extends along the axis X and is supported to the other boundary of the environment (ext) with temperature $T_e<T_s$, then at any point of a homogeneous layer of myocardium it can be described by the following expression:

$$-\gamma_\rho\frac{\partial T}{\partial x} = h_i\cdot\left(T - T_e\right), \quad h_i = C_\rho dT, \tag{19}$$

where h_i – heat transfer coefficient for the i – point in the myocardium. Substituting this expression into the formula for the equation of heat conductivity, we obtain the solution of the problem in time in one spatial coordinate – the axis X.

Substituting this expression into the formula for the equation of heat conductivity, let's obtain the solution of the problem in time in one spatial coordinate – the axis X:

$$-\frac{\partial}{\partial x}\left(\gamma_\rho\frac{\partial T}{\partial x}\right)_{x=i} = \frac{\partial}{\partial x}\left(-\gamma_\rho\frac{\partial T}{\partial x} + \rho h_i\upsilon_i\right). \tag{20}$$

For a small part of the myocardium, which is an infinitely thin layer δ=dx along the axis X, the change in the temperature field will be expressed in terms of expression:

$$\theta(x) = \frac{T - T_s}{T_e - T_s} = \left(\exp\left(\frac{\rho C_\rho\upsilon_i}{\gamma_\rho}x\right) - 1\right)\Big/\left(\exp\left(\frac{\rho C_\rho\upsilon_i}{\gamma_\rho}\delta\right) - 1\right), \tag{21}$$

where υ_i – the rate of distribution of heat flow for i – points of the environment.

Substituting this expression into the formula for the heat flow, let's obtain the heat transfer coefficient in the myocardium h_i for the i – point of the medium:

$$h_i = \rho C_\rho \upsilon_i \Big/ \left(\exp\left(\frac{\rho C_\rho \upsilon_i}{\gamma_\rho} \delta \right) - 1 \right). \tag{22}$$

Provided if in the selected temperature interval $dT=T_s-T_e$ given temperature of myocardium γ_ρ and the coefficient of heat transfer in the myocardium h_i is a constant, the differential equation of heat conductivity has the properties of linearity and homogeneity. This allows to solve the heat conduction equation with respect to the rate of distribution of the heat flow in the myocardium:

$$\upsilon(x,T) = -\frac{h}{\rho C_\rho} \frac{T_e - T_s}{T - T_s} W\left(-\exp\left(-\frac{h}{\gamma_\rho} \frac{T_e - T_s}{T - T_s} x \right) + 1 \right), \tag{23}$$

where W(x, t) is Lambert's function.

If limit the values $x \geq -1/e$ and believe that $W(x,t) \geq -1$, then Lambert's function is defined as an unambiguous function.

The solution to the problem of thermal conductivity shows that in the surface layer of the myocardium, temperature fluctuations can be established with a period $T=2\pi\omega$, which corresponds to the period of thermal waves of heat sources. Temperature fluctuations in the surface layer of the myocardium occur with a phase shift [10], so the depth of penetration of heat into the surface of the myocardium depends on the period of temperature fluctuations on the heart surface. The amplitude of the temperature wave in the surface layer is proportional to the depth:

$$T(x) = T_s \cdot \exp\left(-\omega \sqrt{\alpha} \cdot \chi \right), \tag{24}$$

where χ is time delay of maxima and minima of the temperature in the myocardium.

Taking into account the process of penetration of temperature waves into the depth of the surface layer of the myocardium let's obtain an expression for changing the temperature field, which depends on the frequency of temperature variations ω:

$$\frac{T(x) - T}{T} = \exp\left(-\sqrt{\frac{\omega}{2\alpha}} x \right) - 1. \tag{25}$$

The ratio shows that the longer the period of temperature fluctuations, the less depth of penetration of temperature waves in the depth of the myocardium [11]. A solution for the heat conduction problem taking into account the temperature waves in one spatial coordinate relative to the rate of distribution of the heat flow in the myocardium υ will be described by expression of the form:

$$\upsilon(x,\omega,T) = -\frac{h}{\rho C_\rho \theta(x)} \frac{T_s}{T - T_s} \left(\exp\left(-\sqrt{\frac{\omega}{2\alpha}} x \right) - 1 \right) \times$$
$$\times W\left(-\exp\left(-\frac{h}{\gamma_\rho} \frac{T_e - T_s}{T - T_s} x \right) + 1 \right). \tag{26}$$

Provided that the differential equation of heat conductivity has the properties of linearity and homogeneity, the expression for the rate of propagation of the heat flux has the form:

$$\upsilon(x,\omega,T) = -\frac{h}{\rho C_\rho} \frac{T_s \Delta T}{(T - T_s)^2} \left(\exp\left(-\sqrt{\frac{\omega}{2\alpha}} x \right) - 1 \right) \times$$
$$\times W\left(-\exp\left(-\frac{h}{\gamma_\rho} \frac{T_e - T_s}{T - T_s} x \right) + 1 \right). \tag{27}$$

8. Results of studies on the distribution of temperature in the myocardium

During controlled cooling and warming, the uneven distribution of temperature in tissues is manifested. In inflammatory processes in the myocardium, temperature zones are defined, in which the temperature difference with the surrounding tissues is recorded. With a chronic inflammation, the temperature difference is 0,7–1 °C, with acute illness1–1,5 °C, and when the destructive process reaches 1,5–2 °C [12, 13]. The propagation of the temperature wave on the myocardium surface can be observed in the process of hypothermia (**Fig. 2**) and hyperthermia (**Fig. 3**) of the heart, consistently recorded in conditions of artificial blood circulation [14].

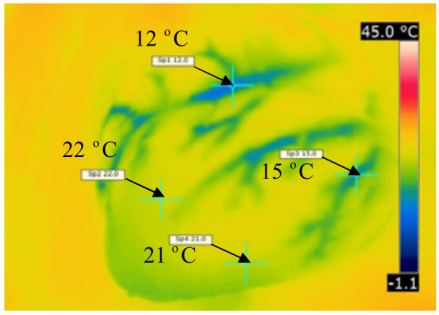

Fig. 2. Thermographic representation of temperature wave propagation on the surface of the myocardium for isolated heart in the process of controlled hypothermia

In the process of hypothermia and hyperthermia of the heart using a thermal imager, the temperature on the surface of the myocardium was not invasively recorded [15]. The temperature data on the surface of the myocardium (**Fig. 2, 3**) show the presence of a temperature difference in the coronary channel 2–3 °C, which indicates the heterogeneity of the temperature distribution on the myocardium surface under artificial blood circulation.

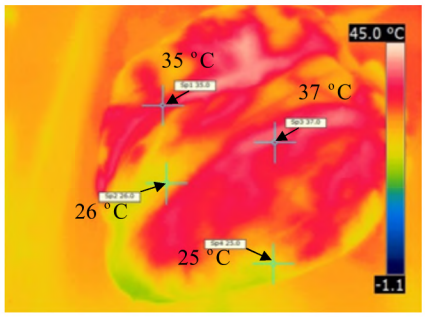

Fig. 3. Thermographic representation of the temperature wave propagation on the myocardium surface for the isolated heart in the process of controlled hyperthermia

As for the distribution of the temperature field, the initial temperature of the myocardium, recorded at the beginning of the process of cooling the isolated heart, was not less 21–22 °C and no more 25–26 °C at the beginning of warming up the heart. The temperature gradient between the tissues of the myocardium and the coronary solution is from 6 °C and more (to 10 °C). When warming the heart, the coronary bed in the myocardium stands out at a temperature gradient from 9 °C and more (to 12 °C).

The evaluation of the rate of propagation of temperature waves in the myocardium can be made on the basis of the obtained equation for the rate of the heat flux distribution $\upsilon(x, T)$ in moments of time t, which correspond to the completion of the processes of hypothermia and hyperthermia. For calculation of the rate of distribution of heat flow in the myocardium $\upsilon(x, T)$ the values of constant coefficients and physical parameters of tissues [16] and the values of the temperature of the walls of the myocardium were used:

T_s=23 °C – temperature of the external wall of the myocardium,

T_e=17 °C – temperature of the internal wall of the myocardium.

The rate of flow of heat in the myocardium depending on the temperature on the surface of the myocardium and the cooling depth along the axis X shown in **Fig. 4.**

The obtained dependences (**Fig. 4**) for the rate of the heat flow distribution in the myocardium υ(x, T) show that the magnitude of the rate of distribution of the heat flow in the absence of additional sources of heat in the myocardium is practically unchanged with the depth of penetration of the heat flow in the myocardium. The distribution of heat flux significantly depends substantially depends on the temperature on the surface of the heart, it increases in exponential law from the value $\upsilon=0{,}1\times10^{-3}$ m/s to size $\upsilon=1{,}5\times10^{-3}$ m/s with temperature rise.

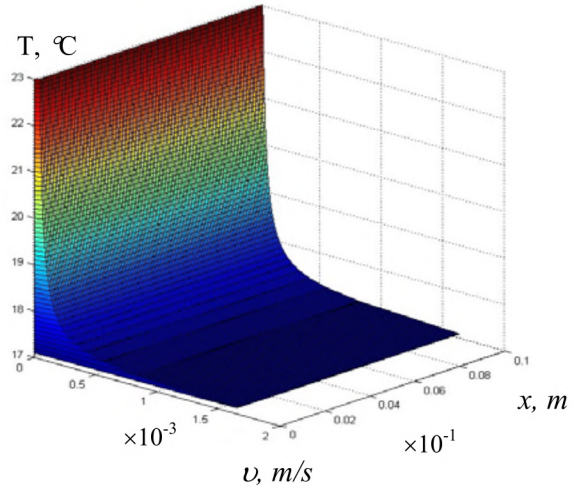

Fig. 4. Dependence of the rate of the heat distribution flow υ(x, T) in the myocardium from the temperature *T* in the depths *x* layer of myocardium.

The source of heat sources in the myocardium may be temperature waves due to uneven flow of cooled or warmed blood due to rotation of the rollers of the pump of the artificial blood circulation device. Accelerated the rate of distribution of heat flow in the depth of the myocardium υ(x, ω, T) taking into account temperature waves T(x) in the surface layer on one spatial coordinate, depending on the temperature difference between the outer and inner heart of the heart, is shown in **Fig. 5.**

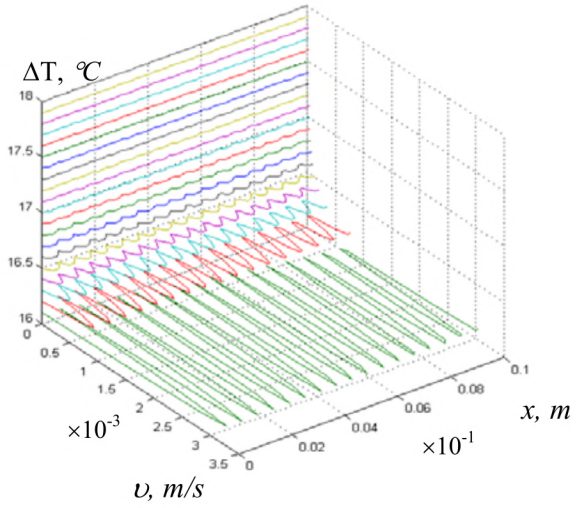

Fig. 5. Dependence of the rate from distribution of heat flow υ(x, ΔT) in the depths of x layer in temperature difference ΔT between the outer and inner walls of the myocardium, taking into account the temperature waves

Obtained dependencies (**Fig. 5**) for the rate of distribution of heat flow in the myocardium $\upsilon(x, \omega, T)$ show that for the frequency ω=250 rpm the amplitude of the temperature waves is maximal in the surface of the myocardium and significantly decreases in the direction of the propagation of the heat flux. Moreover, the rate of distribution of the heat flow in the myocardium significantly decreases from the value $\upsilon=2{,}5\times10^{-3}$ m/s at gradient ΔT=16 °C to size $\upsilon=0{,}1\times10^{-3}$ m/s at gradient ΔT=16,5 °C.

If to take into account that during the operation of the apparatus of artificial blood circulation the blood flow may warm up with a temperature gradient 0,2–0,5 °C or cool with a large gradient 0,5–1,7 °C then, taking into account the temperature waves in the homogeneous layer of the myocardium, the temperature between the external one T_e and inside T_s the wall of the myocardium changes the faster, the higher the density of the heat flow q_s through the surface with the thickness δ.

9. Conclusions

The overall reactivity and course of pathological processes in the myocardium are largely determined by the rate of propagation of temperature waves in the tissue layer. Moreover, the temperature difference between the blood in the contour and the patient's body should not differ by more than 15 °C. The temperature gradient between the blood in the vessels and the myocardium leads to a temperature difference between the outer and inner layer of the heart (**Fig. 4**), which, according to the function of the rate of propagation of the heat flux, changes in exponential law.

Periodic changes in the temperature in the operating field and in the circulatory circuit lead to the appearance of temperature waves on the surface and in the depth of the surface layer of the myocardium.

The estimated values of the rate of propagation of temperature waves in the myocardium under artificial blood circulation correspond to the density of the flow of heat in the process of hypothermia and hyperthermia of the heart, the regulation of which ensures the survival of the myocardium during the operation. Further studies of temperature wave propagation in the heart under artificial blood circulation should be directed to increasing the effectiveness of non-invasive methods for controlling temperature in order to determine the extent and location of contours of the coronary arteries, which will allow reliable and effective determination of the degree of absolute and relative violations of myocardial blood supply.

References

[1] Gurev, V., Lee, T., Constantino, J., Arevalo, H., Trayanova, N. A. (2010). Models of cardiac electromechanics based on individual hearts imaging data: Image-based electromechanical models of the heart. Biomechanics and Modeling in Mechanobiology, 10 (3), 295–306. doi: 10.1007/s10237-010-0235-5

[2] Vetter, F. J., McCulloch, A. D. (1998). Three-dimensional analysis of regional cardiac function: a model of rabbit ventricular anatomy. Progress in Biophysics and Molecular Biology, 69 (2-3), 157–183. doi: 10.1016/s0079-6107(98)00006-6

[3] Nickerson, D., Smith, N., Hunter, P. (2005). New developments in a strongly coupled cardiac electromechanical model. Europace, 7, 118–127. doi: 10.1016/j.eupc.2005.04.009

[4] Helm, P. A., Tseng, H.-J., Younes, L., McVeigh, E. R., Winslow, R. L. (2005). Ex vivo 3D diffusion tensor imaging and quantification of cardiac laminar structure. Magnetic Resonance in Medicine, 54 (4), 850–859. doi: 10.1002/mrm.20622

[5] Lunkenheimer, P. P., Redmann, K., Kling, N., Jiang, X., Rothaus, K., Cryer, C. W. et. al. (2006). Three-dimensional architecture of the left ventricular myocardium. The Anatomical Record Part A: Discoveries in Molecular, Cellular, and Evolutionary Biology, 288 (6), 565–578. doi: 10.1002/ar.a.20326

[6] Vadakkumpadan, F., Arevalo, H., Prassl, A. J., Chen, J., Kickinger, F., Kohl, P. et. al. (2010). Image-based models of cardiac structure in health and disease. Wiley Interdisciplinary Reviews: Systems Biology and Medicine, 2 (4), 489–506. doi: 10.1002/wsbm.76

[7] Helm, P., Beg, M. F., Miller, M. I., Winslow, R. L. (2005). Measuring and Mapping Cardiac Fiber and Laminar Architecture Using Diffusion Tensor MR Imaging. Annals of the New York Academy of Sciences, 1047 (1), 296–307. doi: 10.1196/annals.1341.026

[8] Sivukhin, D. V. (2005). Obshhiy kurs fiziki. Vol. 2. Termodinamika i molekulyarnaya fizika. Moscow: Fizmatlit/MFTI, 544.

[9] Lobasova, M. S., Finnikov, K. A., Milovidova, T. A., Dekterev, A. A., Serebrennikov, D. S., Minakov, A. V. (2009). Teplomassoobmen. Krasnoyarsk: IPK SFU, 295. Available at: http://files.lib.sfu-kras.ru/ebibl/umkd/1536/u_lecture.pdf

[10] Irodov, I. E. (1999). Volnovye protsessy. Osnovnye zakony. Moscow: Laboratoriya bazovykh znaniy, 256.

[11] Pushkareva, A. E. (2008). Metody matematicheskogo modelirovaniya v optike biotkani. Saint Petersburg: SPbGU ITMO, 103.

[12] Kotovskyi, V. Y. (2009). Obgruntuvannia vymoh do umov provedennia termohrafichnykh doslidzhen biolohichnykh ob`yektiv. Visti akademii inzhenernykh nauk Ukrainy, 2 (39), 6–11.

[13] Nicholas, A., Diakides, B., Joseph, D., Bronzino, A. (2008). Medical Infrared imaging. London: CRC Press Taylor Group LLC, 451.

[14] Ghosh, S., Falter, F., Cook, D. J. (Eds.) (2009). Cardiopulmonary Bypass. New York: Cambridge University Press, 207. Available at: https://suny-perfusion-knowledge.wikispaces.com/file/view/Cardiopulmonary+bypass+book+-+Ghosh.pdf

[15] Shlykov, V., Danilova, V., Maksymenko, V., Maryna, S. (2017). Application of Model of Heat Exchange for Miocardium Provided Stationary Convection Laminar Flow. Journal of Cardiology & Current Research, 10 (1). doi: 10.15406/jccr.2017.010.00350

[16] Lokshin, L. S., Lur'e, G. O., Dement'eva, I. I. (1998). Iskusstvennoe i vspomogatel'noe krovoobrashhenie v serdechno-sosudistoy khirurgii. Moscow: Nauchnyy tsentr khirurgii, Rossiyskaya akademiya meditsinskikh nauk, 93.

Original Research Article: full paper

(2018), «EUREKA: Physics and Engineering»
Number 2

RESEARCH ON USE OF LOW CONCENTRATION INVERSE SOLUBILITY POLYMERS IN WATER FOR HARDENING MACHINE COMPONENTS AND TOOLS

Nikolai Kobasko
Intensive Technologies Ltd
68/1 Peremohy ave., Kyiv, Ukraine, 03113
nkobasko@gmail.com

Anatolii Moskalenko
Institute of Engineering Thermophysics of NASU
2A Zhelyabova str., Kyiv, Ukraine, 03057
an.moskalenko@gmail.com

Volodymyr Dobryvechir
Intensive Technologies Ltd
68/1 Peremohy ave., Kyiv, Ukraine, 03113
dobrivecher@yahoo.com

Abstract

There is an optimal water concentration of inverse solubility polymers (1 %) where in many cases film boiling is absent. Based on accurate experimental data of French and data of authors, it was shown that during quenching from 875 oC in cold water solutions of optimal concentration film boiling is completely absent for those steel parts initial heat flux densities of which are below critical value. It is established that initial heat flux density decreases with increase sizes of tested samples. Initial process of quenching (formation of boundary boiling layer), which makes further history of cooling, is not investigated deeply and widely yet enough. When film boiling is absent, mathematical model includes only transient nucleate boiling process and convection. In this case, cooling time within the transient nucleate boiling process can be calculated using average effective Kondratjev numbers Kn. They were evaluated for inverse solubility polymers depending on their concentration and sizes of tested samples. As a result, an improved technology of hardening large gears and bearing rings is proposed by authors. Its essence consists in interruption of accelerated cooling or turning off agitation of quenchant when dissolving of surface polymeric layer starts. Examples of performing improved technology are provided by authors. Developments can be used by engineers to switch from carburized large gears quenched in oil to gears made of optimal hardenability steel and quenched in water solutions of optimal concentration.

Keywords: polymers of inverse solubility, optimal concentration, initial heat flux, boiling process, effective Kn numbers, recipes, large gears, improved technology.

DOI: 10.21303/2461-4262.2018.00582

1. Introduction

As a rule, water polymers are widely used in the practice as a quenchant of medium and high concentration (5 %, 10 %, 20 %, and rarely 30 %) to compete with mineral and vegetable oils. Cooling process is performed like in oil which continues almost to bath temperature. Standard cooling curves and cooling rates characteristics of water polymers are provided by manufactures to maintain polymeric quenchants within the given requirements. Cooling curves and cooling rates data cannot be used for making calculations and developing recipes. As a result, in heat treating industry sometimes a big distortion is observed after quenching machine components in water polymer solutions. Author [1] explained such behavior by non-uniform dissolving surface polymeric layer when quenching in water polymer solution of inverse solubility. Moreover, a long ago authors [2, 3] came to conclusion that low water concentration of inverse solubility polymers (≈1 %) provides maximal cooling rate of standard probes and this important fact in not yet used in the practice to intensify quenching processes. The goal of this paper is research concerning low concentration of water polymers solutions of inverse solubility for hardening machine components and tools like large gears of wind power stations, large bearing rings, rollers, etc. A method of calculation is dis-

cussed to prevent non-uniform dissolving of polymeric surface layer which can be performed by interruption the process of cooling or turning off the quenchant agitation. The results of investigations can be used by engineers for improving quality of hardened machine components and tools.

2. Initial and critical heat flux densities

To predict film boiling present during quenching steel parts or probes in liquids, one should compare initial heat flux density (q_{in}) with critical heat flux density (q_{crl}). If initial heat flux density is below the first critical heat flux density q_{crl}, film boiling is absent [4–6]. If it accedes q_{crl}, full film boiling takes place. It should be noted that initial processes taking place during immersion heated steel parts into cold liquid are not investigated yet. The cooling process starts as follows:

– At the very beginning steel parts or probes have initial temperature T_0 (850 °C) and quenchants have a temperature 20 °C.

– Within the time interval T_0–A (**Fig. 1**) the double electrical layer is formed when quenching in electrolytes or insulating surface layer is created when quenching in water solutions of inverse solubility polymers.

– When quenching in agitated water salt solution of optimal concentration, the time interval T_0–A is almost the same for different sizes and forms of steel parts.

– Within the time interval T_0–A the liquid of boundary layers is heated above of its boiling point to develop transient nucleate boiling process which starts at point A.

– Within the time interval T_0–A hyperbolic heat conductivity equation preferably should be used for calculating temperature field and initial heat flux density in steel parts or probes.

– After transient nucleate boiling starts, conventional parabolic heat conductivity (1) with the boundary condition (2) can be used.

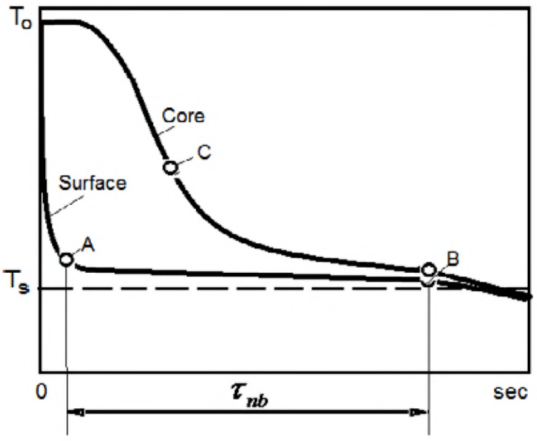

Fig. 1. A scheme explaining cooling time calculation during transient nucleate boiling process: T_0 is initial austenitzing temperature; A is initial surface temperature of developed transient nucleate boiling process; B is finish surface temperature of boiling process; C is core temperature of product for which cooling time should be calculated within interval AB; T_s is saturation temperature; τ_{nb} is duration of transient nucleate boiling process

To be sure that film boiling during quenching can be absent, authors calculated initial heat flux densities using own experimental data and experimental data of French shown in **Table 1** [7]. For solving inverse problem IQLab software was used [8]. More information on inverse problem one can find in literature [9–11]. Material thermal properties of probes are provided in **Table 2.** The main issue was to find out how size of probe affects initial heat flux density because standard probes are small and real steel parts are large. The results of calculations are shown in **Fig. 2, *a*, *b***.

When quenching spherical probe 12.7 mm in diameter from 875 °C in 5 % water solution of NaOH at 20 °C agitated with 0.914 m/s initial heat flux density is 17 MW/m^2 that is below q_{crl} for given concentration and agitation. It means that film boiling is absent. With increase the size of probe, initial

heat flux decreases (**Fig. 2, *b*).** It means that film boiling can be easily prevented for large steel parts. However, large steel part during quenching in liquid increases its average temperature that decreases critical heat flux density and by this way increases probability of existing film boiling. To prevent heating of quenchant, its volume should be appropriate and liquid should be agitated.

Table 1

Time required for the surface of steel spheres of different sizes to cool to different temperatures when quenched from 875 °C in 5 % water solution of NaOH at 20 °C agitated with 0.914 m/s (French, 1930)

Size, Inches, (mm)	Time, sec							
	700 °C	600 °C	500 °C	400 °C	300 °C	250 °C	200 °C	150 °C
0.5" (12.7)	0.028	0.042	0.058	0.071	0.11	0.15	0.26	0.60
4.75" (120.6)	0.043	0.066	0.09	0.12	0.17	0.21	0.29	0.95
7.15" (181.6)	0.040	0.070	0.100	0.140	0.240	0.310	0.42	1.15
11.25" (285.8)	0.043	0.120	0.190	0.330	0.570	0.960	1.26	2.18

Table 2

Thermal properties (diffusivity and conductivity) of Inconel 600 and stainless steel depending on temperature in °C

Temperature, °C	Inconel 600		Stainless steel AISI 304	
	$a \times 10^{-6}$, m^2/s	λ, W / mK	$a \times 10^{-6}$, m^2/s	λ, W / mK
100	3.7	14.2	4.55	17.5
200	4.1	16	4.63	18
250	4.3	16.9	4.66	18.8
300	4.5	17.8	4.7	19.6
400	4.8	19.7	4.95	21
500	5.1	21.7	5.34	23
600	5.4	23.7	5.65	24.8
700	5.6	25.9	5.83	26.3
800	5.8	26.3	6.19	27.8
900	6.0	28	6.55	29.3

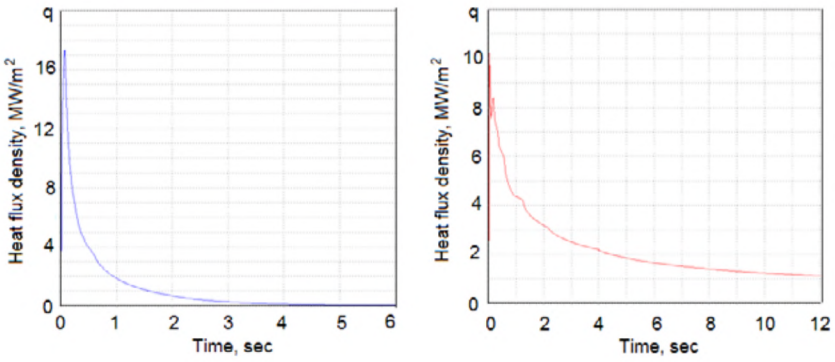

a *b*

Fig. 2. Heat flux density versus time when quenching spherical steel samples in 5 % water NaOH solution at 20 °C agitated with 0.914 m/s: *a* – 12.7 mm in diameter; *b* – 286 mm in diameter

According to investigations [4], very fast cooling increases critical heat flux density and it prevails the initial heat flux density that eliminates completely film boiling process.

3. Optimal concentration of inverse solubility polymers in water

As seen from **Fig. 3**, there is an optimal concentration of inverse solubility polymer in water where probability of destroying vapor blanker is maximal. This optimal concentration combined with agitation of quenchant can completely prevent film boiling during hardening.

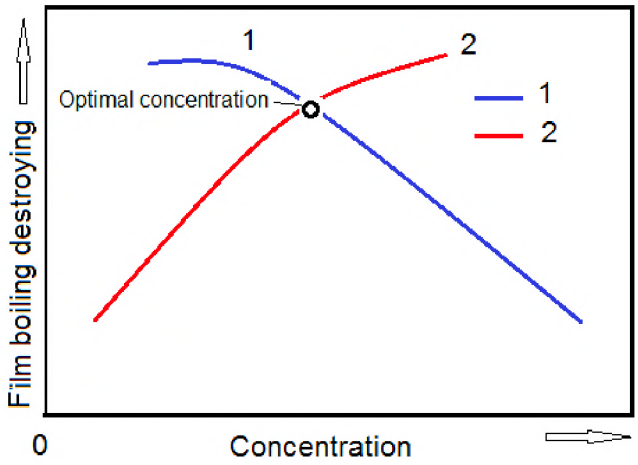

Fig. 3. Probability of film boiling destroying with decreasing the first critical heat flux density (curve 1) and formation of the surface insulating layer (curve 2) versus concentration of inverse solubility polymer in water

Our experiments showed that optimal concentration of inverse solubility polymers in water can be rather low (about 1 %) that makes a bath quenchant less expensive.

4. Cooling time calculation during quenching in polymers

If the film boiling process is absent and the transient nucleate boiling takes place immediately, the cooling process is governed by the following equations (1)–(6), [12–14]:

$$c\rho\frac{\partial T}{\partial \tau} = \mathrm{div}\left(\lambda \mathrm{grad} T\right), \tag{1}$$

$$\left[\frac{\partial T}{\partial r} + \frac{\beta^m}{\lambda}\left(T - T_S\right)^m\right]_{r=R} = 0, \tag{2}$$

$$T\left(r,0\right) = T_0. \tag{3}$$

After transient boiling process is completed, a convection mode of heat transfer starts and the third kind of boundary condition (4) is used instead of boundary condition (2):

$$\left[\frac{\partial T}{\partial r} + \frac{\alpha_{conv}}{\lambda}\left(T - T_m\right)\right]_{r=R} = 0. \tag{4}$$

The initial temperature for the convection mode is the temperature distribution at the end of the transient nucleate boiling process:

$$T\left(r,0\right) = T\left(r,\tau_{conv}\right). \tag{5}$$

It means that

$$T\left(r,\tau_{nb}^{\ end}\right)=T\left(r,\tau_{conv}^{\ start}\right)$$

and it's chosen as an initial condition for the convection mode.

A transition from the nucleate boiling process to the convective mode of heat transfer is determined by equalizing the heat fluxes and the end of boiling and at the beginning of convection (6), i. e.

$$q_{nb}\equiv q_{conv}. \tag{6}$$

A generalized equation for calculating duration of the transient nucleate boiling process, based on solution of Eq. (1)–(3), was proposed [15]:

$$\tau_{nb}=\Omega k_F\frac{D^2}{a}. \tag{7}$$

The value of Ω is a function of the convective Biot number.

According to author [1, 15], an average effective Kondratjev number Kn can be find which allows calculating cooling time within the transient boiling nucleate boiling process using simple Eq. (8):

$$\frac{a\tau}{K}=\frac{0.24k+\ln\theta}{Kn}. \tag{8}$$

Fig. 4 provides average effective Kondratjev numbers Kn for inverse solubility polymers of different concentrations.

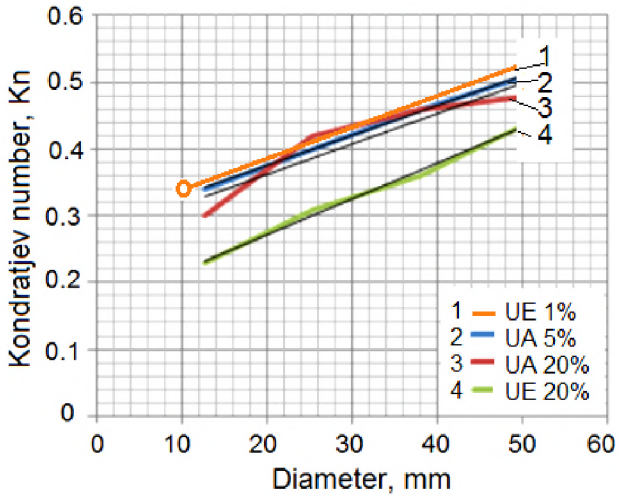

Fig. 4. Effective Kondrtjev numbers Kn for inverse solubility water solutions of polymers depending on their concentrations and size of product: 1 is 1 % of UCON E in water; 2 is 5 % of UCON A in water; 3 is 20 % of UCON A in water; 4 is 20 % of UCON E in water at 20°C

New results in **Fig. 4** are data concerning 1 % UCON E in water at 20 °C depending on size of probes changing from 10 mm to 50 mm in thickness.

Obtained data from **Fig. 4** and Kondratjev form coefficients K from **Table 3** allow calculating cooling recipes when quenching steel parts in water solutions of inverse solubility polymers. Principal scheme of quenching process is shown in **Fig. 5.**

Table 3

Kondratjev coefficients K depending on different shapes and sizes of solid bodies [16]

Shape	Kondratjev coefficient K, m^2
Slab of thickness L	$\frac{L^2}{\pi^2}$
Infinite cylinder of radius R	$\frac{R^2}{5.784}$
Infinite square bar with sides of L	$\frac{L^2}{2\pi^2}$
Cylinder of radius R and height Z	$\frac{1}{\frac{5.784}{R^2}+\frac{\pi^2}{Z^2}}$
Plate with sides L_1, L_2, L_3	$\frac{1}{\pi^2\left(\frac{1}{L_1^2}+\frac{1}{L_2^2}+\frac{1}{L_3^2}\right)}$
Sphere	$\frac{R^2}{\pi^2}$

Note: R is radius, L is thickness, Z is height

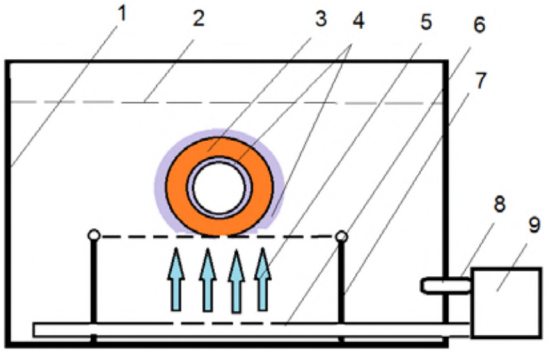

Fig. 5. Prinsipal scheme of performing IQ -2 process with use of low concentration polymers: 1 is quench tank; 2 is level quenchant in a tank; 3 is steel parft (large gear or large bearing ring); 4 is surface polymeric layer; 5 is liquid stream; 6 is perforated tube; 7 is holder; 8 is outlet tube; 9 is pump

An example

A large ring 40 mm in thickness and 120 mm height, made of AISI 52100 steel, is quenched from 860 °C in 1 % water solution of inverse solubility polymer agitated with 0.5 m/s (**Fig. 5)**. To prevent dissolving surface polymeric layer which causes distortion of a ring, cooling should be interrupted when core temperature approaches 400 °C. For calculating cooling time Eq. (8) is used.

Initial data: k=1;

$$K = \frac{1}{\frac{9.87}{0.04^2}+\frac{9.87}{0.12^2}} = 145.7\times10^{-6}\,m^2 \text{ (Table 3)};$$

$$a = 5.36\times10^{-6}\,m^2/s;$$

Kn=0.48 (**Fig. 4**);

$$\text{Ln}\theta = \text{Ln}\frac{860\ ^{\circ}\text{C} - 20\ ^{\circ}\text{C}}{400\ ^{\circ}\text{C} - 20\ ^{\circ}\text{C}} = 0.793.$$

According to Eq. (8) interruption cooling time is:

$$\tau = (0.24 + 0.783) \times \frac{145.7 \times 10^{-6}\ \text{m}^2}{5.36 \times 10^{-6}\ \text{m}^2/\text{s} \times 0.48} = 58\ \text{s}.$$

6. Discussion

At present time wind power stations (wind mills) are working worldwide to provide the potential economic, environmental, and social benefits. In the USA plan is to supply by wind mills 10 % of the nation's electrical demand in 2020, 20 % in 2030, and 35 % in 2050. The main attention is paid to reducing the cost of electricity, and accelerating the deployment of wind power. The typical wind power station (wind mill) containing large gears is shown in **Fig. 6** [22].

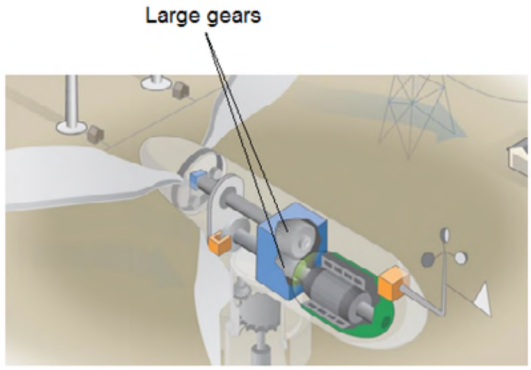

Fig. 6. Typical wind mill station containing large gears [22]

That is why decreasing cost of large gears and increasing their service life is very important. Authors of the paper are proposing to manufacture large gears from alloy low hardenability steel [23] and quench them in agitated 1 % water solution of inverse solubility polymers to eliminate carburizing process, improve resistance against corrosion and increase service life of large gears. Further work in this field is needed to investigate properly initial hardening processes including crisis of boiling to provide correctly boundary condition for hyperbolic heat conductivity equations used for governing initial quenching processes [24–26]. Also, extremely important is problem concerning protection gears from corrosion [27]. Authors believe that tendency to corrosion of gears will decrease if carburizing process is eliminated.

However, accelerated hardening of complicated steel parts requires control of cooling process and its interruption at proper time that is possible when process is automated and special software for developed technology is available. Currently, the problem is being solved by Intensive Technologies Ltd (ITL), Kyiv, Ukraine.

7. Conclusions

1. There is an optimal low concentration (≈1 %) of inverse solubility polymers in water where film boiling is absent.

2. During quenching machine components and tools in optimal concentration of inverse solubility polymers, film boiling is completely absent due to initial heat flux density is below critical value caused by creation of the surface insulating layer.

3. When diameter of spherical probe increases from 12.7 mm to 286 mm, initial heat flux density during quenching in electrolytes decreases from 17.2 MW/m^2 to 10.2 MW/m^2. That simplifies preventing film boiling process during quenching large steel parts in water solution of poly-

mers due to increased size of real steel parts and presence on their surfaces insulating layer that decreases initial heat flux density.

4. Low concentration of inverse solubility polymers can be used as a perfect quenchant for hardening large steel parts like large bearing rings, large gears for wind power stations, rollers, etc.

5. Accelerated quenching in water solutions of polymers should be interrupted before polymeric surface layer at the bottom of a load is dissolved that prevents quench crack formation and decreases cardinally distortion. For this purpose IQCalc2 software can be used which is available from Intensive Technologies Ltd, Kyiv, Ukraine.

6. To perform correctly cooling time interruptions, authors experimentally evaluated effective dimensionless Kondratjev numbers Kn for polymers of inverse solubility depending on their concentration and size of machine components (**Fig. 4**).

7. In contrast to existing cooling curves and cooling rates data provided by manufactures, authors of the paper proposed simplified method of cooling time calculation in water solutions of polymers to decrease distortion and increase service life of hardened machine components in two or more times [13].

8. Further investigations in the field are needed; especially initial process of quenching requires careful investigations to study critical heat flux densities and mechanism of surface polymeric layer formation.

References

[1] Kobasko, N. (2017). Cooling intensity of inverse solubility polyalkylene glykol polymers and some results of investigations focused on minimizing distortion of metal components. EUREKA: Physics and Engineering, 2, 55–62. doi: 10.21303/2461-4262.2017.00294

[2] Kobasko, N. I., Moskalenko, A. A. (1996). Intensification the methods of quenching by means of use water polymer solutions. Promyshlennaya Teplotekhnika, 18 (6), 55–60.

[3] Moskalenko, A. A., Kobasko, N. I., Tolmacheva, O. V., Totten, G. E., Webster, G. M. (1996). Quechants Characterization by Acoustical Noise Analysis of Cooling Properties of Aqueous Poly (Alkylene Glycol) Polymer Quenchants. Proceedings of the Second International Conference on Quenching and Control of the Distortion. Cleveland: Cleveland Marriott Society Center, 117–122.

[4] Tolubinsky, V. I. (1980). Teploobmen pri kipenii [Heat transfer at boiling]. Kyiv: Naukova Dumka, 320.

[5] Kutateladze, S. S. (1963). Fundamentals of Heat Transfer. New York: Academic Press, 485.

[6] Kutateladze, S. S. (1950). Hydrodynamic Crisis Model of Heat Transfer in Boiling Liquid at Free Convection. Journal of Engineering Physics, 20 (11), 1389–1392.

[7] French, H. J. (1930). The Quenching of Steels. Cleveland: American Society for Steel Treating, 177.

[8] Kobasko, N. I., Dobryvechir, V. V. (2010). Inverse Problems in Quench Process Design. Intensive Quenching Systems: Engineering and Design. West Conshohocken: ASTM International USA, 210–229.

[9] Tikhonov, A. N., Glasko, V. B. (1967). On the Issue of Methods of Determination of the Part's Surface Temperature. Journal of Computational Mathematics and Mathematical Physics, 7 (4), 910–914.

[10] Alifanov, O. M. (1975). Outer Inverse Heat Conduction Problems. Eng. Phys. Jour., 29 (1), 13–25.

[11] Beck, J. V., Osman, A. M. (1992). Analysis of Quenching and Heat Treating Processes Using Inverse Heat Transfer Method. Proceedings of Quenching and Distortion Control Conference. Chicago: ASM International, 147–154.

[12] Lykov, A. V. (1967). Teoriya Teploprovodnosti [Theory of Heat Conductivity]. Moscow: Vyschaya Shkola, 596.

[13] Kobasko, N. I., Aronov, M. A., Powell, J. A., Totten, G. E. (2010). Intensive Quenching Systems: Engineering and Design. West Conshohocken, ASTM International, 234. doi: 10.1520/mnl64-eb

[14] Guseynov, Sh. E., Buikis, A., Kobasko, N. I. (2006). Mathematical statement of a problem with the hyperbolic heat transfer equation for the intensive steel quenching processes and its analytical solution. Equipment and Technologies for Heat Treatment of Metals and Alloys (OTTOM-7). Kharkov, 2, 22–27.

[15] Kobasko, N. I. (2009). Transient Nucleate Boiling as a Law of Nature and a Basis for Designing of IQ Technologies. Proc. of the 7th IASME/WSEAS International Conference on Heat Transfer, Thermal Engineering and Environment (HTE'09). Moscow, 67–76.

[16] Kondratev, G. M. (1957). Teplovye Izmereniya [Thermal Measurements]. Moscow: Mashgiz, 245.

[17] Liscic, B., Tensi, H. M., Luty, W. (Eds.) (1992). Theory and Technology of Quenching. Berlin, Heidelberg: Springer, 484. doi: 10.1007/978-3-662-01596-4

[18] Liscic, B., Tensi, H., Canale, L., Totten, G. (Eds.) (2010). Quenching Theory and Technology. Boca Raton: CRC Press, 725. doi: 10.1201/9781420009163

[19] Dossett, J. I., Totten, G. E. (Eds.) (2013). ASM Handbook. Vol. 4A: Steel Heat Treating Fundamentals and Processes. ASM International, 784.

[20] Totten, G. E., Bates, C. E., Clinton, M. A. (1993). Handbook of Quenchants and Quenching Technology. Ohio: ASM International, Materials Park, 507.

[21] Totten, G., Howes, M., Inouer, T. (Eds.) (2002). Handbook of Residual Stress and Deformation of Steel. Ohio: ASM International, Materials Park, 499.

[22] How do Wind Turbines Work. A New Era for Wind Power in the United States. Wind Energy Technologies Office. Available at: https://www.energy.gov/eere/wind/how-do-wind-turbines-work

[23] Kobasko, N. I. (2017). Pat. 114174 UA. Alloyed Low Hardenability Steel and Method of its Designing. MPK C22C 38/40, C22C 38/12, C21D 1/18, C22C 38/24, C22C 38/08, C22C 38/46, C21D 9/00. No. a 2013 11311; declareted: 23.09.2013; published: 10.05.2017, Bul. No. 9.

[24] Liscic, B. (2003). Critical Heat-Flux Densities, Quenching Intensity and Heat Extraction Dynamics During Quenching in Vaporizable Liquids. Proceedings of the 4th International Conference on Quenching and the Control of Distortion. Beijing, 21–28.

[25] Buikis, A. (2009). Some new models and their solutions for intensive steel quenching. Daugavpils, 27–30.

[26] Buikis, A., Buike, M., Vilums, R. (2017). Several Intensive Steel Quenching and Wave Power Models. WSEAS transactions on heat and mass transfer, 12, 107–121.

[27] Hermann, S., Holm, A.-P. (2009). Protecting Gears in Wind Power Applications. Available at: http://gearsolutions.com/article/detail/5882/protecting-gears-in-wind-power-applications

Original Research Article: full paper

(2018), «EUREKA: Physics and Engineering»
Number 2

METHOD OF OBTAINING APPROXIMATE FORMULAS

Konstantin Ludanov
Institute for Renewable Energy NAS of Ukraine
20A Gnata Hotkevicha str., Kyiv, Ukraine, 02094
k.i.ludanov@ukr.net

Abstract

The two-parameter method of approximating the sum of a power series in terms of its first three terms of the expansion, which allows one to obtain analytic approximations of various functions, decomposes into a Maclaurin series. As an approximation function of this approximation, it is proposed to use elementary functions constructed in the Nth degree, but with a "compressed" or "stretched" variable x due to the introduction of the numerical factor M ($x \equiv \varepsilon \cdot m$, $M \neq 0$) into it. The use of this method makes it possible to significantly increase the range of very accurate approximation of the obtained approximate function with respect to a similar range of the output fragment of a series of three terms. Expressions for both the approximation parameters (M and N) are obtained in a general form and are determined by the coefficients of the second and third terms of the Maclaurin series. Also expressions of both approximation parameters are found for the case if the basis function and the approximant function decompose into the Maclaurin series in even powers of the argument. A number of examples of approximation of functions on the basis of the analysis of power series into which they decompose are given.

Keywords: approximation of functions, power series expansion, Maclaurin series, sum of a power series, two-parameter approximation, Newton's binomial.

DOI: 10.21303/2461-4262.2018.00589

1. Introduction

In the analysis of fundamentally important regularities, from which our understanding of new phenomena develops, the role of analytical methods remains extremely high. Their role is also high in the qualitative determination of the parameters of complex physical phenomena, noted in [1]. Therefore, various methods of perturbation theory are so important, which are the main analytical tool for investigating nonlinear physical and technical problems. It is usually possible to calculate only a few terms of the perturbed decomposition, usually no more than two or three. The resulting rows often converge slowly or even diverge. Nevertheless, these several members contain significant information, from which it is necessary to extract all that is possible, is summarized in [2].

How important is the approximation method, which approximates not only the values of the approximating function-basis, but its derivatives, is noted by Russian mathematicians [3] who believe that in the case of an analytically given function it is often useful to replace a too complicated mathematical expression with a simpler one, the basic properties of the function are preserved. Indeed, when approximation of functions is important, not only the accuracy of the approximation, but also the form and properties of the approximating function is important. This is due to the fact that often the approximating function must correspond to the physics of the investigated process. A more accurate reflection of the physics of the process can often be achieved by approximating the function together with the derivatives. Approximating approximations with a small number of parameters have become most widespread in practical investigations. Such expressions are more easily amenable to physical interpretation [3].

Thus, it is very important to develop new methods for reconstructing unknown functions from small fragments of power series into which they decompose, as well as to search for simple approximations for complex functions based on the use of their decompositions into Maclaurin series. Such methods will make it possible to significantly increase the range of their exact approximation, and also to be able to interpret experimental data within the framework of linear dependence in the event that the variable in a complex function is implicitly expressed.

2. Literature review and problem statement

Historically, the first method of accelerating the convergence of power series is the fractional-rational transformation of a variable (small parameter) in the form of an Euler transformation:

$\mathbf{x}=\varepsilon/(1+\varepsilon)$, [2]. The goal of the Euler transformation is the transfer of the singularity $\varepsilon=-1$ to the point at infinity. Moreover, if there are no other singularities in the complex plane, then the radius of convergence of the series becomes infinite [2, 4].

From the low-parametric methods of approximation in mechanics, the so-called Shanks "nonlinear transformation" is rather well known. It consists precisely in approximating the sum of the power series in terms of its first three terms. The application of the Shanks nonlinear transformation to the first three terms of the power series $\sum=1+a\varepsilon+b\varepsilon^2+\ldots$ gives a simple rational fraction

$$\sum=[a+(a^2-b)\varepsilon]/(a-b\varepsilon),$$

which is often a more accurate approximation to the sum of the series than its fragment representing the sum of the original three terms. For example, this sum gives an exact value if the series is a geometric progression (both convergent and divergent) [4].

The problem of maximizing the extraction of such information is usually solved by methods of approximating the sum of a power series (Maclaurin) by analytic functions with respect to the coefficients of the first terms of the expansion. The most powerful method of approximation is the Padé method [5–7], in which it is carried out in the framework of approximation by rational functions. However, in many cases [8], the Padé approximation method is unacceptable in principle. First, when as a basis for approximation it is necessary to use non-rational, and other functions, for example, trigonometric. Or when in the solution by the method of a small parameter only a few terms of the expansion are obtained, the coefficients of which must then receive a certain physical interpretation.

In cases when the formula approximating the exact expression or the fragment of the power series into which this expression decomposes, it is sufficient to coincide only the first two derivatives of this function, the most optimal solution is the use of two-parameter approximations of the sum of the Maclaurin series.

In this sense, the most promising method for approximating the sum of a power series in terms of its first three terms is the Ludanov method [9], which abstract (9B 832 DEP) was published in the RZh "Matematika" more than thirty years ago (in No. 9, 1984). A method is developed for two-parameter approximation of the power series of Maclaurin with respect to its first three terms in the form of the Nth power of an arbitrary elementary function y(x) in which the variable x is written as the product of the argument ε by the parameter **M** ($x=\mathbf{M}\varepsilon$).

3. Methods of research

To solve this problem, a powerful method such as the theory of power series was used in this paper. According to Euler [4], there are an infinite number of functions, each of which has an excellent expression for the power series into which it decomposes. Mathematical operations on functions are equivalent to operations on their power series. Analysis of the combination of two mathematical operations on power series: the construction of the Maclaurin series in the Nth power and the introduction of the factor in the composition of its variable ($x=\mathbf{M}\varepsilon$), showed the possibility of obtaining an identical decomposition (in fact of some function) of an identical fragment from the first three terms of the series of the elementary function thus modified. This mathematical fact formed the basis for the development of a new method for obtaining approximate formulas, which in the presence of many advantages has a significant drawback: a not very large range of exact approximation. But in many practical cases this approximation accuracy is quite sufficient.

4. Research results

4. 1. Approximation of functions that decompose into a power series in the variable *x*

Let's consider the general case when, as a result of solving a nonlinear problem, a fragment of the Maclaurin series is obtained:

$$\sum c_i\varepsilon^i=1+a\varepsilon+b\varepsilon^2+\ldots, \quad (1)$$

the sum of which should be approximated as the Nth power of the function f(x) (where x=**M**·ε), chosen on the basis of additional considerations (for example, in accordance with the physics of the described phenomenon).

The expansion of the function **y**=f^N in the Maclaurin series has the following form:

$$\mathbf{y}(x)=1+\mathbf{y}'_{(0)}\frac{x}{1!}+\mathbf{y}''_{(0)}\frac{x^2}{2!}+..., \tag{2}$$

Let's express the derivatives $\mathbf{y}'_{(0)}\,\mathbf{y}''_{(0)}$ in terms of the corresponding derivatives of the chosen function $f_{(x)}$

$$\mathbf{y}'_{(0)}=\mathbf{N}\cdot f^{N-1}{}_{(0)}\cdot f'_{(x)},$$

$$\mathbf{y}''_{(0)}=\mathbf{N}\cdot f^{N-2}{}_{(0)}\cdot[(N-1)(f'_{(x)})^2+f_{(x)}f''_{(x)}]. \tag{3}$$

At the point of expansion x=0 for (3) let's obtain:

$$\mathbf{y}'_{(0)}=N\cdot f'_{(x)},$$

$$\mathbf{y}''_{(0)}=N\cdot[(N-1)\cdot(f'_{(0)})^2+f''_{(0)}]. \tag{4}$$

Taking into account the fact that x=Mε, the series (2) can be rewritten as:

$$f^N{}_{(M\varepsilon)}=1+N\cdot f'_{(0)}\cdot M\frac{\varepsilon}{1!}+N\cdot[(N-1)\cdot(f'_{(0)})^2+f''_{(0)}]\cdot M^2\frac{\varepsilon^2}{2!}+\ldots \tag{5}$$

Equating the coefficients of the corresponding powers of the variable ε for the series (1) and (5), let's obtain a system of two equations with two unknowns:

$$\begin{cases} a=M\cdot N\cdot f'_{(0)}, \\ b=(M^2\cdot N/2)\cdot\left[(N-1)\cdot(f'_{(0)})^2+f''_{(0)}\right]. \end{cases} \tag{6}$$

Solving the obtained system of equations for the unknown parameters M and N, we obtain their expressions through the known coefficients a and b of the series (1) and the derivatives of the function $f_{(x)}$ chosen as the basis for the approximation f′(x) and f″(x) in point (0,1):

$$N=(a/f'_{(0)})^2\cdot[f''_{(0)}-(f'_{(0)})^2]/(2b-a^2);$$

$$M=(f'_{(0)}/a)\cdot(2b-a^2)/[f''_{(0)}-(f'_{(0)})^2]. \tag{7}$$

A particularly simple expression for the parameters M and N is in the case when the function f (x) is used as the function f (x)=1+x. In addition, the function y (x) is obviously expressed in the form of a Newton binomial $y(x)=(1+x)^N$.

The first and second derivatives in this case take the values f (x)=1, f (x)=0. And the approximation parameters take the following values:

$$M=a\cdot(1-2b/a^2),\ N=(1-2b/a^2)^{-1}. \tag{8}$$

The same values of the parameters M and N can also be obtained directly, i. e. equating the coefficients a and b of the series (1) to the coefficients for the corresponding powers of the binomial series:

$$(1+M\cdot\varepsilon)^N=1+N\cdot M\cdot\frac{\varepsilon}{1!}+N\cdot(N-1)\cdot M^2\cdot\frac{\varepsilon^2}{2!}+... \tag{9}$$

Here, it should be noted that if the series (1) is a geometric progression (for $b=a^2$), then the approximation of this sum in the Newton binomial for $y=(1+M\cdot\varepsilon)^N$ gives its exact value, as well as the Shanks nonlinear transformation:

$$[a+(a^2-b)\cdot\varepsilon]/(a-b\cdot\varepsilon)\big|_{a^2=b}=(1-a\cdot\varepsilon)^{-1}. \quad (10)$$

The values of the approximation parameters obtained in this case ($b=a^2$) from (8) are equal to $M=-a$, $N=-1$, i. e. coincide with the parameters of the right-hand side of (10), the exact expression for the sum of the geometric progression.

Example 1

Let's compare the error of approximation with the developed method with the error of the well-known Padé approximation method. Let's consider here an example given in [7], where an approximation is given of a fragment of the Maclaurin series (i. e., its first three terms) into which the function $\mathbf{y}(z)=[\ln(1+z)]/z=1-z/2+z^2/3-...$ In [7] three Padé approximations are given: [1/0], [0/1] and the most accurate of them $[1/1]=(1+z/6)/(1+2\cdot z/3)$, which gives an error of 1 % for z=1. If the approximated series is approximated by a new method, for example, within the framework of Newton binomial (in this case, the values of the approximation parameters calculated according to formulas (8): M=5/6, and N=3/5), then let's obtain the approximate formula $\mathbf{y}(z)=(1+5\cdot z/6)^{-0,6}$, which for z=1 gives an error of less than 0.3 %. Thus, it is obvious that the method developed in the paper for approximating the first three terms of the Maclaurin series is more accurate in this case than the known Padé approximation method.

Example 2

In applications it is often necessary to express the variable of the resulting solution (x) in an explicit form: x=f(y). This is the case, for example, in inverse problems in the definition of physical properties. However, in many solutions the variable (x) can't be explicitly expressed, for example, if the solution is obtained in the form $y=[1-\exp(-x)]/x$, [10]. To obtain the explicit expression for x, let's use the approximation of the relation y=f(x) in the form of a Newton's binomial. Using the formula (8) for y (x), it is possible to obtain the following approximation:

$$\mathbf{y}(x)=[1-\exp(-x)]/x\approx(1+x/6)^{-3}. \quad (11)$$

From the found approximation, it is easy to express the variable (x) in the form:

$$x=f(\mathbf{y})\approx 6\cdot[\sqrt[3]{(1/\mathbf{y})-1}]. \quad (12)$$

This approximation has sufficient approximation accuracy in the range (0-2).

And if a more accurate approximation is needed, then for $x\geq 0$, it is possible to use double approximation here and get its approximation by a more complicated function:

$$\mathbf{y}(x)=[1-\exp(-x)]/x\approx\exp(\cos\sqrt{x-1}). \quad (13)$$

From this approximation, the variable x can be expressed in a more complicated way:

$$x=f(\mathbf{y})=\arccos^2(1+\ln\mathbf{y}). \quad (14)$$

This approximation has not only higher accuracy, but also a wider range of applications (0–3).

Sometimes it is necessary to find an approximation for the function $\mathbf{y}=x/\ln(1-x)^{-1}$, which describes the dependence of the "efficiency" y (x) in the range $0\leq x\leq 1$. If we use Newton's binomial as a basis here, we obtain the following approximation

$$\mathbf{y}\approx(1-x/1{,}2)^3.$$

4. 2. Approximation of functions that decompose into a power series in the square of the variable x^2

In a number of cases, when solving nonlinear problems by the small parameter method, the result is a fragment of the series in the form of an expansion in even powers of the argument. This is often the case in periodic processes described by trigonometric functions, for example, cosine:

$$\cos(x)=1-\frac{x^2}{2!}+\frac{x^4}{4!}-\frac{x^6}{6!}+... \tag{15}$$

In such cases, the fragment of the series is obtained in the following form:

$$\sum c_i x^i=1+ax^2+bx^4+\ldots \tag{16}$$

To approximate such series, as a basis, let's use functions that decompose into a Maclaurin series with respect to even powers of the argument:

$$f^N(x)=1+N\cdot f''_{(0)}\cdot\frac{x^2}{2!}+N\cdot\left[3(N-1)\left(f''_{(0)}\right)^2+f^{iv}_{(0)}\right]\cdot\frac{x^4}{4!}+\ldots \tag{17}$$

Carrying out in (17) a change of variable $x=\varepsilon\sqrt{M}$ and equating the coefficients of the corresponding ε powers of series (11) and (12), let's obtain the system:

$$\begin{cases} a=(M\cdot N/2)\cdot f''_{(0)}, \\ b=\left(M^2\cdot N/24\right)\cdot\left[3(N-1)\cdot\left(f''_{(0)}\right)^2+f^{IV}_{(0)}\right]. \end{cases} \tag{18}$$

Solving the obtained system of equations for the unknown parameters M and N, let's obtain their expressions through the known coefficients a and b of the series (1) and the derivatives of the function $f_{(x)}$ chosen as the basis for the approximation f′(x) and f″(x) in point (0,1):

$$N=(a/f''_{(0)})^2\cdot[f^{iv}_{(0)}/3-(f''_{(0)})^2]/(2b-a^2),$$

$$M=2(f''_{(0)}/a)\cdot(2b-a^2)/[f^{iv}_{(0)}/3-(f''_{(0)})^2]. \tag{19}$$

Example 3

If it is necessary to approximate functions that decompose into series in even powers of the argument, it is very simple to use Newton's binomial as a basis. In this case, first we need to change the variable $\varepsilon=x^2$, and then use formulas (8).

For example, for the cosine function: $\cos(x)\approx(1-x^2/3)^{1,5}$. The function **y**=x/arth(x) that is implicit with respect to x is also expressed in terms of the square of the variable $x/\text{arth}(x)\approx\approx(1-13x^2/15)^{1/2,6}$. And for the Bessel function of the first kind of order zero, the approximation by the Newton binomial in terms of the square of the variable is very simple: $J_o(x)\approx(1-x^2/8)^2$.

A more complicated expression, but less precise, can be obtained by expressing the Bessel function via the cosine function: $J_o(x)\approx[\cos(x\cdot\sqrt{3/2})]^{2/3}$. However, in this case it is necessary to use the general approach (7).

4. 3. Estimation of the approximation error

If, as a result of solving a nonlinear problem, a solution is obtained in the form of a fragment of a power series of the first three terms of the Maclaurin expansion, then it is obviously impossible to estimate the error of approximate formulas obtained by this method. But if, as a result of the solution, a fragment is obtained from the first four terms, it becomes possible to estimate the approximation error. There is also this possibility in the other two cases considered above: if necessary, obtain an approximate formula in the case when for an exact function one can't obtain an explicit

expression of the argument, and also in cases of simplification of very complicated formulas by simple expressions without significant loss of accuracy.

For example, if as a result of solving a nonlinear problem by a small parameter method, a solution is found in the form of a fragment of a power series of the first four terms of the Maclaurin expansion:

$$\mathbf{y}(x) = 1 + \mathbf{y}'_{(0)} \cdot \frac{x}{1!} + \mathbf{y}''_{(0)} \cdot \frac{x^2}{2!} + \mathbf{y}'''_{(0)} \frac{x^3}{3!}, \tag{20}$$

then, as a result of approximation for the solution of the problem obtained above, the approximate formula f (x) (that is, $\mathbf{y}(x) \approx \mathbf{f}(x)$), is obtained by the proposed method, which expansion in the power series has the following form:

$$\mathbf{f}(x) = 1 + \mathbf{f}'_{(0)} \cdot \frac{x}{1!} + \mathbf{f}''_{(0)} \cdot \frac{x^2}{2!} + \mathbf{f}'''_{(0)} \cdot \frac{x^3}{3!} + \ldots \tag{21}$$

In this case, as an accurate estimate of the absolute error Δ(x) of the approximation, it is possible to use the difference of two series $\mathbf{R}(x)=\mathbf{f}(x)-\mathbf{y}(x)$. Since the first three terms of the series (21) and (20) are respectively equal, the result of the subtraction is also expressed by a power series whose first term is:

$$\mathbf{R}(x) \approx x^3(\mathbf{f}'''_{(0)} - \mathbf{y}'''_{(0)})/6 + x^4 \cdot \mathbf{f}^{IV}_{(0)}/24 + \ldots \tag{22}$$

As a rough estimate of the absolute error of approximation Δ(x) in this case, it is possible to use the value of the first term of this series:

$$\Delta(x) \approx x^3(\mathbf{f}'''_{(0)} - \mathbf{y}'''_{(0)})/6. \tag{23}$$

A similar result can be obtained in the other two cases mentioned, only then the power series **R**(x) will have the following form:

$$\mathbf{R}(x) \approx x^3(\mathbf{f}'''_{(0)} - \mathbf{y}'''_{(0)})/6 + x^4(\mathbf{f}^{IV}_{(0)} - \mathbf{y}^{IV}_{(0)})/24 + \ldots \tag{24}$$

And as a rough estimate of the relative error of approximation in this case, it is possible to use the expression:

$$\boldsymbol{\delta}(x) \approx x^3(\mathbf{f}'''_{(0)} - \mathbf{y}'''_{(0)})/[6\mathbf{y}(x)]. \tag{25}$$

An analysis of the above approximate estimates of the error in the approximation of functions by the method developed in the article showed that Δ(x) is proportional to the third power of the variable, that is, x^3. And to approximate functions that decompose with respect to even powers of the argument Δ(x), its proportionality to the sixth power of the argument is obvious, that is, x^6.

5. Discussion of research results

The method for approximating the sum of a power series developed in the article can also be used in the case of approximation of functions that decompose into a Taylor series, for example, in the cases when $x_{(0)}=d$, then the power series has the form:

$$\mathbf{y}(x)=\mathbf{y}(d)+\mathbf{y}'(d)\cdot(x-d)+\mathbf{y}''(d)\cdot(x-d)^2/2+ \ldots \tag{26}$$

Normalizing the coefficients of the obtained series (15) by dividing them by the value of **y** at the point d: y(d) (obviously, the condition: d: y(d) easily transforms the series (15) into a

Maclaurin series. The subsequent sequence of parameter determination in the approximation is described above.

In this case, the choice of a number of proposed approximants is as follows. It is necessary to compare the coefficients of the third (or sixth) degree of the variable expansion of the proposed functions, with the corresponding coefficient for the third (or sixth) power of the variable ε of the expansion of the original function in a Taylor series. In this case, the criterion for choosing the approximant is, obviously, the minimum of the relative error of approximation of this coefficient.

6. Conclusions

For functions decomposing into Maclaurin series, a new analytical method for obtaining approximate formulas in the form of the Nth power of the functions f(Mx), adopted a priori as a function of the basis of approximation, is developed.

In general terms, expressions for the approximation parameters (N and M) of the approximate formula are obtained from the coefficients of the first three terms of the expansion of the function; therefore, even a small fragment of the series found as a result of solving the nonlinear problem by the small parameter method can serve as the initial function.

The developed method can also be used to obtain approximate formulas in cases where it is impossible to express the argument explicitly from exact functions, and also in cases where it is necessary to simplify complex formulas by simple expressions without significant loss of accuracy.

The error of approximations is analyzed and expressions are obtained for estimating the absolute and relative error of approximation.

References

[1] Koul, Dzh. (1972). Metody vozmushheniy v prikladnoy matematike. Moscow: MIR, 275.

[2] Van-Dayk, M. (1967). Metody vozmushheniy v dinamike zhidkosti. Moscow: MIR, 311.

[3] Popov, V. A., Tesler, G. S. (1980). Priblizhenie funktsiy dlya tekhnicheskikh prilozheniy. Kyiv: Naukova dumka, 353.

[4] Krylov, V. I. (1988). Matematicheskiy analiz. Uskorenie skhodimosti. Minsk: N i T, 175.

[5] Baker, G. A. Jr. (1965). The theory and application of the Pade approximant method. Advances in Theoretical Physics, 1, 1–58.

[6] Baker, G. A. Jr. (1975). Essentials of Pade approximants. New York: Academic Press, 318.

[7] Baker, G. A. Jr., Graves-Morris, P. (1981). Pade Approximants. Addison-Wesley Publishing Co.

[8] Vinogradov, V. N., Gay, E. V., Rabotnov, N. S. (1987). Analiticheskaya approksimatsiya dannykh v yadernoy i neytronnoy fizike. Moscow: Energoatomizdat, 128.

[9] Ludanov, K. I. (1984). Metod approksimatsii summy stepennogo ryada po ego pervym trem chlenam. Uk-84, Dep. № 763 v UkrNIINTI. Kyiv, 7.

[10] Fisher, M. E. (1965). The nature of critical points. Boulder: University of Colorado Press, 159.